AN ABSTRACT OF THE THESIS OF

CARL ALBERT BOWER, JR. for the M. S.
(Name) (Degree)

in METEOROLOGY presented on May 8, 1968
(Major) (Date)

Title: THE RELATIONSHIP BETWEEN SNOW CRYSTAL TYPES AND THE PREVAILING ATMOSPHERIC CONDITIONS ASSOCIATED WITH THE PASSAGE OF PACIFIC STORMS OBSERVED AT SANTIAM PASS IN THE OREGON CASCADES

Abstract approved [redacted]
Dr. Fred W. Decker

Detailed analyses of snow crystal sequence and atmospheric conditions were accomplished utilizing macrophotographic techniques for obtaining the snow crystal record at Santiam Pass in the Oregon Cascades on 19-20 January, 14-15 February, and 9-10 March, 1967. The photographic equipment consisted of a 35 millimeter single lens reflex camera, bellows, and extension tubes which facilitated macrophotography. To conduct crystal studies, problems inherent with crystal photography required solutions. The synoptic data for this study were extracted from teletype reports, facsimile charts, radiosonde soundings, and surface observations from U. S. Weather Bureau and Federal Aviation Administration weather stations.

The several storms analyzed indicated a crystal sequence commencing with high altitude crystal types progressing to low altitude

crystal types with the passage of a warm front occlusion, and a sequence of low altitude crystal types changing to a wide, intermittent crystal type spectra representative of convective and orographic activity following the passage of a cold front occlusion. A relationship between ceiling heights and crystal types was noted in two synoptic situations involving frontal passages. Low ceilings over the valley stations were associated with crystal types from high altitudes and high ceilings were associated with crystals from low altitudes which exhibited riming.

The Relationship between Snow Crystal Types and the Prevailing Atmospheric Conditions Associated with the Passage of Pacific Storms Observed at Santiam Pass in the Oregon Cascades

by

Carl Albert Bower, Jr.

A THESIS

submitted to

Oregon State University

in partial fulfillment of
the requirements for the
degree of

Master of Science

June 1968

APPROVED:

[redacted]

Associate Professor of Meteorology
in charge of major

[redacted]

Chairman of Department of Physics

[redacted]

Dean of Graduate School

Date thesis is presented May 8, 1968

Typed by Marion F. Palmateer for Carl Albert Bower, Jr.

ACKNOWLEDGMENT

Thanks and appreciation are extended to Dr. Fred W. Decker, my major professor, for his help on this study and for his initial guidance and interest concerning my desire to enter the Meteorological field during my tour with the U. S. Army.

Additionally, thanks is extended to my father, Mr. Carl A. Bower, for the use of his photographic equipment which greatly facilitated this study and to Mr. Robert M. Black, Agricultural Advisory Meteorologist with the U. S. Weather Bureau for his help in securing meteorological data. To my wife, Geraldine, recognition is given for help and encouragement during my studies at Oregon State University.

TABLE OF CONTENTS

LIST OF FIGURES

LIST OF TABLES

THE RELATIONSHIP BETWEEN SNOW CRYSTAL TYPES AND THE PREVAILING ATMOSPHERIC CONDITIONS ASSOCIATED WITH THE PASSAGE OF PACIFIC STORMS OBSERVED AT SANTIAM PASS IN THE OREGON CASCADES

INTRODUCTION

One might ask, why study snow crystals beyond seeking aesthetic values or understanding their formation from a crystallographic standpoint? Understanding and study of snow crystals certainly has interest beyond aesthetics and crystallography. A snow crystal can reveal in its form the precise meteorological conditions under which its formation occurs. A crystal grows as a particular form until meteorological conditions change, thus favoring other crystalline forms. Consequently, a snow crystal is a document in which the size and structure give information about atmospheric layers in which it develops and passes through on its fall to the ground.

Grunow (1960) suggests that use of snow crystals as aerological sondes exists at locations lacking radiosonde flights and for continuous studies on development of meteorological conditions within the upper air layers. The objective of such a use is to obtain indications on the structure of precipitation cloudiness from typical snow crystal samples. If the crystal form depends uniquely upon airmass conditions, it can be expected that the passage of a cyclone, and its

frontal systems, is indicated by a typical crystal sequence. Rime-coated crystals infer the existence of supercooled water clouds, and conclusions are drawn on existence of hazards for flying owing to a potential icing of aircraft. For evaluation of the process of rain-out and wash-out of radioactive fission products, crystal forms could give essential data if it is possible to know from these forms at what altitudes the snow crystals originate and through what thickness of layers they fall.

Early workers made extensive observations on snow crystals reaching the ground and attempted to correlate the relative frequencies of various crystal forms with temperature at the place of observation, but very little in the way of consistent results emerged at first. Failure to find clearly marked correlations between predominant crystal habit and temperature at the ground was not surprising since only the conditions aloft during growth of the snow crystal are of major importance in determining its form. Recently, crystals have been collected from different types of clouds having widely differing temperature conditions, water vapor concentration, and supersaturation relative to ice (Table 4). More recently, considerable work has been done on qualitative and quantitative work with snow crystals (Nakaya, 1954; Grunow and Huefner, 1959; Kuettner, Aldaz, and Boucher, 1958; Magono, et al., 1959, 1960, 1962, 1963, and 1964; Power, 1962; and Weickmann, 1957). Results

of these studies are summarized (see Literature Review in this study).

To date, a study has not been conducted in the Pacific Northwest where meteorological conditions are quite different from those encountered in studies in Japan, Germany, and the Northeastern United States. It is, therefore, the purpose of this study to: (1) describe the methods employed and the problems involved in crystal sampling, and (2) relate snow crystal types and distributions to: (a) the synoptic situation, (b) the associated nearby atmospheric conditions as indicated by radiosonde soundings at Salem, Oregon, and (c) empirical studies.

DEVELOPMENT OF THE SNOW CRYSTAL SPECTRA

Formation of Hydrometeors

Growth of Cloud Droplets

An airmass cools by expansion when forced to ascend, either through gradual ascent associated with cyclonic activity or under orogenic influence. With decreasing temperature the relative humidity increases and in the absence of condensation nuclei may increase seven or eight times that necessary for saturation (Mason, 1962). Condensation nuclei in the air range from 10^{-7} centimeters to greater than 10^{-3} centimeters in size. When the airmass cools nearly to saturation, water vapor condenses on the condensation nuclei. The growth rate of individual droplets is dependent on surface tension and hygroscopic forces, the humidity of the air, and the rate at which heat of condensation transfers from the water vapor to a droplet. When considering numerous droplets, the preceding factors make the process extremely complicated. With all droplets competing for the available water vapor, individual growth rates depend upon the size, concentration, and cooling rate of the air (Mason, 1962).

Mason (1962) states two processes by which droplets may grow large enough to form clouds: (1) diffusion of water vapor to the

surface of a droplet and condensation upon it, and (2) growth of a droplet through collision and coalescence caused by the relative motion of one droplet to another. Variations in cloud-drop sizes may be attributed to nonuniform rates of diffusion because of variations in the size of the nuclei, vertical velocities, relative humidity gradient, and other factors (Haltiner and Martin, 1957).

Growth of Hydrometeors

On the basis of theoretical and experimental work, two basic processes of precipitation propagation are recognized: (1) The Bergeron-Findeisen mechanism of ice crystal-cloud-droplet coexistence and (2) the coalescence (accretion) mechanism.

In 1928, the Swedish meteorologist, Tor Bergeron recognized ice growth at water saturation; therefore, ice supersaturation was important in natural clouds. The cornerstone of the ice crystal-cloud-droplet mechanism is the fact that at temperatures below freezing, the saturation vapor pressure is less over ice than liquid water. Measurements show that vapor pressure over supercooled water at -20°C exceeds by 22 percent that over ice at the same temperature (Langmuir, 1948). Thus, in a cloud consisting of ice crystals and supercooled waterdrops, a vapor pressure gradient from the waterdrops, toward the ice crystals exists. The ice crystals grow by diffusion from the

supersaturated environment at the expense of evaporation from the waterdroplets for which the same environmental air appears subsaturated. Their growth is at a rate dependent upon the gradient of vapor concentration between the ambient cloudy air and the immediate boundary layer of the crystal. Finally, the large crystals can no longer be sustained by the air currents and fall to the ground. If they pass through a deep layer of warmer air, they melt and reach the ground as rain. Battan (1962, p. 61) described the process in steps:

> Assume now that some ice crystal nuclei are suddenly introduced into the cloud and that a small number of ice crystals are formed. As soon as this occurs, the cloud system becomes unstable. The air is saturated with respect to water, but is supersaturated with respect to ice crystals. As a result, water vapor molecules deposit on the ice crystals. As soon as this happens, the air is no longer saturated with respect to water. Consequently, some water evaporates from the cloud-droplets to make up for the losses to the crystals. This evaporation again leads to supersaturation with respect to the ice, the crystals grow larger, and the cycle continues.

The preceding steps occur continuously in a cloud, and under suitable conditions, snow crystal growth is thousands of times faster than waterdroplets. The Bergeron-Findeisen Theory is the generally accepted explanation for the formation of large drops associated with clouds extending above the freezing level in large cyclonic storms in middle and high latitudes and is the prevailing precipitation formation mechanism except for some tropical showers and usual drizzle

situations. Byers and Hall (1955) determined that the ice phase is not required for initiating precipitation over tropical oceans and probably is not required over humid tropical landmasses.

In 1950, Tor Bergeron (Weickmann, 1957) introduced the idea that noteworthy precipitation is the result of a "releaser cloud" and a "spender cloud." The water content is small in the "releaser cloud," but sufficient to generate trigger particles adequate in size and number to sweep out a "spender cloud" containing a continuous supply or large storage capacity of precipitable water. Hall (1957) observed the Bergeron Process operating with various distributions of ice crystals and supercooled droplets in general rainstorms in western Washington. He noted frequent cases with an upper and lower cloud deck; the lower containing the primary water supply and the upper furnishing ice crystals which fell into the lower deck and rapidly increased in size. Braham (1966) observed that ice crystals from upper levels could seed clouds containing supercooled droplets and indicated that cirrus crystals can play an active role in cloud microphysics by serving as a source of ice particles able to nucleate supercooled clouds in the middle and low levels. It was determined that cirrus crystals not only exist below cirrus clouds, but can survive falls of several thousand feet in clear air in concentrations adequate for seeding lower clouds.

A brief account of droplet growth through coalescence

(accretion) is presented since crystal growth can be involved in the coalescence (accretion) process both by collision between crystals and collision with supercooled droplets. Measurements show a considerable drop-size range in any given region of a cloud (Houghton, 1950). Because the larger drops fall faster than the smaller drops, larger drops will overtake and "sweep out" the smaller ones. In the coalescence process, some of the smaller drops escape the "sweeping out" process. The drops collected comprise a fraction of the total (called the collection efficiency) which depends upon the size of the collecting and collected drops and their relative velocity (Houghton, 1950). The growth rate of a droplet by this method depends on the mass of the particle, the median cloud-drop diameter, the liquid water content of the cloud, and the breadth of the cloud-drop size spectra (Houghton, 1950). Braham (1965) constructed a flow diagram (Figure 1), illustrating the principal precipitation processes and their interrelationships.

Snow Crystal Genesis

Crystallization Nuclei

The assumption that adequate quantities of effective condensation nuclei exist in the troposphere so that the transition from water vapor to water always takes place at or near water saturation cannot

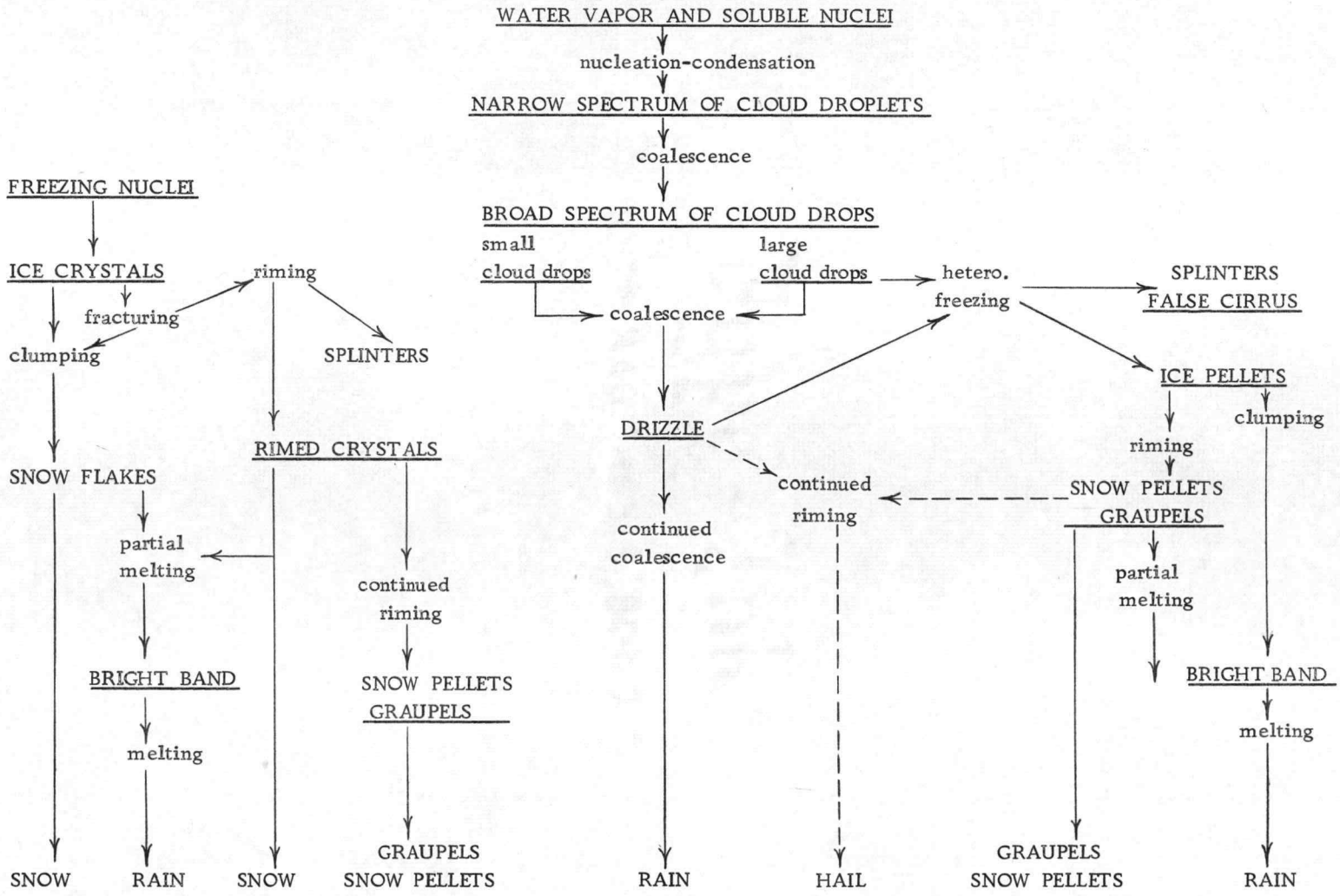

Figure 1. Flow diagram of precipitation processes (Braham, 1965, p. 494).

be made for the transition between water vapor and ice (deposition). In the atmosphere, deposition probably occurs seldomly near ice saturation. Therefore, layers of several hundred meters in thickness may often be supersaturated with respect to ice.

Ice crystals usually do not form naturally in clouds unless the supersaturation with respect to ice is approximately ten percent. This behavior is different from that of water condensation where supersaturation of less than one percent may suffice for crystallization.

Some available nuclei in the atmosphere serve only if a considerable degree of supersaturation occurs. Among these are the small ions and small particles studied by physicists in cloud chambers. In the nucleation process for the passage from vapor to crystallization, conditions are not the same as those for condensation and at low temperatures supersaturation with respect to ice is noted. This indicates that those suitable for condensation are not very suitable for crystallization.

Natural freezing nuclei appear mainly as insoluble substances, active only at large supersaturations (Byers, 1965). Information concerning substances which serve as natural ice nuclei in the atmosphere has been obtained by Kumai (1961, 1962) and Isono (1955). Of 271 snow crystals from Houghton, Michigan, studied in detail, Kumai found that 87 percent contained clay mineral particles as

nuclei. Of 356 snow crystals collected on the elevated icecap of northern Greenland in the summer, 85 percent revealed clay mineral particles at their centers. Four of the total number of center particles were hygroscopic substances and in 13 snow crystals, center nuclei were not discernable, suggesting the possibility of homogenous nucleation.

Snow Crystal Growth

Pristine snow crystals present in cirrus clouds or in ice fog are the same type of ice crystals formed in the air by condensation of water vapor by deposition. The ice crystal is first formed in the formation of a natural snow crystal by (1) the spontaneous transformation of a supercooled waterdroplet at cirrus temperature, (2) the result of natural or artificial seeding at warmer temperatures, or (3) the direct deposition of water vapor on a solid nucleus. Minute fragments of an ice crystal may be included in the seeding materials as the most efficient one. The preceding processes lead to the same result in the sense that small ice crystals or germs of snow crystals make their appearance in the atmosphere (Nakaya, 1954). The form and structure of the snow crystal grown from a germ are determined by the meteorological conditions after the germ is formed.

At temperatures a little below 0°C, concentrations of ice crystals formed in clouds are extremely low, and the difference in the

saturation vapor pressures over ice and liquid water is so small that the growth rate of a crystal appearing in a supercooled cloud is little different from that of the cloud-droplets. At temperatures below -10°C, however, crystals may appear in concentrations significant for the production of appreciable precipitation, and yet low enough to allow a moderate rate of ascent of air, keeping the air nearly saturated with respect to liquid water. Air saturated with respect to liquid water at -10°C, is supersaturated relative to ice by ten percent and at -20°C by 21 percent; hence, ice crystals grow more rapidly at these temperatures than will the cloud-droplets for which the supersaturation will usually be less than one percent (Mason, 1962). This growth is maintained for the duration of required supersation. The growth by diffusion is extremely rapid at first (the droplet or crystal growing from the size of the nucleus to visible size in a fraction of a second), but soon slows down (Byers, 1965).

Extensive areas of supercooled water in the snow region are unusual and tend to be localized in regions where stronger ascents are induced by topography or convection. In general, well above the melting level there are only snow crystals. It follows that the freezing of droplets cannot be the source of crystals which is needed to replace those falling out of layer clouds as snow. It is thought that the splintering of the large, fragile, fern-like snow crystals provides these crystals (Mason, 1962).

In the absence of riming or electrostatic effects it is probable that snow crystals seldom coalesce with each other. At such cold temperatures that even the lowest clouds have turned to ice crystals, only the rudimentary pristine crystal forms occur. It is a common observation, however, that the largest snowflakes occur with the temperatures very near freezing; under these conditions there is always strong evidence of riming. The reason that riming helps collision and coalescence is twofold: (1) rimed particles have size dependent fall speeds making collisions possible, while unrimed planes have similar rates of fall regardless of size, and (2) the presence of liquid on the surfaces helps cement crystals together.

From the preceding arguments it appears that needles possessing size dependent fall speeds, could collide more easily; this is exactly what has been observed since needles often occur in bunches, sheaths, or even in clumps with nonparallel axes. Since the needle crystal represents a growth habit characteristic of temperatures near 0°C, it is often formed in an environment favorable for riming (Byers, 1965).

Classification of Snow Crystals

The solid hydrometeors observed in the atmosphere can be classified into four main types: (1) individual ice crystals or groups of crystals having a common nucleus, (2) snowflakes, (3) ice pellets,

and (4) hailstones. Needles, columns, and plates are fundamental crystal structures. The first two develop mainly in the principal axis and the last predominantly in the lateral axis. Pyramids and bullets are included among columnar forms. The plates range from simple hexagons, through sectored hexagons and stars, to the highly branched dendrites. Under exposure to successively different diffusive fields, combinations occur such as capped columns, spatial dendrites, and other combined forms. Clumping and riming produce such forms as large, cottonlike snowflakes, thick plates, rimed crystals, low density snow grains, dense pellets, and miscellaneous irregular particles (Byers, 1965).

Although solid precipitation elements are generally allocated to one of ten main classes (Nakaya, 1954), detailed observations reveal many variations. To correlate observations, scientists agree on and work in terms of an International Classification (Table 1). Each class and basic feature of snow is designated by a code figure or a symbol. Additional letters and figures indicate additional characteristics such as the physical state, size, and degree of aggregation (Mason, 1957).

The International Classification of snow crystals was progressive and essential in correlating results from different geographic areas, but many workers found it unacceptable because it lacked the detail which crystal classification needed. Consequently, many

Table 1. Classification of solid precipitation as agreed by the International Commission on Snow and Ice in 1949 (Mason, 1957 n. p.).

Type of Particle (F)

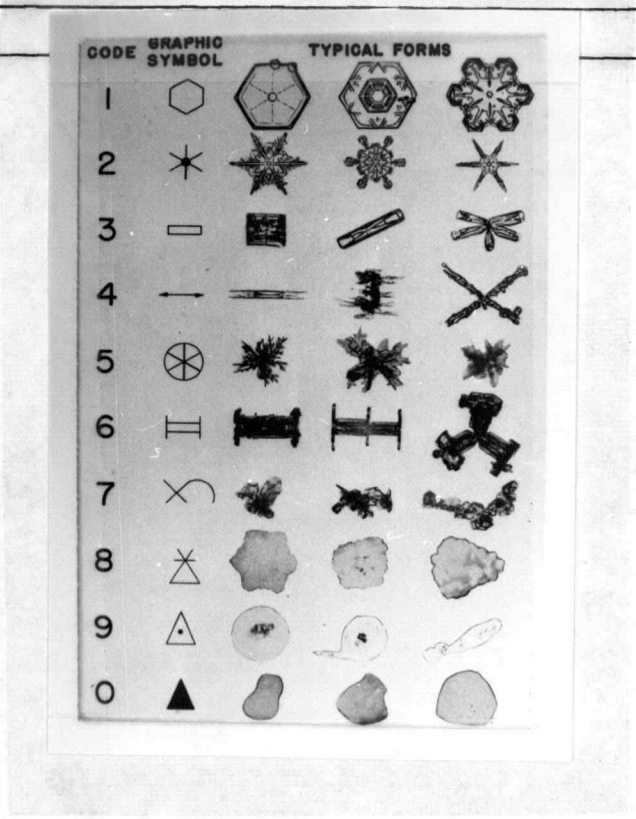

Term	Remarks
Plates; also combinations of plates with or without very short connecting columns	
Stellar Crystals; also parallel stars with very short connecting columns	
Columns; and combinations of columns	
Needles; and combinations of needles	
Spatial dendrites; spatial combinations of feathery crystals	
Capped columns; columns with plates on either or one end	
Irregular particles; irregular aggregates of microscopic crystals	
Graupel (soft hail); isometric shape, central crystal cannot be recognized	
Ice pellets--ice shell; inside mostly wet	
Hail	

Additional Characteristics

m	-	Broken
r		Rimed
f		Flake
w		Wet

Size of Particle (D)

a	0-0.49 mm	Very small
b	0.5-0.99 mm	Small
c	1.0-1.9 mm	Medium
d	2.0-3.99 mm	Large
e	4.0 or larger	Very large

workers have used the General Classification of Snow Crystals introduced by Nakaya (1954) (Figure 2 and Table 2), comprised of 41 crystal types arranged according to form and combinations that are possible between main forms.

If crystals listed in the General Classification are arranged according to their formation conditions, concentrations combining qualitative and quantitative analyses into a less complicated system can be made. Nakaya accomplished this by concentrating the many types of crystals into eight main types, bringing them into relation with the temperature-saturation diagram (Figure 3).

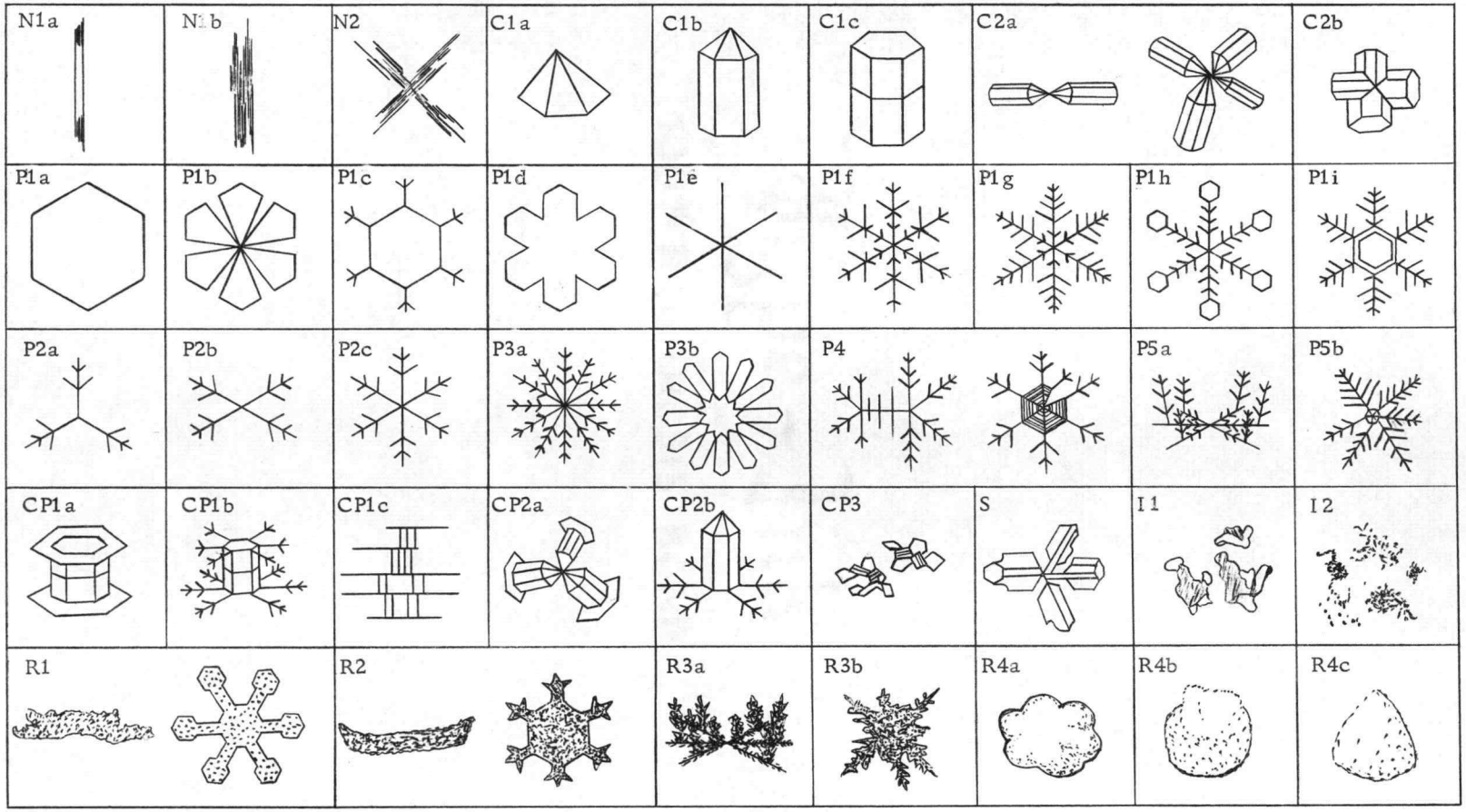

Figure 2. General classification of snow crystals, sketches (Nakaya, 1954, p. 81).

Table 2. General classification of snow crystals (Nakaya, 1954, p. 80).

I	N	Needle Crystal	1.	Simple needle	a.	Elementary needle
					b.	Bundle of elementary needles
			2.	Combination		
II	C	Columnar Crystal	1.	Simple column	a.	Pyramid
					b.	Bullet type
					c.	Hexagonal column
			2.	Combination	a.	Combination of bullets
					b.	Combination of columns
III	P	Plane Crystal	1.	Regular crystal developed in one plane	a.	Simple plate
					b.	Branches in sector form
					c.	Plate with simple extensions
					d.	Broad branches
					e.	Simple stellar form
					f.	Ordinary dendritic form
					g.	Fernlike crystal
					h.	Stellar crystal with plates at ends
					i.	Plate with dendritic extensions
			2.	Crystal with irregular number of branches	a.	Three-branched crystal
					b.	Four-branched crystal
					c.	Others
			3.	Crystal with twelve branches	a.	Fernlike crystal
					b.	Broad branches
			4.	Malformed crystal		Many varieties
			5.	Spatial assemblage of plane branches	a.	Spatial hexagonal type
					b.	Radiating type
IV	CP	Combination of column and plane crystals	1.	Column with plane crystals at both ends	a.	Column with plates
					b.	Column with dendritic crystal
					c.	Complicated capped column
			2.	Bullets with plane crystals	a.	Bullets with plates
					b.	Bullets with dendritic crystals
			3.	Irregular assemblage of columns and plates		
V	S	Columnar crystal with extended side planes				
VI	R	Rimed crystal (crystal with cloud particles attached)	1.	Rimed crystal		
			2.	Thick plate		
			3.	Graupellike snow	a.	Hexagonal type
					b.	Lump type
			4.	Graupel	a.	Hexagonal graupel
					b.	Lump graupel
					c.	Conelike graupel
VII	I	Irregular snow particle	1.	Ice particle		
			2.	Rimed particle		
			3.	Miscellaneous		

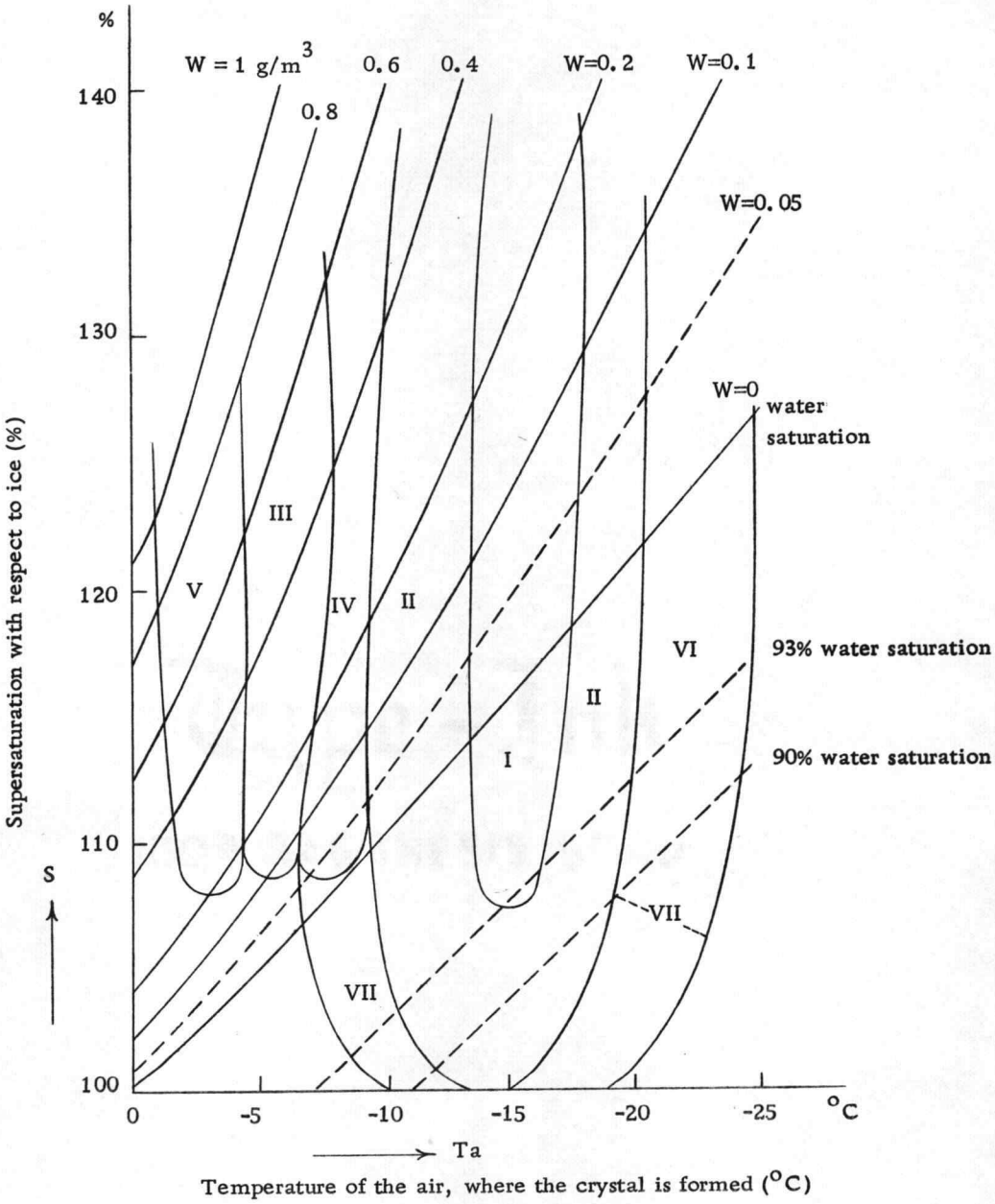

I	Dendrite
II	Plate, Sector
III	Needle
IV	Scroll and Cup
V	Irregular Needle
VI	Spatial Plate
VII	Column

Figure 3. Ta-S diagram, showing conditions of snow crystal formation as a function of temperature and supersaturation.

LITERATURE REVIEW

Historical

During the middle of the 13th Century the first report of complicated crystalline forms inherent with the formation of snow crystals recognized first with the naked eye was made in Europe. Nakaya (1954), cites the history of snow crystals in Europe as detailed by Hellman, and reports that the first sketch of snow crystals observed with the unaided eye was made by Claus Magnus, the Archbishop of Uppsala, about 1550. Sketches at that time did not indicate that snow crystals had hexagonal symmetry, but Keppler, at a later date did point out the fact that snow crystals belong in a grouping with hexagonal crystals. In 1635 Descartes observed snow crystals with the naked eye and published his sketches in Amsterdam. Hellman's detailed history is further cited by Nakaya (1954) and brings the observation of snow crystals up to the period when the microscope first came into prominence. It is reported that Robert Hooke published in Mirographia in 1665 various sketches of snow and frost crystals. Friedrich Martens sailed from Spitzbergen to Greenland and reported on snow crystals observed in the Arctic regions. In his report is perhaps the first reference on the relation between crystal forms and weather conditions. Donat Rosetti, in 1681, while a mathematician and priest at Reverno, Italy, collected sketches of 60 snow crystals

and made the first attempt to classify them. In 1820, William Scoresby, a whaler from England wrote, in a book on the history and status of whale fishing, a complete description of snow crystals he had observed, and clarified the structure of new types previously overlooked.

With the development of photomicrography in Europe, the study of snow crystals progressed rapidly. Among the people making significant contributions during the last part of the 19th Century were Hellmann of Berlin and Nordenskiöld of Stockholm. In the United Stated, Bentley (1931) made a contribution of now famous photomicrographs. Dobrowolski, of Poland did an extensive study on snow crystals and published the results. The fact that the results are not too well known is most likely attributable to the unpopularity of the Polish language.

In 1932, Nakaya and colleagues started snow crystal studies with extensive observations. A general classification of snow crystals was proposed from results of their observations (Nakaya, 1954). Further research with respect to mass, speed of fall, electrical nature, and frequency of occurrence of each snow crystal type was conducted. By 1944, Nakaya and colleagues (Nakaya, 1954) were able to produce every type of snow crystal artificially and hence were able to determine conditions of crystal formations.

Experimental

Attempts to determine the dependence of ice crystal shape on the variables involved in crystal growth indicate that primary parameters affecting crystal habit are temperature and ambient pressure of water vapor; the presence of fog droplets and the fall velocity of the growing crystal may also be involved. Finally, it is possible that foreign particles or vapors exert appreciable influence on the growing ice crystal.

Laboratory experiments on ice crystal growth are divided into two general categories. The first deals with ice crystals grown under conditions close to water saturation in a droplet fog, while in the second, the crystals grow in a droplet-free vapor with temperature and supersaturation independently variable. The droplet fog environment simulates more closely cloud conditions in the atmosphere, but gives more limited information about the growth process.

Perhaps the best known experiments on snow crystal growth are those conducted by Nakaya (1954), who suspended growing ice crystals on a fine filament in a cylindrical cold chamber. The bottom of the cold chamber contained a beaker of water maintained at a warm temperature, producing a slowly ascending fog which became supercooled before reaching the crystals. The crystals were growing in an environment which was probably above water saturation but

which also contained fog droplets. The growth habit of the crystals was studied as a function of ice crystal temperature and of the water bath temperature. The presence of the fog drops makes it difficult to estimate the true supersaturation of the environment; thus, results are difficult to interpret. Nakaya developed a diagram illustrating the dependence of different growth habits on temperature and to some extent on the supersaturation (Figure 3). The boundaries entered empirically separate the different crystal forms. The diagram has been generally verified in studies of snow forms from natural clouds of known temperatures.

Marshall and Langleben (1954) re-analyzed Nakaya's results and attempted to express them in terms of true supersaturation instead of the supersaturation utilized by Nakaya. They determined that the crystal habit is caused primarily by the active vapor excess rather than any temperature effects. Experimental evidence against such an interpretation was obtained by Shaw and Mason (1955) who examined the growth rate of single ice crystals growing on a cooled metal plate under conditions of controlled temperature and supersaturation. They concluded that crystal habit was primarily a function of temperature with supersaturation having a much smaller, nonsystematic effect.

Nakaya (1955) reported that aerosol particles profoundly affect ice crystal habit, but this was not confirmed by Hallet and Mason

(1958) who noted that habit changes are not affected by the pressure, the nature of the carrier gas, or the presence of aerosols.

Typical studies of growth from a fog are those of aufm Kampe, Weickmann, and Kelly (1951) and of Mason (1953) who initiated crystal formation by seeding a supercooled fog formed in a room-sized cold chamber with dry ice or silver iodide. Crystals were collected on glass plates coated with formvar solution, which left permanent replicas of the crystal when the formvar dried. From these experiments, results indicated a habit sequence: plates → prisms → plates → prisms as the temperature was lowered.

Mason and Hallett (1958) grew crystals on a thin nylon fiber running vertically through the center of a diffusion cloud chamber in which the vertical gradients of temperature and supersaturation were accurately controlled and measured. Detailed boundary conditions between different crystals were determined by growing different crystal forms simultaneously on the fiber. The movement of the fiber either up or down in the environment, caused original crystals to assume the crystal habit peculiar to the particular temperature and saturation characteristics in the new environmental surroundings. The changes in crystal shape were not produced by varying the supersaturation at constant temperature, but in some cases were produced by only one centigrade degree change in temperature at constant supersaturation. This experiment demonstrated that very large

variations of supersaturation do not change the basic crystal habit, although supersaturation does control the growth rate.

More recent experiments in which crystals were grown at supersaturations of only a few percent showed that the supersaturation also controls the aspect ratio or the relationship between the c "major" axis and the a "minor" axis. Thus, at temperatures where plate-like crystals appear, increasing supersaturation causes transitions from very thick plate to thick plate, to sector plate to dendrite. In the prism regime, the development is from short, solid prism to longer, hollow prism to needle. Needles, sector plates, and dendritic crystals grow only if the supersaturation exceeds values corresponding roughly to the air being saturated with respect to liquid water. Consistent results of Mason's and Hallett's experiments showed the crystal habit to vary along the fiber in the manner illustrated in Table 3.

Table 3. Crystal habit as determined by Mason and Hallett (1958).

Temperature Range	Crystal Type
0°C to - 3°C	Thin hexagonal plates
- 3°C to - 5°C	Needles
- 5°C to - 8°C	Hollow prismatic columns
- 8°C to -12°C	Hexagonal plates
-12°C to -16°C	Dendritic, fern-like crystals
-16°C to -25°C	Hexagonal plates
-25°C to -40°C	Hollow prisms

Field Studies

Weickmann, cited by Mason (1957), made a comprehensive collection of ice crystals from natural clouds at different tropospheric levels up to the cirrus level, with the temperatures being measured at the various levels. In proceeding from high to low level clouds, a gradual transition from prisms through thick plates to thick hexagonal plates was noted. Weickmann's observations were compiled (Table 4) and illustrate the various temperature and cloud characteristics in which various crystalline forms appeared. Not included in Weickmann's cloud observations are needle crystals which Gold and Power (1952) reported as originating from clouds in which the temperature was between -3°C and -8°C. Weickmann's data have been substantiated by Gold and Power (1952) who estimated the temperatures from radiosonde data. They estimated the height of snow formation from data on tephigrams and examined the relationships between shape of observed snow crystals at the earth's surface and the temperature of the layer in which the crystals were estimated to have formed.

Weickmann (1957) observed the time sequence of snow crystal forms during continuous precipitation and suggested that the snow crystal could be used as an aerological sonde. The dependence of snow crystal shape on temperature in the upper atmosphere was in

Table 4. Predominant crystal forms in different cloud types according to Weickmann (Mason, 1957, p. 177).

Level of Observation	Temperature Range	Cloud Types	Crystal Forms
Lower troposhpere	0° C to -15° C	Nimbostratus	Thin hexagonal plates
		Stratocumulus Stratus	Star shaped crystals showing dendritic structure
Middle troposphere	-15° C to -30° C	Altostratus	Thick hexagonal plates
		Altocumulus	Prismatic columns--single prisms and twins
Upper troposphere	less than -30° C	Isolated Cirrus	Clusters of prismatic columns containing funnel-shaped cavities. Some single hollow prisms.
		Cirrostratus	Individual, complete prisms

reasonable agreement with that obtained in the laboratory as confirmed by Kuttner and Boucher (1958). Grunow and Huefner (1959) conducted a qualitative analysis obtained by a general survey of all crystal forms appearing simultaneously. From this, a quantitative analysis was made to derive layer thicknesses and to construct cross-sectional analyses based on crystal results.

Gold and Power (1960) determined that the dependence of snowfall density on crystal type may give insight into the physical basis for part of the areal variation in the water equivalent of snow during storms. Power, Summers and D'Avignon (1964) showed that a good relationship between the density of newly fallen snow and the form of the predominant crystal which comprises the snowfall exists. Riming had a marked influence on the density of the snowfall. In cases, high snow growth levels were associated with high relative humidities at the bases of frontal inversions.

To fill the gap existing on areal studies, Nakaya and Higuchi (1960) conducted studies to determine the areal distribution of snow crystals during a snowfall. Observations were conducted simultaneously over an area of 5200 square kilometers utilizing 14 observation points. From the study, dependence of snow crystals on the prevailing atmospheric conditions showed agreement with experimental results, and areas where crystals of like shape were observed appeared related to upper air isotherms.

Magono, et al. (1959) conducted a series of field observations to determine the growth rate of natural snow crystals in the atmosphere utilizing a series of observation points situated vertically on a mountain. They determined the existing atmospheric conditions at each of the stations used and more accurately determined the conditions under which the crystals grew. It was observed that snow crystals of various types grew at humidity values near ice saturation and at times a little below ice saturation. Dendritic crystals were found in heavy snowfalls, but generally occurred in very light snowfalls in the absence of observable clouds. In some cases the air within clouds was not saturated, expecially in most cases near the cloud base.

In 1960 Magono, et al. (1960) continued studies of the previous year to define humidity conditions more precisely. With improved humidity measurements snow crystals still appeared to grow in and fall from, a nonsaturated air layer. The extension of cloud layers to 85 percent relative humidity rendered observed results comparable to experimental results. Dendritic crystals were observed to grow in nonsaturated air layers with respect to ice, as noted in preceding studies.

Accurate humidity measurements in clouds require more development. To accomplish this, Magono, et al. (1963) changed their

observation techniques. A dropsonde was employed to better ascertain the temperature and humidity conditions prevalent in the cloud from which the snow crystals fell. One item of noteworthy interest determined from these investigations was that although spatial dendrites were observed to fall, the associated inversion layer usually experienced at -20° C did not appear in the dropsonde data.

During the winter of 1963 (Magono, et al. 1964), a three dimensional observation network was used for cloud and snowfall observations on the west coast of Hokkaido. From a cloud, source of falling crystals, it was determined that heavy snowfalls originated first from lower stratocumulus of band structure and after initial considerations were increased by orographic influence.

METHODS OF RECORDING SNOW CRYSTAL SPECTRA

Various techniques are used for recording snow crystal types. The technique used depends on the quality of results desired, operating conditions, and type of study. Basically, sampling methods are considered as either continuous or periodic. Sampling techniques must meet the following requirements: (1) samples must provide a representative survey of different crystal forms appearing simultaneously, and (2) for form analyses, the observation material must provide an exact image of the outside surfaces of individual crystals.

Visual Method

The visual method of snow crystal observation requires the least sophistication with respect to equipment and procedure. Use of the visual method requires a sampling board, faced with black velvet which facilitates inspection of the snow crystals under a low-power magnifying glass. Compound snow crystal forms are not easily identified and only general characteristics about a snowfall are noted when using the visual method. Detailed requirements for problems of cloud physics and physics of precipitation are not satisfied by visual observation methods because classification schemes used are necessarily general.

Replica Technique

Schaefer (1956) devised a widely used method of preserving crystal forms. Snow crystals are embedded in a plastic casing which hardens around them, leaving a faithful reproduction of the snow crystals. The technique utilizes polyvinyl formal (obtained under the brand name of Formvar 15-95), dissolved in dichloro-ethane. For most crystal work, a solution of one to two parts by weight of Formvar to 100 parts of dichloro-ethane is used. A thin coating of the liquid is applied to a glass plate or other suitable material and exposed to snow crystals until the desired crystal density is obtained. The resulting replicas are suitable for microscopic inspection at a later date or lend themselves to direct photography.

Schaefer (1962) improved the replica technique by utilizing precoated glass slides. The crystal samples desired are deposited on precoated slides. When the desired number of crystals are obtained, the sample is exposed to the vapor of the solvent used, thus liquifying the polyvinyl formal which then envelops the sample. The improved method is useful in situations in which the particle life is limited because of evaporation, sublimation, or other conditions where particle stability is a function of delicate equilibrium.

An adaption of the replica technique to a method enabling continuous replication described by Power, Summers, and D'Avignon

(1964), utilizes a polyester film base as the material on which the Formvar solution is deposited. The film is passed through a Formvar bath by means of a driving sprocket. A sampling chimney located over the film allows crystals to fall on the wetted film base. A blower system facilitates drying of the Formvar solution, enabling continuous snow crystal sampling.

Photographic Methods

The photography of snow crystals can be grouped into three major types. Shadow photography is used for recording crystal sizes as they appear naturally. Macrophotography is that photography concerned with magnifications up to four power. Microphotography can be accomplished either by enlargement of prints or by use of a microscope with an adapter facilitating direct microscopic photography.

LOCATION OF STUDY

Physiography

Geography

Within the Pacific Northwest are a variety of physiographic settings; more locally, several divisions are noted in Oregon. Important in this study is Western Oregon; that part of the state extending from the Cascade Mountains on the east to the Pacific Ocean on the west.

The Coast Range extends from the Columbia River in the north to the Klamath Mountains in the south. The crestline is about 1500 feet in elevation, although peaks are higher and passes lower. Marys Peak, 4094 feet in elevation, is the highest peak in the Coast Range (Baldwin, 1959).

The Willamette Valley separates the Coast Range and the Cascades in the northern half of Oregon. The Cascade Range is divided into two regions: (1) the Western Cascades with more even crests, and (2) the high Cascades which include the well known peaks. The high Cascades divide the state into the marine western portions and the much drier, continental interior. The Cascades rise somewhat abruptly 60 to 100 miles inland from the Pacific shore and are 50 to 100 miles wide with general summit elevations of 6000 to 8000 feet

in the north and 4000 to 6000 feet in the south. Above the summit level rise such well known peaks as Mt. Hood, 11, 360 feet; Mt. Jefferson, 10, 495 feet; and the Three Sisters, 10, 354 feet (Baldwin, 1959).

Climatology

The several regions of the Pacific Northwest have different climatic settings attributable in part to surface form and elevation. Location near the coast and some distance inland is another important factor with the parallelism of the coastline and mountain ranges enhancing the effect of this factor.

The Pacific Ocean is especially effective in restricting annual temperature ranges along the coast where landforms allow marine influence to penetrate inland to the Cascade Mountains. The mountains form an effective barrier, increasing the effect of the landmass on temperature between winter and summer east of the mountains (Highsmith, 1962).

Weather

Much of the precipitation in the Pacific Northwest is associated with the movement of cyclonic storms through the area. With these storms occurs the inherent meeting of airmasses having contrasting temperature and moisture content along frontal discontinuities.

Ascending air in the low pressure center and up frontal surfaces cools, resulting in cloud and precipitation formation. Mountain barriers, cause of orographic lifting, also influence precipitation totals significantly, contributing to a comparatively wet Western Oregon with windward slopes and the drier Eastern Oregon.

Polar maritime Pacific airmasses affecting North American weather have the North Pacific, dominated by the Aleutian Low and its strongly cyclonic circulation, as a source region. The eastern part of the Pacific in mid-latitudes is a region of relatively warm surface waters. These waters surround the maritime Pacific "mP" source region so most of the air entering this region originates in cold continental areas to the north and west, and is drawn into the region by the strong northwesterly flow converging on the Aleutian Low. Heating and humidifying the continental Polar "cP" air at its base by the warm water transforms it rapidly from a cold, dry, stable airmass into one relatively unstable with mild and humid lower layers.

Site Selection

Selection of Santiam Pass in the Cascades (44° 25'N., 121° 52'W.) with an elevation of 4, 748 feet, made it possible to attain sufficient elevation and the associated cold temperatures necessary for snow crystal photography. The facilities of Santiam Lodge, a summer

camping facility and winter retreat site administered by the Presbyterian churches in the area, proved adequate for data collection. Higher relief to the north, northwest, and west, and trees to the southwest and south provided wind breaks. The photographic equipment was located underneath an "A" frame building used as living quarters by the lodge manager (Figure 4). Temperatures under the building of one to two fahrenheit degrees warmer than the ambient temperature in the open were encountered during calm conditions. Quarters which could be used for rest and warmth were available to the researcher. Shelter from the cold is extremely desirable, if not a necessity. The relative inactivity of the researcher, even with suitable clothing made keeping warm difficult under prolonged subfreezing conditions. Working in the open, during subfreezing conditions, for extended periods is exhausting work, and working alone for periods longer than 12 hours approaches the impossible.

Figure 4. Area underneath "A" frame dwelling in which photographic equipment was located for snow crystal studies.

EQUIPMENT USED FOR SECURING SNOW CRYSTAL RECORD

Camera and Accessories

Photographic work was accomplished with a Yashica TL-Super 35 millimeter single lens reflex camera containing a focal plane shutter and a 50 millimeter lens. A through-the-lens light metering system was incorporated in the camera for exposure control. In addition to the camera, a Kopil belloscope and Vivitar extension tube set were used as complementary equipment for macrophotography. The least magnification possible with the extension tube set was X 0.20. The range of magnifications possible with the bellows was X 0.67 to X 2.68.

Equipment Mounting and Problems

Two problems encountered in macrophotographic work are depth of field reduction and camera vibration. A X 4 magnification has a depth of field (vertical depth for which everything is in focus) of approximately 0.3 millimeters and a slight deviation from parallel of the film plane to the sampling platform can cause serious focusing problems.

Contrasted to photography requiring rapid shutter speeds and distant objects in which slight vibration of the camera, supporting tripod, or subject movement does not markedly affect the photographic

quality, the slightest vibration of the camera or subject yields unsatisfactory results in macrophotography, utilizing slow shutter speeds. The use of a rigid tripod and a remote shutter release or delay type shutter is a requisite for minimizing vibrations. The ten-second shutter delay of the camera was utilized for photography in this study.

The camera, tripod, and sampling platform were mounted as an integral unit (Figure 5) to minimize vibrations. A pocket level was utilized to insure that the film plane of the camera mounted on the tilting panhead of the tripod was level and parallel to the sampling platform.

Fine focusing difficulties were avoided by utilizing the coarse adjustment of a dismantled, inexpensive microscope to achieve correct focal lengths at various magnifications. The coarse adjustment of the microscope was adapted to a shoe attached at the base of the camera and mounted on the panhead of the tripod. The adaptation made camera movement with respect to the fixed platform on the tripod possible. The coarse adjustment of the microscope adapted to the tripod complemented the adjustment obtained by moving the vertical shaft of the tripod up or down.

Problems Encountered with Camera

A problem encountered with the camera was that of seizing[1] during extended crystal sampling. On arrival at Santiam Pass the photographic equipment was acclimated to minimize the affect of excess heat on the crystals. In relocating the camera from a warm to a cold environment, immediate problems were not noticed, but after prolonged exposure under extreme conditions, the camera on occasion would not function properly. The diaphram in the lens barrel would seize and not respond to manual setting from f 1.7, used for focusing and viewing to f 16 used for crystal photography. Warming the lens barrel freed the diaphram but caused excessive condensation on the lens and possibly in the lens barrel.

In addition to the diaphram malfunction, the mirror utilized for viewing and focusing through the lens often remained in a retracted position assumed during film exposure. When the mirror would not return to the viewing and focusing position, snow crystal photography was not possible. Warming the camera freed the viewing mirror.

---

[1] By "seize" is meant that through freezing of condensation or through the change in viscosity of lubricants used the camera ceases to function properly.

Figure 5. Mounting of camera on tripod, showing light source, working platform, bellows and vertical focusing adjustment.

SAMPLING, RECORDING AND GROUPING OF THE SNOW CRYSTAL SPECTRA

Sampling Technique

One method of snow crystal sampling was used with different sampling plates, depending on results desired. A sampling board covered with black, deep nap velvet was used for visual crystal observation. Photography utilizing transmitted light required lantern slides for crystal sampling.

When snow crystals fell in a less than vertical trajectory, interception was difficult because the wind blew the crystals off the sampling board or slide, or the crystals bounced off. Because sampling periods were often windy, a small box which functioned as a wind screen was utilized, thus reducing the horizontal velocity of the snow crystals, allowing them to settle on the sampling board or slide.

During snow crystal sampling, several samples per hour were taken for visual classification or for direct photography. The closest interval used for survey sampling was ten minutes. Shorter periods of time were often used for photography at high magnifications. To capture representative samples of the crystals, the sampling box was covered until the immediate area around the "A" frame shelter (Figure 4) was clear of the sampling area. The sampling box was then uncovered and exposed for a measured length of time

(usually 10 - 20 seconds) dependent on the snow crystal density on the plate, and then recovered. Occasionally the sampling exposure was less than ten seconds and at other times greater than 20 seconds.

When gusty winds blew snow off trees and the "A" frame shelter, sampling was carried out during lulls. Crystal samples contaminated by snow blown off trees or buildings were discarded.

Methods Used in Obtaining Crystal Record and Problems Encountered

Visual Methods

The visual method, used to complement photographic methods consisted of noting predominant crystal types falling at a particular time, or of noting unusual crystalline forms observed during photographic work. Crystals observed visually are classified according to the General Snow Crystal Classification (Figure 2). Visual observations give a general survey of crystals observed but are not suitable for statistical analyses.

Photographic Methods

Early crystal photography utilized black and white film (commercially available as Kodak Panatomic X) with an ASA rating of 32. It was thought that crystal analyses could be accomplished from prints of the negatives, but it was later determined that crystal

magnifications up to X 2 prints were difficult to identify. Prints with magnifications of X 12 to X 15 were easily identified, but prints of this nature did not represent sufficient crystal numbers to conduct a general survey of crystal types falling at the time photography was accomplished. Because of the difficulty encountered in crystal identification from the prints of Panatomic X negatives, a change was made to colored slide film (Kodachrome II) with an ASA rating of 25.

A continuous light source which could be metered accurately without the necessity of computing exposure time on the basis of film tests was used for transmitted lighting of the crystal samples. The light source utilized a light reflector, frosted bulb, and light diffuser to achieve uniform lighting of the crystal samples photographed.

Satisfactory results were obtained using transmitted light, but problems existed. The incandescent light source supplied heat, causing snow crystal melt. Consequently, it was necessary to change the size of the frosted bulb used for lighting from a 40-watt bulb to a 25-watt bulb, depending on the temperature, and to ventilate the lighting system in an attempt to minimize heating effects from the bulb. During marginal temperature situations it was necessary to use the light for a period of time just long enough to accomplish focusing and film exposure. Unless the temperature was 30° F or colder, crystal photography was difficult to impossible. Heat from the hands while handling the sampling plate and the presence of the body during

focusing was often sufficient to cause crystal melt.

Computation of magnifications used in the crystal photography consisted of dividing the total distance between the film plane of the camera and the lens by the focal length of the lens. This method allowed slight error because of inaccuracy in measurement of lens to film plane distance obtained with a metric scale.

Various crystal magnifications were tried to arrive at a magnification providing best results. For the anticipated use of prints for crystal analyses it was determined that a magnification leading to a 2X enlargement when the film was processed and printed in jumbo prints would be suitable. Slides were taken at X 0. 38 with the idea in mind that a greater field of crystals would be photographed. Most of the work for analyses was accomplished at X 0. 38 and X 0. 68.

Grouping of the Snow Crystal Spectra

Procedure

To obtain a complete classification of snow crystals that would lend itself to further manipulation, the General Classification of snow crystals (Figure 2, Table 2) was used. A Bausch and Lomb Model HD 557 stereo-microscope with variable magnifications ranging from X 13 to X 80 aided the analyses of the snow crystal slides. By using transmitted light for microscopic viewing, it was possible to easily

identify snow crystal forms from the slides at X 26 on the microscope. The X 26 enlargement of slides which were X 0.4, enlarged crystals enough for identification. Magnifications up to X 1 on the slides yielded suitable crystal images when viewed under the microscope. Magnifications greater than X 1 on the slides were over enlarged when viewed under the stereo-microscope; consequently crystal detail was lost and faded into the emulsion contained on the film.

A plastic overlay with an etched grid was constructed and placed in the slide mount on top of the individual negative to aid snow crystal analyses. The grid consisted of 35 squares, numbered in an order, making later checking possible if verification was needed. Each square in the grid was five millimeters on a side. The numbering system was such that the first 15 squares included the central portion of each slide. Positioning the first 15 squares in the middle of the slide was necessary because the transmitted lighting used in the crystal photography left the edges of the slides underexposed and the camera lens introduced distortion on the edges of the slides.

Validity of Sample Count

With a representative sample collected during snowfall, the crystals arrange themselves in a random manner, and random sampling of the slide is not necessary.

In tabulating crystals by type and number, the researcher is faced with conducting a complete analysis entailing the counting and classification of every crystal observed on each slide or a compromise dealing with partial counts of crystals. Obviously, a compromise is in order since some slides contained up to 1200 crystals. For statistical purposes, there is a number of crystals that must be counted to have ratios between various crystal types at a particular sampling period remain constant. Thus, if one counts enough crystals, the ratios between various crystal types in a sample will closely approximate the ratios in a total count of the specimen.

Generally an attempt was made to classify at least 200 crystals on each slide. Some slide counts were less than 200 because of the snow crystal density and some had more. While counts greater than 200 would have stabilized the ratios more between crystal types, it is felt that knowledge of the accuracy encountered is sufficient.

Dryden (1931) constructed a nomogram illustrating the percent error on the abscissa and number counted along the ordinate. On this, curves were entered for various percentages. Use of the nomogram (Figure 6) makes possible the determination of the percentage error encountered for each percentage group of crystals appearing as one type. The formula on which the nomogram is based is:

$$\text{p. e. (in no. of crystals)} = 0.6745 \sqrt{n\,p\,q}$$

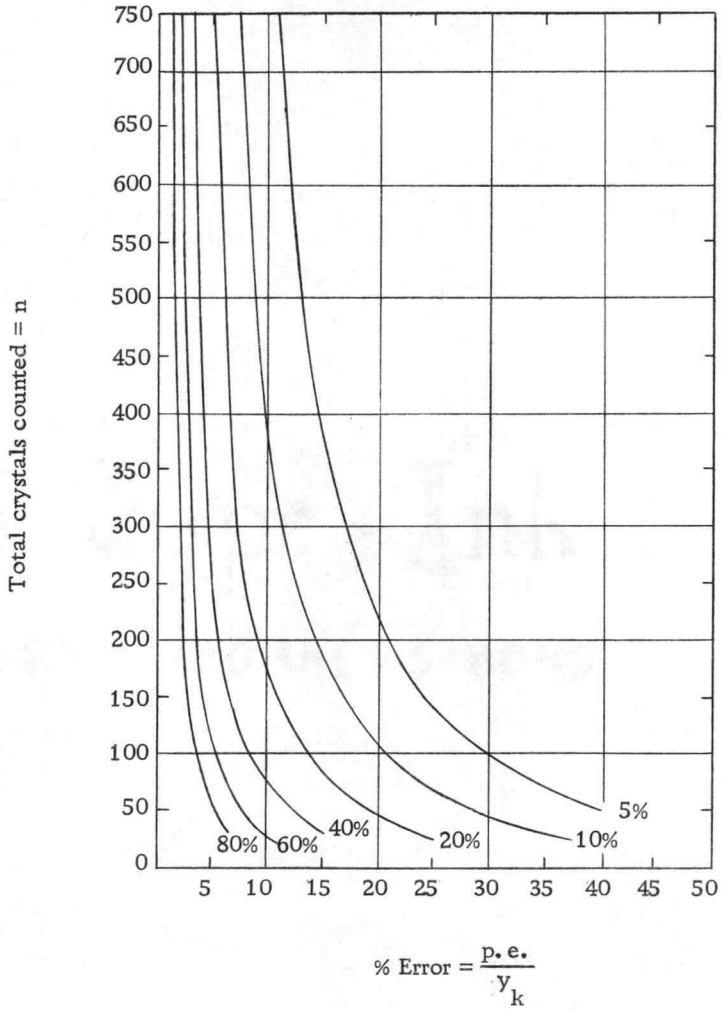

Figure 6. Nomogram of percent error for individual crystal counts versus total crystal count.

where p. e. is the probable error involved in counting n crystals, p is the probability that a crystal will belong to a specific type and q the chance that a crystal will not belong to a specific crystal type. The percent error is based on the relationship that p. e. in percent = p. e. $/y_k$ where y_k = the number of crystals of any type found in n crystals of the slide. Thus, for each crystal type with its percentage of frequency in the whole slide, there can be plotted a curve of p. e. in percent and n.

This consideration reveals the fact that the p. e. of the abundant types will be much lower than the p. e. of the less abundant types. Also for a type having a given frequency, p and q will not vary and p. e. will be a function of n; more specifically will vary directly as the $\sqrt{n.}$. Thus, for a sample count of 200 with 20 percent of the sample represented by a given crystal type, one has an accuracy of plus or minus nine percent (Figure 6).

DATA ANALYSIS

Case Selection and Data Presentation

Because Santiam Pass is marginal with respect to subfreezing temperature conditions in winter compared to temperatures in Europe and Japan which are subfreezing for extended periods (Nakaya, 1954, and Grunow and Huefner, 1959), not all major storms lent themselves to snow crystal sampling. Average maximum and minimum monthly temperatures compiled for Santiam Pass over a period of eight years (Appendix A, Table 8) show warmer mean temperatures than those encountered in studies conducted on the Island of Hokkaido and in Germany. Although the available climatological data for Santiam Pass are not reliable, climatologically speaking, one does have an idea of the temperatures likely during the winter months. Daily data are presented for January, February and March of 1967 (Appendix A, Tables 9 - 11).

Climatic Conditions for January, February and March 1967

During January 1967, average temperatures of 8° to 10° F above normal were common in Northcentral Oregon while 4° to 5° F above normal were fairly common everywhere except along the coast. Of four major storms passing over Oregon during the month, one was suitable for snow crystal analyses. In January, Santiam Pass

experienced 134 total inches of snow, leading all recording stations in Oregon (U. S. W. B. Climatological Data, 1967).

Only one date in February had considerable snowfall at Santiam Pass, although six consecutive days through the middle of the month had appreciable precipitation. Of these, three were not suitable for crystal studies because of high maximum temperatures (Appendix A, Table 10).

Temperatures for March averaged 3° F below normal. One major storm occurred during the month, with substantial snowfall over much of Southcentral, Northeast, and Southeast Oregon (U. S. W. B. Climatological Data, 1967).

Case Selection

Selection of atmospheric disturbances on which atmospheric variables at Santiam Pass were clearly represented by radiosonde data from Salem, Oregon, necessitated the selection of storms with wide-spread and continuous precipitation mechanisms. Continuous precipitation, associated with warm fronts, occlusions, westerly waves, cold fronts, and suitable orographic conditions, is considered to last at least one hour at a rate of about one inch in 24 hours.

The snow crystal sequence and its dependence on the snynoptic situation are discussed in detail for three cases: (1) a cold front occlusion, (2) warm front occlusion, and (3) the southern edge of a

cold cyclone. The results of snow crystal surveys are associated and compared to the synoptic and upper air conditions. Synoptic situations are illustrated with the aid of surface weather maps and upper air maps for 850 and 500 millibar levels (Appendix C, Figures 20-47). In addition to isobars, the sea level maps contain fronts. Upper air conditions are further illustrated by use of time-height cross-sectional analyses (Figures 7, 10 and 13) to an altitude corresponding to the 400 millibar pressure height. The time-height cross-sections contain isotherms on 5°C intervals and isohumids at ten percent intervals on the basis of saturation with respect to ice. Wind speed and direction are included for mandatory levels when available. The wind shaft indicates the direction from which the wind blows, and the barbs on the shaft denote wind velocities. A long barb represents ten knots and a half barb represents five knots. A blackened triangle symbolizes 50 knots. In addition to the cross sectional analyses, individual radiosonde flights (Appendix D, Figures 48-59) for Salem, Oregon, are included for crystal sampling periods.

Data Presentation

Results of snow crystal analyses are presented in general surveys (Appendix E, Tables 12-14) in the form suggested by Weickmann (1957). The surveys have two rows of crystals; the top row contains typical forms requiring only slight ice supersaturation, and the

bottom row contains forms whose growth occurs at or near water saturation. Crystals of the top row are formed either as a result of weak updraft and a small number of crystals, or with strong updraft and numerous crystals. A strong updraft combined with a number of crystals tends to produce crystals in the bottom row and a still smaller number of crystals result in rimed crystals. A third row on the tables depicts the principal temperature ranges in which the various crystal types are most often associated. The presentation used for this study contains all crystals observed for given observation times. To realize more exacting results than those achieved by Weickmann (1957), and Grunow and Huefner (1959), the various percentages of crystal types are entered for corresponding observation times. Crystals on the top sides of the time lines represent crystals contained in the top row and crystals on the bottom of the time lines represent those of the bottom row. Percentages of crystal types were rounded off to the nearest whole percent. In cases where the the crystal type observed was less than one percent of the total crystal count, or when visual observations were conducted and crystal counts not made, an "X" was used. In addition to time, temperature, crystal counts, number of squares of each grid counted, and riming notation, crystal forms not appearing within the temperature groupings are also included.

The crystal types classed according to the General

Classification (Table 2 and Figure 2) and tabulated as General Surveys (Appendix E, Tables 12-14) were summarized on the crystal time-height cross sectional analyses (Figures 8, 11 and 14) by temperature ranges. In addition to the isotherms, isohumids, and crystal types, cloud cover data were entered for Salem, Eugene, and Redmond, Oregon (U. S. W. B. Surface Observations) when available. Primary emphasis was placed on the overcast heights and in cases of high overcast conditions, broken conditions were also considered to determine the highest cloud deck from which crystals may have originated. Cloud heights were adjusted to mean sea level in order to have cloud cover data at uniform heights for all stations. By way of example, cloud heights for Redmond, Oregon, were increased by 3,000 feet. With high cloudiness, cloud layers on either side of the Cascades were probably the same height above mean sea level. Lower cloudiness on the west side of the Cascades would be subject to orographic lifting, but cloudiness above the summit level of the mountains probably consisted of decks transversing the mountain. Therefore, if breaks in cloudiness at lower levels at one of the observing stations reveal higher cloudiness, it is assumed that the higher cloudiness exists for the other stations during the widespread storms considered in this study.

Along the bottom of each crystal-time-height cross-sectional analyses are observation times with radiosonde flight times

corresponding to 0400 PST and 1600 PST. Isotherms are represented by solid lines and isohumids with respect to ice by dashed lines. Consideration is not given crystal type frequencies as that data are available in the General Surveys (Appendix E, Tables 12 - 14). Crystals types are the crystal-time-height cross sections (Figures 8, 11 and 14) are represented by the letters employed in Nakaya's General Classification (Figure 2, and Table 2). Station symbols and cloud cover data used on the crystal-time-height cross sections are included in Table 5.

Table 5. Station symbols and cloud cover designation used on crystal time height cross sectional analyses.

Station	Symbol	Cloud Cover	
Salem	△	▲ overcast	10/10 cover
		◭ broken	6/10 to 9/10 cover
		◬ scattered	1/10 to 5/10 cover
Eugene	□	■ overcast	10/10 cover
		◨ broken	6/10 to 9/10 cover
		◫ scattered	1/10 to 5/10 cover
Redmond	○	● overcast	10/10 cover
		◑ broken	6/10 to 9/10 cover
		◐ scattered	1/10 to 5/10 cover

The 41 types of the General Classification were combined into the ten groups of the International Classification according to Nakaya's interpretation (1954) (Table 6).

The International Classification (Table 1), while less exacting

than the General Classification (Figure 2 and Table 2), reveals general crystal trends. The various crystals of the International Classification are expressed graphically as percentages. The curves for each crystal type appear, one above the other, and total 100 percent. The order of the crystal groups is such that crystals of the warmer regions appear at the bottom of the figure. Thus, graupel, needles, spatial dendrites, dendrites, capped columns, plates, irregular crystals, and columns are in order of warmest to coldest formation temperature. Time is entered along the bottom of the figure.

Table 6. Conversion of General Classification to Internation Classication (Nakaya, Appendix n. p. 1954).

International Classification	General Classification
Plates	P1a, P1b, P1c, P4
Stellar	P1d, P1e, P1f, P1g, P1h, P1i, P2a, P2b, P2c, P3a, P3b, P4
Columns	C1a, C1b, C1c, C2a, C2b
Needles	N1a, N1b, N2
Spatial	P5a, P5b
Capped Columns	CP1a, CP1b, CP1c, CP2a, CP2b
Irregular Crystals	CP3, S, I, I2, I3 (Spatial Plates)
Graupel	R4a, R4b, R4c

The preceding surveys represent crystal types observed simultaneously at the ground. Simultaneous crystal appearance does not imply simultaneous snow crystal formation, since crystals formed at high altitudes fall greater distances and in the presence of winds aloft, travel considerable distances. Conclusions on upper levels of cloudiness must consider the distances crystals travel. Nakaya (1954) determined the fall rates of various crystal types, where fall velocities vary depending on the mass of the various crystal types (Table 7).

Table 7. Mean values of dimensions, mass and rate of fall for various types of crystals (Nakaya, p. 116, 1954).

Type of Crystal	$\bar{d}$ (mm)	$\bar{m}$ (mg)	$\bar{v}$ (cm/sec)	$\bar{v}/v_r$
Needle	1.53	0.004	50	1/2
Plane Dendritic	3.26	0.043	31	1/6
Spatial Dendritic	4.15	0.146	57	1/5
Powder Snow	2.15	0.064	50	1/4
Crystal with droplets	2.45	0.176	100	1/5
Graupel	2.13	0.80	180	1/2.5

Crystal velocities of plane dendritic, powder, and spatial dendritic are all independent of their dimensions (Nakaya, 1954). Attached water droplets increase the velocity of crystals. Not included in the table is small graupel having a velocity of 100 cm/sec. The

fall velocities of needles are size dependent, thus the velocity for larger needles is 70 cm/sec and that of small needles, 30 cm/sec. The notation, $\bar{v}/v_r$ is the velocity ratio of a snow crystal to that of a raindrop of similar mass (Nakaya, 1954).

Cold Front Occlusion

Synoptic Situation, 19-20 January 1967

Examination of the 0400 PST map on the 19th revealed a deep 500 millibar low over the gulf of Alaska with strong west-southwest flow aloft. The morning (ESSA II and Nimbus II) weather satellite photographs revealed a broad band of dense clouds over Washington and Western Oregon associated with a front extending from Northwest Oregon, southwest to a position about 35° N. and 140° W. then west (U. S. W. B. Satellite Summary). The area behind the front in the off-shore region was covered by cellular clouds.

The surface front was located across Western Washington and Northwest Oregon, southwest off the coast to possible waves at 134° and 148° W. at 1300 PST (Figure 22). The 0400 PST maps showed the cold 500 millibar trough off-coast with the jet stream across Southern Oregon and Northern California. The surface front was located in Southwestern Idaho across Northern California. Satellite photographs of 1100 PST on the 20th showed Washington and Northern

Oregon covered by cellular instability clouds to a point well off-shore. The northern edge of the frontal clouds covered the southern half of Oregon and extended off the Southern Oregon Coast in a west-southwest direction.

The synoptic situation the evening of the 20th remained unchanged with respect to the low off the British Columbia coast and filling continued (Figure 32).

Synoptic maps are contained in Appendix C (Figures 20-34).

Upper Air Conditions

The discussion of upper air conditions is based on the time-height cross sectional analysis (Figure 7) and Salem radiosonde flights (Appendix D, Figures 48-53).

Cold air advection accompanying the cold front occlusion early the 19th decreased temperatures at all levels with post-frontal temperature falls most rapid. A temperature drop at the 6 km height from -20°C to -35°C was noted between 0400 PST and midnight January 19th. The 2 km level temperature decreased from about 2°C to about -7°C at 0800 PST on the 20th.

During the day, the lower boundaries of the saturated layers descended and by 1900 PST the 19th, the upper layer was saturated between 1.5 km and heights greater than 7 km (Figure 7). The lower layer of saturation extended to 0.3 km by 1600 PST. Drying at

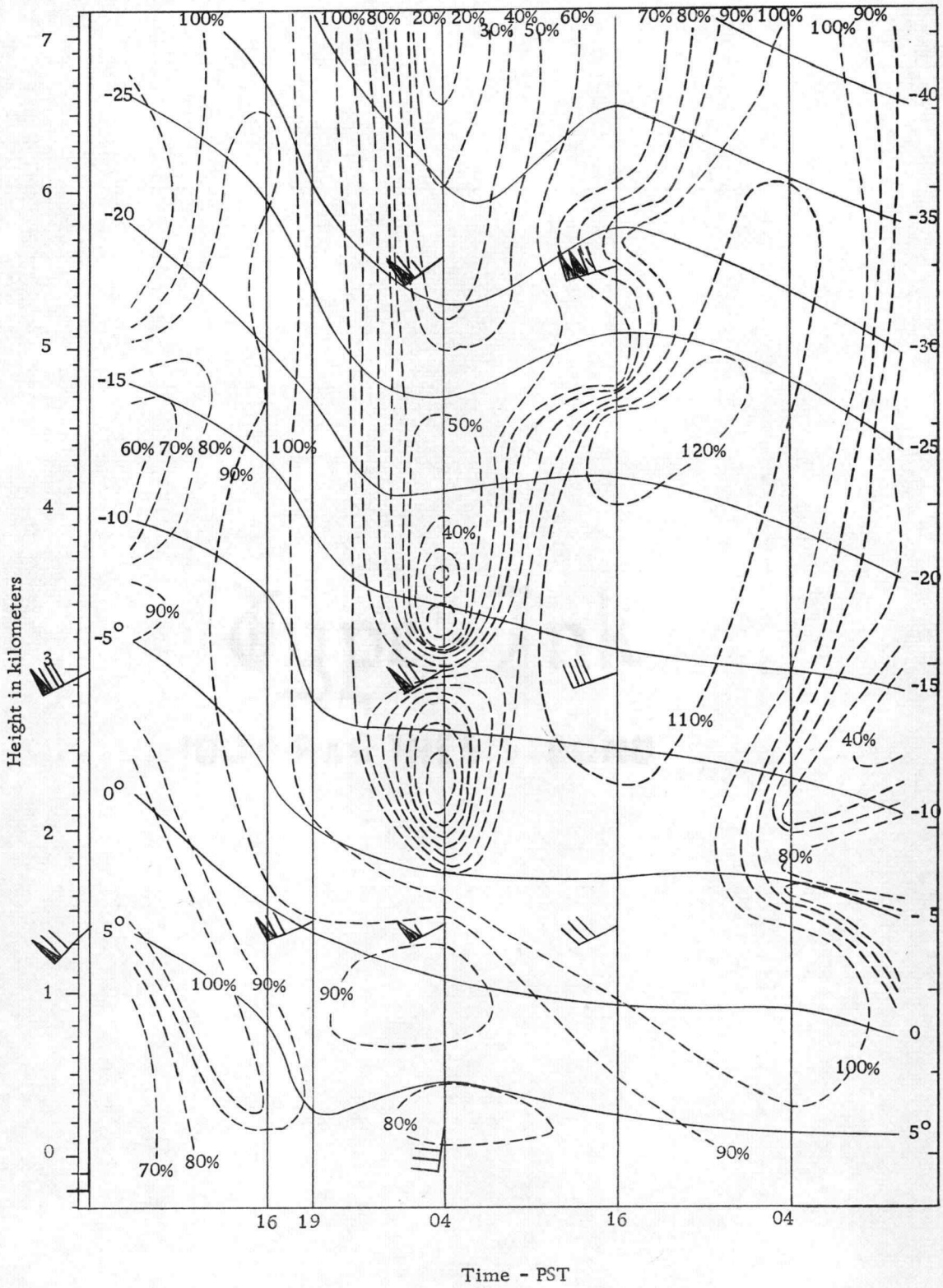

Figure 7. Time-height cross sectional analysis of temperature and relative humidity with respect to ice for 0400 PST 19 January to 0400 PST 21 January 1967.

2100 PST above 2 km corresponded to increasing temperatures aloft and decreasing temperatures below 2 km. A layer of saturation appeared between 1.7 km and 1.5 km. After 0400 PST the 20th, relative humidity increased, forming a supersaturated layer between 4.8 km and 0.9 km by 1600 PST, corresponding to a temperature increase above 4.3 km. Increased relative humidity after 0400 PST on the 20th above 1.8 km was probably associated with the series of waves formed on the front and post-frontal convective activity.

Winds aloft during this period had velocities to 70 knots at 1.4 km on the 19th to in excess of 100 knots at 5.7 km at 1600 PST on the 20th. Wind directions aloft during the crystal sampling period remained southwest to west-southwest.

Weather

Snowfall during the sampling period (1200 PST on the 19th through 2230 PST on the 20th) was continuous. Surface observations indicated that prefrontal precipitation commenced in Salem at 0920 PST and in Eugene at 1111 PST. Prefrontal precipitation at Santiam Pass started as rain about noon and turned to snow. Snowfall intensity diminished briefly around 0500 PST on the 20th at which time stars were clearly visible through a thin cloud deck. Wave formation

on the front contributed to continued heavy precipitation along with orographic and instability showers which diminished slowly as cold air advection commenced in the Northern portion of Oregon (U. S. W. B. Seattle FP 3). During the crystal sampling period, 38.1 inches of snow fell, averaging over one inch per hour and amounted to 3.84 inches water equivalent (U. S. W. B., Climatological Data for Oregon).

The recording barograph at Oregon State University recorded the lowest pressure at 1430 PST on the 19th. It is estimated from the preceding pressure data that the front crossed the Cascades around 1500 PST.

Prior to the sampling period, temperature at Santiam Pass reached 40° F and decreased from 34° F at 1300 PST on the 19th to 28° F at the end of the crystal sampling period on the 20th.

Cloud cover data from Salem, Eugene, and Redmond, Oregon, indicated that broken to overcast conditions prevailed through the crystal sampling period. Cloud cover for the valley stations consisted of stratocumulus with low ceilings to altocumulus with higher ceilings. With the exception of a break in the weather conditions the morning of the 20th, Santiam Pass was under the influence of a complete obscuration.

Crystal Analysis

The crystal-time-height cross section (Figure 8) reveals

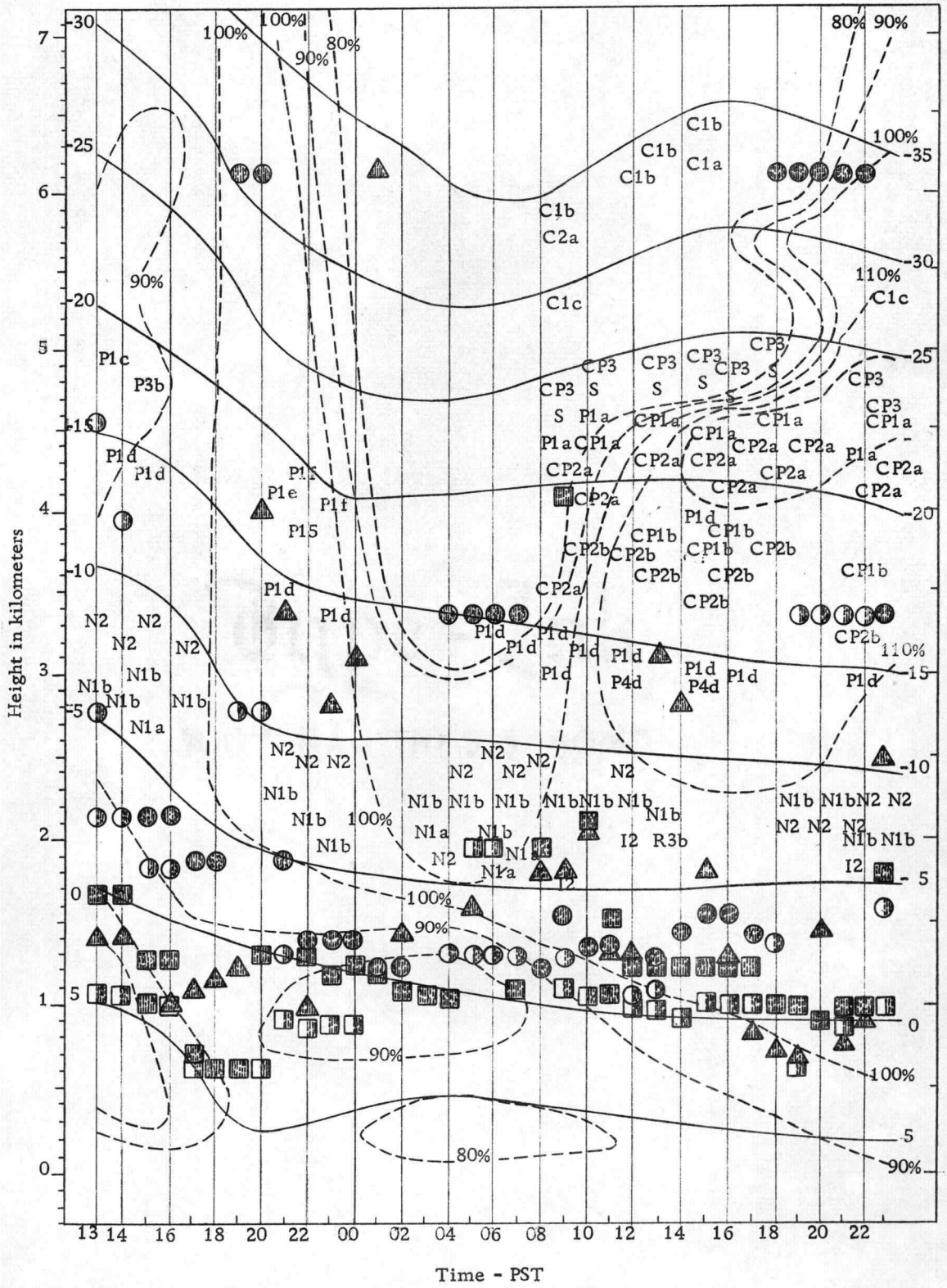

Figure 8. Crystal-time-height cross sectional analysis for 1300 PST, 19 January to 2400 PST 20 January, 1967. See Table 5 for explanation of geometric symbols and Figure 2 and Table 2 for crystal types.

inadequate relative humidity (90 to 100 percent) for the needle "N1b", "N2", and "N1a" (-4° to -8°C) and dendritic crystals "P1d", "P1e", and "P3d" (-14° to -20°C) observed between 1330 PST and 1630 PST on the 19th (Nakaya, 1954). Magono (1963) determined that dendritic growth could occur at relative humidities as low as 90 percent.

Overcast conditions west of the Cascades ranged from 1.7 km to 0.7 km making higher cloud observation impossible, although broken cloudiness at 4.5 km at 1300 PST to overcast at 2.2 km by 1600 PST was noted on the east side. The broken cloudiness, probably indicative of cloud heights west of the Cascades provided the necessary humidity conditions for dendritic crystal growth. Explanations justifying the disagreement between the crystals and time-height cross-section (Figure 8) are: (1) differing meteorological conditions aloft as a result of the distance separating Salem from Santiam Pass, (2) errors in interpolated values of temperature and relative humidity, either as the result of 12-hour intervals between radiosonde flights or of nonrepresentative data resulting from passage of the sounding balloon through a break in overcast conditions or through an isolated cloud, or (3) orographic lifting of the moist low-level airmass resulting in saturated conditions to heights greater than those on the time-height cross section (Figure 7). The orographic lifting undoubtedly caused supersaturation to heights great

enough to encompass the range of temperature necessary for needle growth. Bergeron (1965) indicates that lifting of an airmass can occur to heights 10 to 20 times that of the barrier over which the airmass crosses.

Dendrites "P1f", "P1d", and "P5b" (-10° to -20° C) and needles "N1b" and "N2" (-4° to -8°C) were observed from 2040 PST to 2240 PST and agreed with the humidity conditions present on the time-height cross-section (Figure 7). Irregular crystal forms, if present, were not tabulated.

Selected photographs of snow crystals sampled between 0350 PST and 2240 PST on the 20th appear in Appendix F (Figures 60-71). Needle crystals "N1b" and "N2" (-4° to -8°C) predominated from 0350 PST through 0800 PST, and for approximately 40 minutes around 0500 PST needles fell from a thin, broken cloud layer of fracto-stratus. During this period, partial clearing occurred west of the Cascades and precipitation for Santiam Pass was orographic. The needle crystals agreed reasonably well with the crystal-time-height cross-section (Figure 8) with respect to the saturated layer between 1.7 km and 1.4 km which encompassed the lower portion of the temperature range required for needle growth.

Bullets "C1b" and "C2" started by 0805 PST, and spatial plates "CP3" and columns with side planes "S" appeared at 0820 PST. Needles "N1b" and "N2" gradually disappeared and did not reappear

until 1205 PST. The spatial plates "CP3", columns with side planes "S" and bullets "C1b" and "C2a" did not agree with the time-height cross-section humidity analysis. At 0900 PST an overcast cloud cover existed at 4.1 km for Eugene indicating cloud bases at the lower edge of the crystal formation temperature in nonsaturated air. As early as 0100 PST and as late as 1800 PST, an overcast condition existed to cirrus levels (Figure 8). If it is assumed that clouds at 6 km existed after 0800 PST, but were obscured by lower overcast layers through the remainder of the sampling period, conditions for the crystals from cold regions (-20° to -35°C) would be met. The crystals observed indicate saturation conditions to higher levels than those noted on the cross-section. It is not certain whether bullets originated at high or low levels. If formed at high levels, they would have become capped columns, observed during this time, unless there was not sufficient moisture for plates and dendritic formation on all crystals; if the bullets were from low levels they would not have caps. The genesis of these crystals at low levels would more closely relate the cross section to the crystals observed. Needles "N1b" and "N2" and bullets capped with dendrites "CP2b", requiring low supersaturation values for formation were observed during the 1205 PST observation. Grunow and Huefner (1959) concluded that columns capped with dendrites formed as the result of low supersaturation values. Columns capped with dendrites "CP1b", columns capped with plates

"CP1a", spatial dendrites "P5b", and columns with side planes "S" predominated from 1315 PST to 1740 PST. By 1835 PST most of the crystals were rimed needles "N2" and "N1b" which fell until 2220 PST; at which time columns capped with dendrites "CP2a", spatial plates "CP3", and columns with side planes "S" commenced falling and continued to fall through the remainder of the crystal sampling period (2240 PST). Crystals observed after 1200 PST agreed quite well with the crystal-time-height cross section (Figure 8).

Snow crystal trends are illustrated graphically (Figure 9) by combining crystal types of the General Classification into the groups of the International Classification (Table 6).

Needles (↔) predominated from 0350 PST until shortly after 0700 PST at which time irregular forms (⋏) were observed in predominating quantities and by 0800 PST columns (▭) were noted. The inception of irregular forms probably reflects precipitation associated with cloudiness accompanying the wave formation on the surface front in southern Oregon (Appendix C, Figure 26). Two levels of crystal formation appear: (1) the lower level of needle crystals (↔), the result of orographic influence and (2) the crystals formed above -20°C (⋏). By 1000 PST columns capped by plates (⊨) were observed. Noon on the 20th revealed needles (↔) to be the dominant crystal type along with some dendritic types (✳), capped columns (⊨), irregular forms (⋏), and columns (▭).

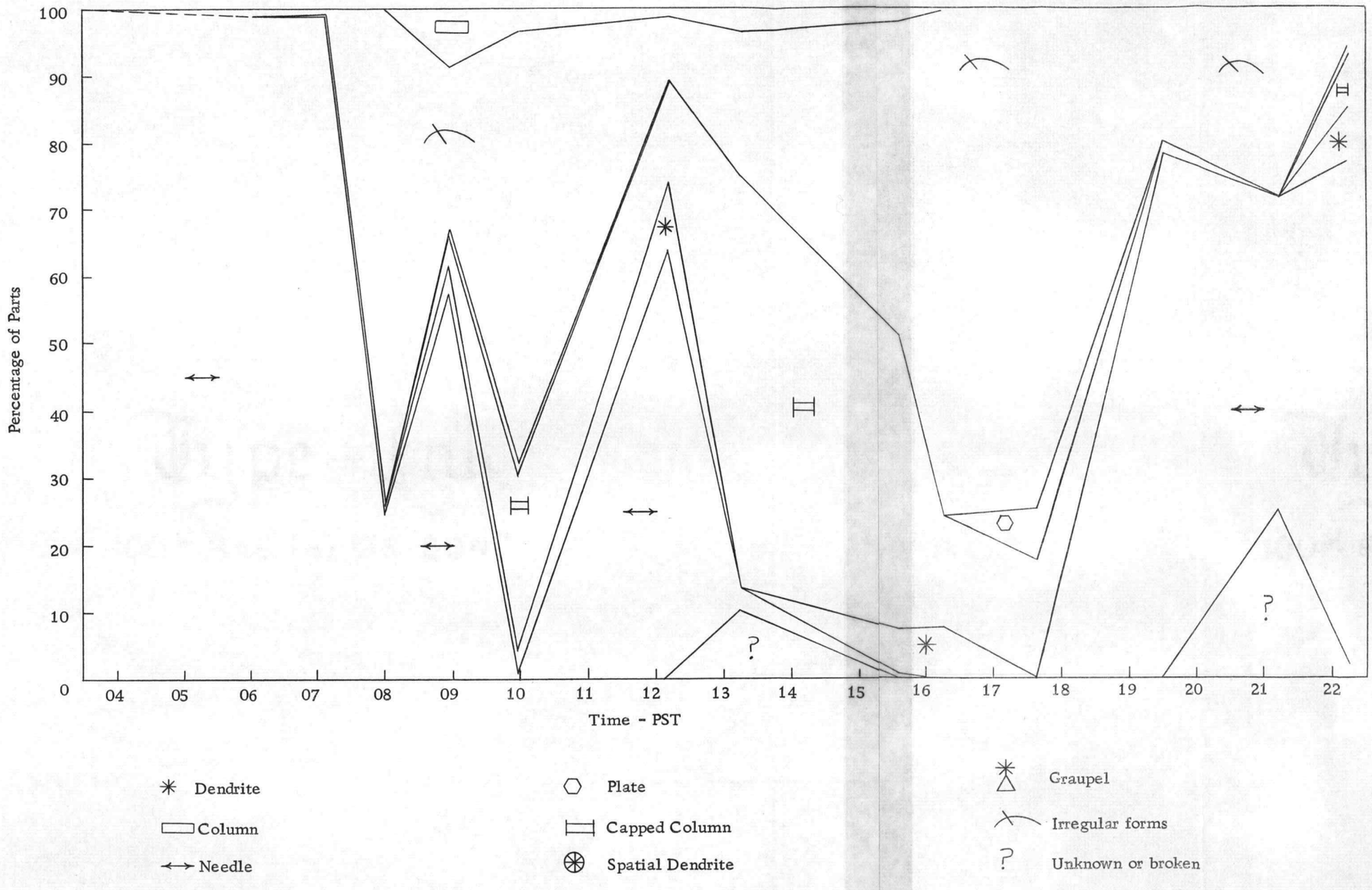

Figure 9. Crystal survey based on International Classification, 20 January 1967.

By 1300 PST, needles had diminished in number with capped columns (⊨⊨) and irregular forms (⋏⋎) dominating. Crystal types representative of -20°C and colder were observed at 1740 PST. From 1900 PST through the remainder of the sampling period, needles (↔) and irregular forms (⋏⋎) predominated. After 2100 PST, dendrites (✳) and capped columns (⊨⊨) were observed in small quantities.

Summary

Wave formation on the front complicated crystal trends. The sequence observed with the approaching front commenced with pre-frontal rain and turned to snow represented by needles and dendrites as the freezing level lowered. These crystal types were observed on both sides of the front. Post-frontal crystals changed to needles as the trailing edge of precipitation diminished and orographic factors prevailed. It is not surprising that crystals from colder temperature regions (less than -20°C) were not encountered because the height of the freezing level was high enough that crystals up to 16,000 feet were in the dendritic temperature range (-15° to -20°C). Humidity conditions above this height were marginal for crystal formation. Needle crystals were observed as a result of low-level orographic influences after post-frontal precipitation from higher levels terminated. Crystals from regions colder than -20°C (CP3 and S) were encountered as high cloudiness from the wave formation on the

front was encountered followed periodically by crystals from the entire temperature spectrum which indicated convective activity resulting from the instability associated with the cold moist airmass. Grunow's findings (1960) verify the preceding sequence.

Dendritic crystals observed required only slight ice supersaturation and formed as the result of strong updraft combined with numerous crystals. Riming present during periods when needles were observed and not present when needles were absent indicates that needles require high supersaturation conditions for their formation. Temperature, saturation, and crystals types for this storm show good agreement with Nakaya's Ta-s diagram (Figure 3).

Warm Front Occlusion

Synoptic Situation, 14-15 February 1967

The 1100 PST (ESSA IV) satellite photographs showed a vortex at 55° N. 142° W. on the 14th. Associated with an occluded front was a 200-mile-wide band of solid cloudiness extending north into British Columbia (U.S.W.B. Satellite Summary).

At 2000 PST on the 14th, the frontal trough was oriented southwestward through the northern Virgin Islands. The 0200 PST weather report on the 15th located the front in the coastal areas of Western Washington and forecast it to reach the Cascades by 0400 PST

(U. S. W. B. Seattle FP3). Minor cooling was experienced in the post-frontal air and drying was confined to high altitudes. On-shore winds contributed to instability showers and orographic cloudiness. Synoptic maps are included in Appendix C (Figures 35-39).

Upper Air Conditions

The time-height cross section (Figure 10) for 14 to 15 February and the Salem radiosonde soundings (Appendix D, Figures 54-56) show two saturated layers at midnight the 14th. The first was between 1. 1 km and 2. 9 km and the second from 3. 8 km to above 7 km. Winds at 1600 PST veered with height, from southwesterly directions near the surface to northwest at 7. 2 km. Wind velocities were 50 knots at higher altitudes and 30 knots near the surface. At 0400 PST on the 15th (Figure 10), two saturated layers remained, the upper between 3. 5 km to above 7. 2 km and the lower between 3. 2 km and 0. 8 km. Post-frontal temperatures at all heights increased with time, with heights above 3 km having the greatest increases. The wind direction remained the same as for 1600 PST on the 14th except that at 5. 6 km, direction was more west than northwest. Upper level wind velocities were greater than those 24 hours earlier. By 0700 PST, drying with time was underway above 3 km and below, the moist layer was decreasing in depth. The afternoon radiosonde flight (Figure 56) revealed continued drying down to 1. 8 km and a shallow saturated layer

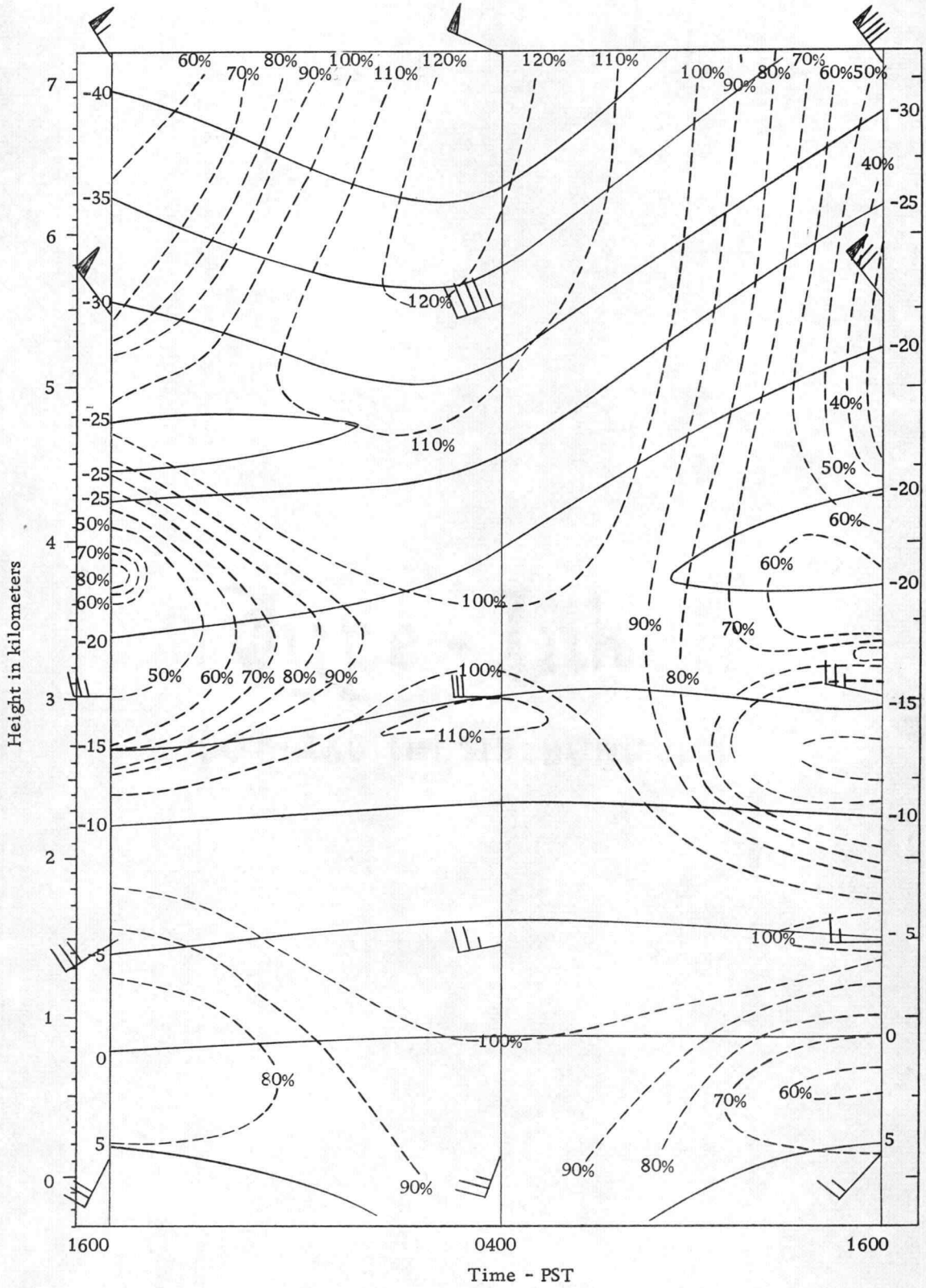

Figure 10. Time-height cross sectional analysis of temperature and relative humidity with respect to ice for 1600 PST 14 February to 1600 PST 15 February 1967.

between 1.8 km and 1.4 km. Warm air advection was evident above 3 km with temperature increases as great as 12°C; below 3 km temperatures remained relatively constant during the sampling period. At the end of the sampling period a temperature inversion between 4.4 km and 5.2 km existed and extended back to back to about 1000 PST on the 15th (Figure 10).

Weather

Light snow commenced around 1800 PST or 1900 PST on the 14th and continued through the night without cease. At midnight the temperature was 24.5°F; 23°F at 0200 PST the 15th and increased to 27°F at 1030 PST. Breaks in the surface obscuration were not noted during the night at Santiam Pass, but cloud cover was breaking up and clear sky was periodically visible through a thin layer of stratus by 0930 PST. Cloud cover over the valley stations consisted of stratus, nimbostratus and stratocumulus during the night and early morning hours (U.S.W.B. Surface Observations, Salem and Eugene). Near the end of the observation period, higher clouds were reported. Ceilings varied from 900 feet prior to and 4000 to 5000 feet after the frontal passage.

Marked precipitation consisted of light rain showers and rain which terminated at Eugene about 0600 PST and at Salem around 0900 PST. Total snowfall at Santiam Pass from 1700 PST on the 14th

to 1700 PST on the 15th totaled ten inches with eight inches falling between 0000 PST on the 14th and 1030 PST the 15th.

The barograph at Corvallis indicated that the front apparently crossed the Cascades by 0400 PST since its pressure reached a low at 0300 PST.

Crystal Analysis

Selected photographs of snow crystals sampled during the storm are in Appendix F (Figures 72-77). Crystal sampling commenced at 0010 PST on the 15th with crystal types observed represented by capped columns of plate and dendritic types "CP1a" and "CP2a" spatial plates "CP3", columns with side planes "S", and malformed "P4" crystals (-15° to -25°C). The snow crystal trend remained relatively unchanged through 0400 PST except that columns and bullets with dendritic caps "CP2a" and "CP2b" increased. Dendritic extensions on the columns and bullets appeared intermediate between dendrites and plates, thus forming broad-branched dendrites.

The crystal-time-height cross section (Figure 11) did not reveal crystals formed between 0° and -10°C (N1b, N2, and C1c), although a saturated layer with respect to ice over that temperature range was present. Rimed crystals were noted from 0100 PST to 0130 PST, at 0230 PST and from 0300 PST to 0345 PST. Cloud droplets causing the riming were probably provided by the lower saturated layer in

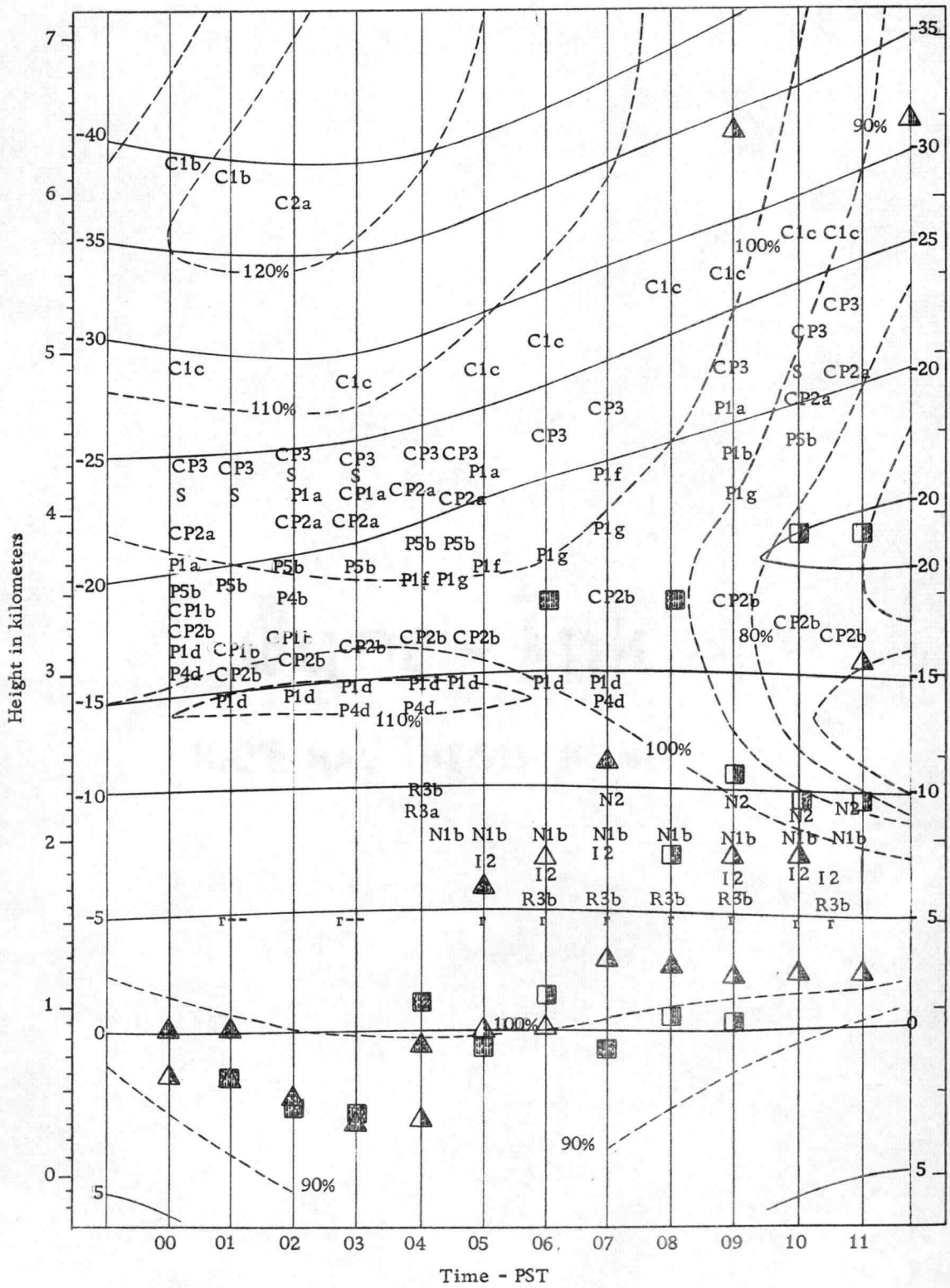

Figure 11. Crystal-time-height cross sectional analysis for 2300 PST, 14 February to 1100 PST, 15 February 1967. See Table 5 for explanation of geometric symbols and Figure 2 and Table 2 for crystal types.

which crystals were absent. Spatial dendrites "P5b" appeared, similar to types Magono (1962) observed to fall from inversion layers in the temperature range of -15° to -20°C. These conditions undoubtedly occurred with overrunning accompanying the warm front occlusion, although an inversion did not appear on the time-height-cross section (Figure 10). An inversion (-25° to -23°C) at 1600 PST was present (Figure 10). Spatial dendrites "P5b" are efficient in sweeping out cloud particles from lower levels (Weickmann, 1957).

Radar reports from the Oregon State University radar facility indicate that pre-frontal precipitation over the Cascades formed at about 5 km, which agreed with the crystal types observed with formation temperatures at the 5 km level.

The crystal trend changed markedly at 0420 PST as needle crystals "N1b" and "N2" fell in significant numbers in addition to the earlier rimed crystal types (Figure 11 and Table 13). Post-frontal crystals were rimed through the end of crystal sampling. After 0420 PST capped columns with plates "CP1a" disappeared until 0830 PST when notable numbers were encountered; after 0830 PST few appeared. Capped columns with dendrites "CP2a" disappeared until 0605 PST. Forms from higher altitudes (CP3 and S) were observed, however. Graupellike forms were noted in significant quantities following the disappearance of capped columns and spatial dendrites. Crystal types observed from 0420 PST to 0830 PST agree with the

crystal-time-height cross section (Figure 11) and Nakaya's Ta-s diagram (Figure 3). After 0830 PST, the contribution of cold crystal types (CP3 and C1c) decreased and the contribution of needles "N1b" and "N2" and rimed particles "I2" increased, which agreed with drying above 2.5 km.

Inspection of the graphical presentation (Figure 12) illustrates that primary crystal forms originated at an altitude higher than 2.7 km, representing precipitation from altocumulus and cirrus cloud decks (⅄, ⊨, ✳ and ⬡).

The post-frontal situation is obvious, as needles and graupel-like forms (✳△) dominated the remainder of the sampling period. Capped bullets (⊨), irregular crystals (⅄), and spatial dendrites (⊛) contributed minor amounts during the peak of the graupellike (✳△) formation. Missing crystal forms (CP2a and CP2b) appeared heavily rimed and were classed as graupellike snow. Graupel (✳△) was decreasing and needles (↔) increasing at the close of crystal sampling. Other crystal forms increased slightly. Toward the end of the observation period, needles were not rimed to the same degree as snow crystals from colder regions, indicating the presence of a saturated layer between the level of needle formation and that of the other crystals. Inspection of the crystal-time-height cross section (Figure 11) revealed cloudiness above the summit level of Santiam Pass (2.2 km) that was probably the source of the cloud droplets

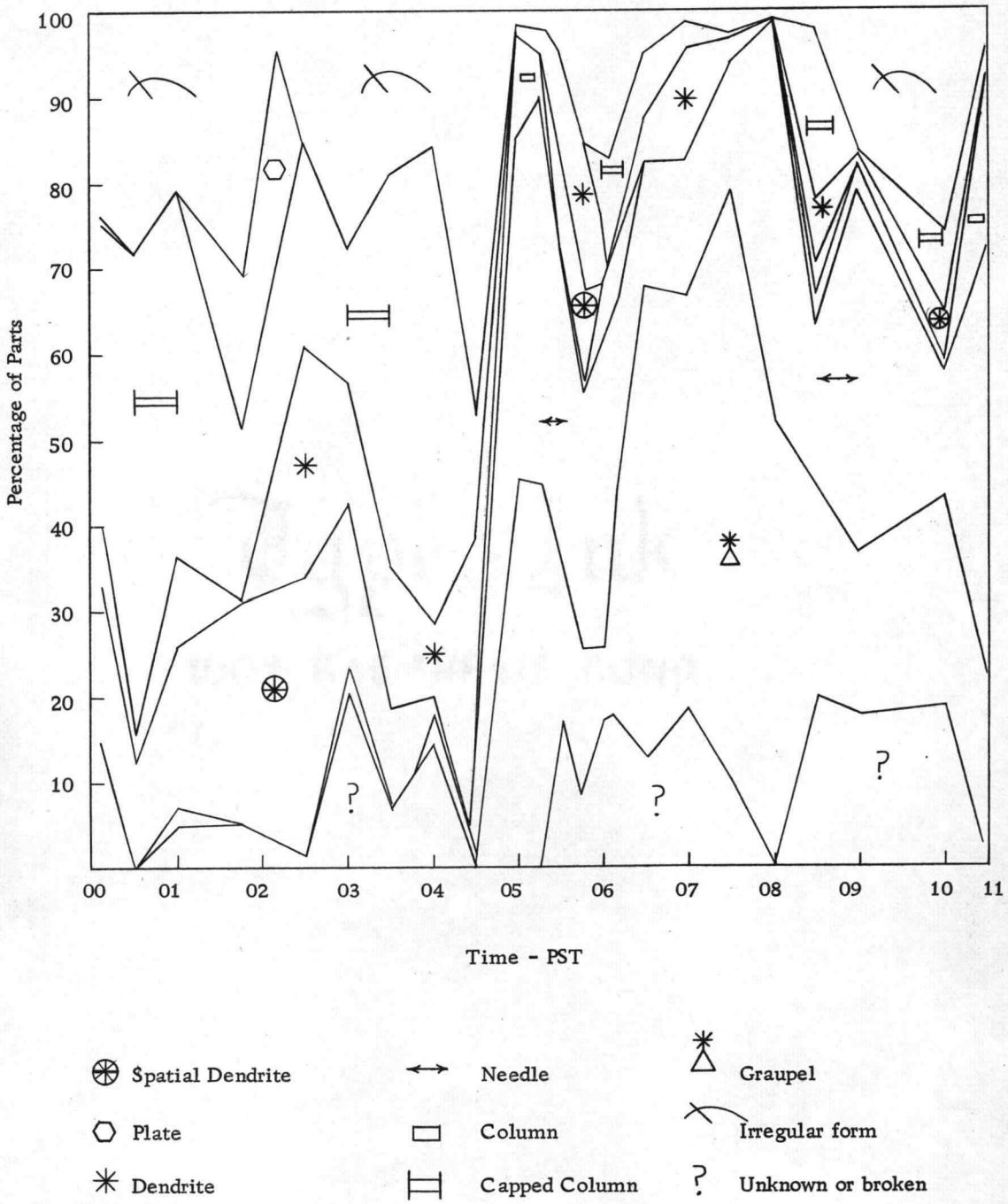

Figure 12. Crystal survey based on the International Classification, 15 February 1967.

noted on crystals formed above 2.2 km. As upper levels of the saturated region diminished in depth, graupellike forms lost their source of riming and reverted to original crystal types. Magono (1962) determined that graupel formation requires a fairly thick cloud consisting of many cloud droplets.

Summary

The trend of crystal forms associated with the warm front occlusion started with crystal forms colder than -15°C (spatial plates, columns with side planes, bullets, capped columns), and as the generating level of the snow descended from the higher levels to lower levels, crystalline forms such as needles and graupel appeared. After the frontal passage, many of the combination crystals (bullets capped with plates, and bullets capped with dendrites) did not appear in the General Crystal Survey (Table 13), although they appeared as graupellike snow (heavily rimed). Many may also have been classed as rimed particles. Good agreement between Nakaya's Ta-s diagram (Figure 3), and the crystal-time-height cross section (Figure 11) is noted for this storm.

The absence of needle crystals prior to the frontal passage is understandable even though saturation existed since the relative humidity was probably less than 105 percent.

The drying above 2.2 km after 0900 PST was quite evident in

that the irregular crystals "S" and "CP3" and combination crystals such as "CP2a" and "CP2b" (bullets capped by plates and bullets capped by dendrites), had very small caps indicating scanty moisture conditions below the -20°C isotherm as compared to similar pre-frontal crystals.

Cold Cyclone

Synoptic Situation, 9-10 March 1967

The 1100 PST (ESSA IV) satellite photographs on the 9th revealed mostly cloudy skies 100 miles off-shore and over Western Oregon, with thin or scattered cloudiness along the east slopes of Washington and Northern Oregon (U. S. W. B. Satellite Summary). An upper trough offshore was centered at 136° W. with an open vortex near 52° N. 135°W. By 1600 PST on the 9th of March, the 500 millibar cold low (Figure 40) had moved south-southeast off the coast with a corresponding movement of its associated surface low. The 0400 PST maps of the 10th had continued the southwestward drift of the 500 millibar low (Figure 43). An Arctic front appeared near the Washington-Canadian border.

Satellite photographs of 1030 PST on the 10th revealed dense cloud cover over most of Eastern Oregon, Northwestern California, and Southwestern Oregon, terminating just off the coast. A vortex

was centered at 47° N. 128° W., northwest of the upper level low. Cloud coverage over Northwestern Oregon appeared convective (U. S. W. B. Satellite Summary). Cold unstable air and associated convective activity continued to influence the weather over Oregon (U. S. W. B., Seattle FP).

Synoptic maps for the period are in Appendix C (Figures 40-47).

Upper Air Conditions

The time-height cross section (Figure 13) revealed a saturated layer between 0. 4 km and 1. 6 km and from 4. 7 km to 5. 5 km at 2300 PST on the 9th. All levels had temperature decreases with the greatest decreases above 2 km. A temperature inversion just colder than -20° C was located between 4. 3 km and 4. 9 km. Winds were southwest to west-southwest at all levels with velocities approaching 100 knots at 7. 2 km.

By 0400 PST on the 10th, two saturated layers appeared on the time-height cross sectional analysis (Figure 13). The upper layer extended from 4. 6 km to 5. 8 km, and above that layer the airmass dried rapidly with height and time. A second saturated layer extended from 2 km to 0. 5 km. Above 4 km, temperature continued to decrease and below 4 km, slight warming occurred. Winds remained unchanged from those of the previous day.

The saturated layer extending between 0. 5 km and 2 km

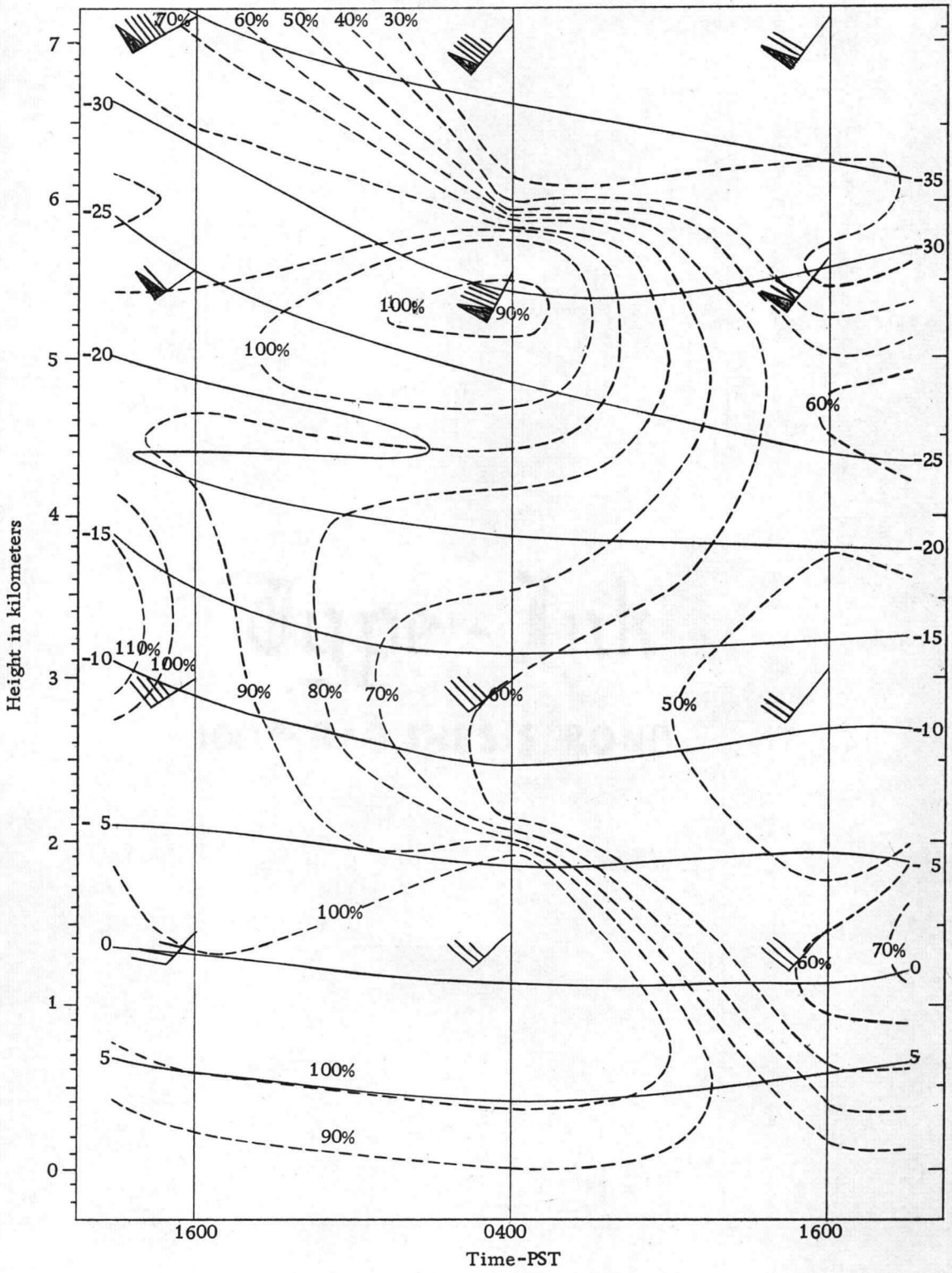

Figure 13. Time-height cross sectional analysis of temperature and relative humidity with respect to ice for 1600 PST 9 March to 1600 PST 10 March 1967.

(Figure 13) experienced drying on its following edge and by 1600 PST on the 10th, the saturated layer had disappeared (Appendix D, Figure 59). The upper saturated layer exhibited drying by 0700 PST. The entire atmospheric column was drying with time by 1600 PST. Winds remained southwest to west-southwest at all levels. Velocities diminished by 35 knots at higher levels, with lesser changes observed at intermediate levels and no change at 1.5 km.

Weather

Snowfall started the afternoon of the 9th and continued through the afternoon of the 10th. Snowfall for Santiam Pass from 1700 PST on the 9th to 1330 PST on the 10th totaled 17 inches with five inches of the total falling before 2330 PST on the 9th. Precipitation for valley stations was showery throughout the day. Rain showers continued at Eugene until 0800 PST on the 10th, and at Salem until about 0500 PST (U. S. W. B., Surface observations, Salem and Eugene).

Temperature on arrival at Santiam Pass was 26° F; increased slightly before falling to 22° F at 0700 PST; to 25° F by noon and to 24° F at 1330 PST.

Multi-layered cloudiness reported by Salem and Eugene (U. S. W. B. Surface observations) consisted of stratocumulus, altocumulus, altostratus and cirrus clouds. Ceilings of 1400 feet over the period prevailed and overcasts occurred generally in the altostratus or

altocumulus cloud layers. After 1000 PST the sun periodically broke through a thin layer of clouds, and snowfall changed to flurries.

Wind conditions at Santiam Pass remained calm through the night.

Crystal Analysis

The majority of the crystals sampled consisted of bullets with plates "CP2a", broad-branched dendrites "P1d", malformed dendrites "P4d", spatial plates "CP3", columns with side planes "S", and ice particles "I1" which occurred until 0800 PST. Riming appeared on all crystals from 0100 PST to 0315 PST. The dendritic forms disappeared after riming ceased and an increase occurred in capped columns with plates "CP1a" and bullets with plates "CP1b". Capped columns "CP2a" and bullets "CP2b" with broad-branched dendrites also appeared.

By 0815 PST, crystals formed primarily at temperatures below -20° C, indicated by spatial plates "CP3", columns with side planes "S", plates "P1a", capped columns with plates "CP1a", capped bullets with plates "CP2b", and bullets "C1b" and "C2a" continued through the end of the sampling period with crystal forms changing almost entirely to spatial plates "CP3" and columns with side planes "S". Spatial dendrites "P5b", indicators of an inversion corresponding to the temperature range in which the overrunning occurred,

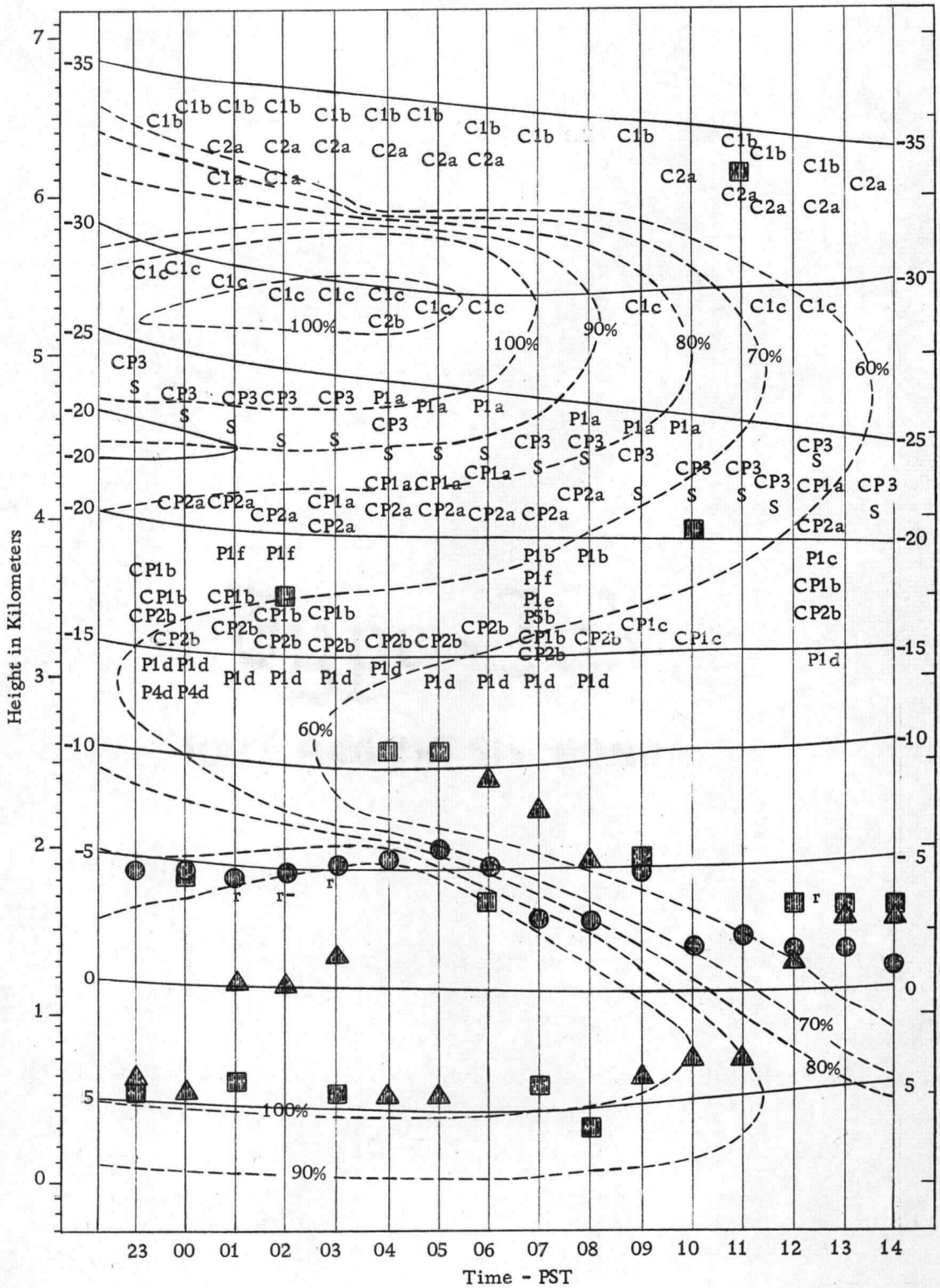

Figure 14. Crystal-time-height cross sectional analysis for 2300 PST 9 March to 1400 PST 10 March 1967. See Table 5 for explanation of geometric symbols and Figure 2 and Table 2 for crystal types.

verified findings (Magono, et al., 1962). The period in which riming and dendrites (-15° to -20°C) occurred corresponded to the saturated layer observed between 0.1 km and 2 km. Between 0010 PST and 0315 PST, the preceding layer reached altitudes higher than Santiam Pass (4800 feet). Only when this occurred was riming possible. After 0400 PST the lower saturated layer dried and the upper saturated layer was limited to a temperature range of -25° to -30°C, corresponding to the range necessary for columns with side planes "S". Magono, et al. (1960) indicated that spatial plates "CP3" can form at temperatures as cold as -29° to -38°C, which agrees better with the crystal-time-height cross section (Figure 14). With respect to higher humidity conditions, the temperature range with which the preceding crystals were associated on the crystal-time height cross section (Figure 14) represents the lower limit of crystal growth.

It is notable that dendrites occurred in the presence of apparently inadequate moisture supplies. The temperature range of dendrites (-15° to -20°C) fell between humidity ranges of 65 to 75 percent. By modifying the time-height cross section (Figure 13), a humidity high of 95 percent could be realized if overrunning conditions were extended. In the inversion layer (0.5 km in extent), dendritic forms apparently originated, although the humidity appeared below saturation. Magono, et al. (1960) concluded that snow crystals can grow at humidities as low as 85 percent with respect to ice. At

humidities this low, he determined that clouds could exist. In this way the discrepancy between humidity and temperature could be reconciled. However, the appearance of the dendritic forms requiring low supersaturation values may reflect saturation conditions not realized on the time-height cross section (Figure 13) as the result of the time span between radiosonde flights.

The crystal trend for the storm as indicated by inspection of the graphical survey on the basis of the International Classification (Figure 15) represents all crystal forms except needles and graupel. From 0000 PST on the 10th, capped columns (⊨⊣) increased markedly and predominated until 0700 PST, corresponding to the time that humidity for dendrites (✳) and plates (⬡) decreased below growth levels, which contributed to a decrease in capped columns (⊨⊣). After 0700 PST, irregular forms (⋏) predominated until the termination of crystal sampling (1330 PST).

Summary

Crystals which appeared at the beginning of the sampling period were forms requiring relative humidities of less than 105 percent. The combination crystal forms such as capped bullets "CP2a" and broad-branched dendrites "P1d" were crystal forms requiring low supersaturation values. Toward the end of the crystal sampling period as middle layers dried, the capped effect on bullets and

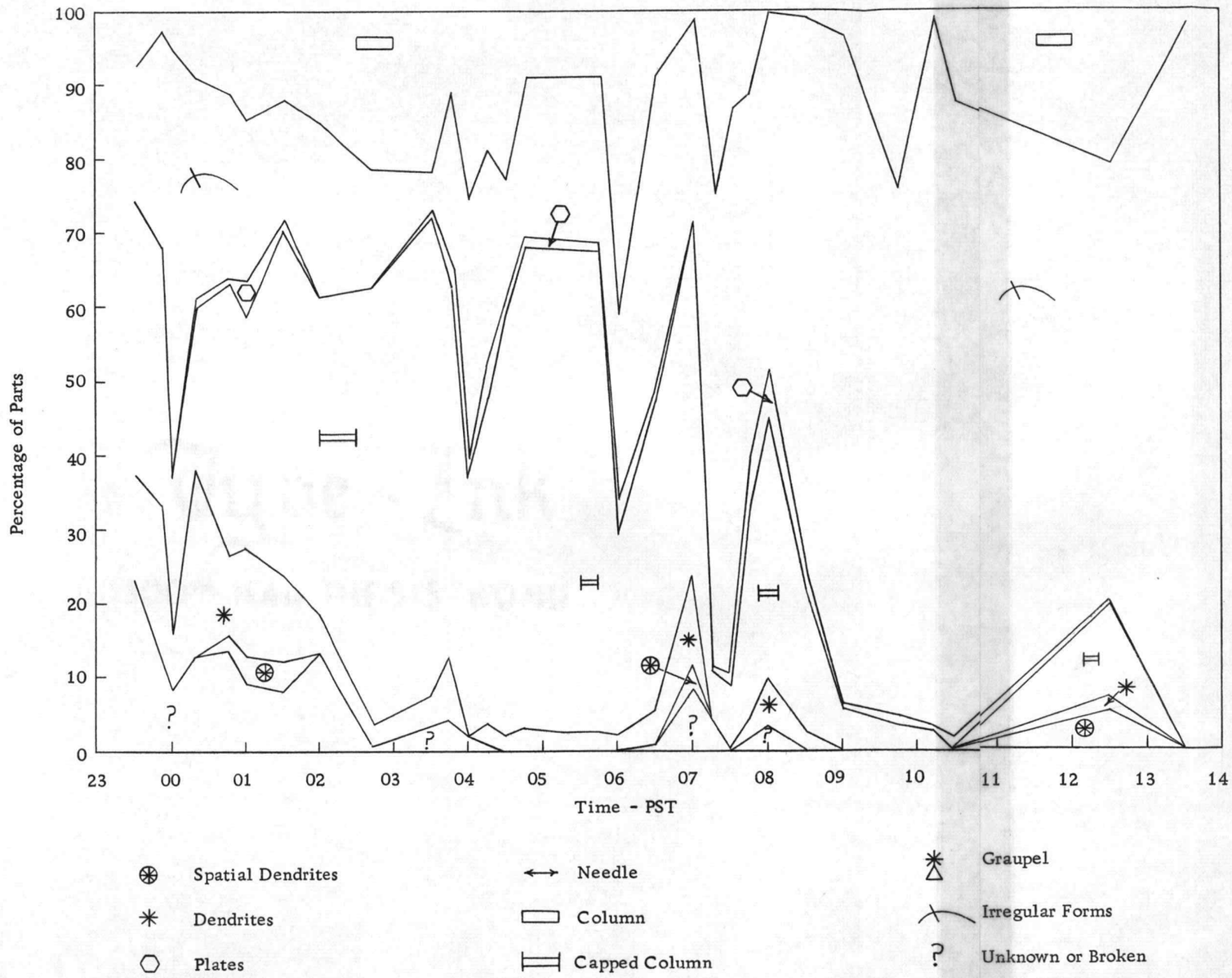

Figure 15. Crystal survey based on the International Classification, 9 and 10 March 1967.

columns was minimal. The presence of crystal forms from non-saturated regions is attributable to the fact that crystals actually grow at relative humidities less than 100 percent or that the growth of crystals reflected conditions not shown by radiosonde cross sections. Occasional high overcast conditions were noted during times and at levels that appeared deficient in moisture on the time-height cross section.

Crystal Types and Precipitation Intensity

Goldman (1951) determined that as the precipitation rate intensified, cloud bases descended. The rate of precipitation intensification is related to the lowering of the generating level of snow as the convergence mechanism spreads to lower levels (Weickmann, 1957). Considering the preceding, and with information on cloud cover data for Salem, Eugene, and Redmond, Oregon, an attempt was made to relate crystal types to the mean cloud base of overcast conditions.

For January, mean heights (average of overcast height for Salem, Eugene, and Redmond) of overcast layers were plotted against time (Figure 16). Predominant crystal types were entered in their corresponding location on the cloud-height presentation (Figure 16) from the International Survey of crystal forms (Figure 9). During periods of high overcast conditions, several crystal groups were noted.

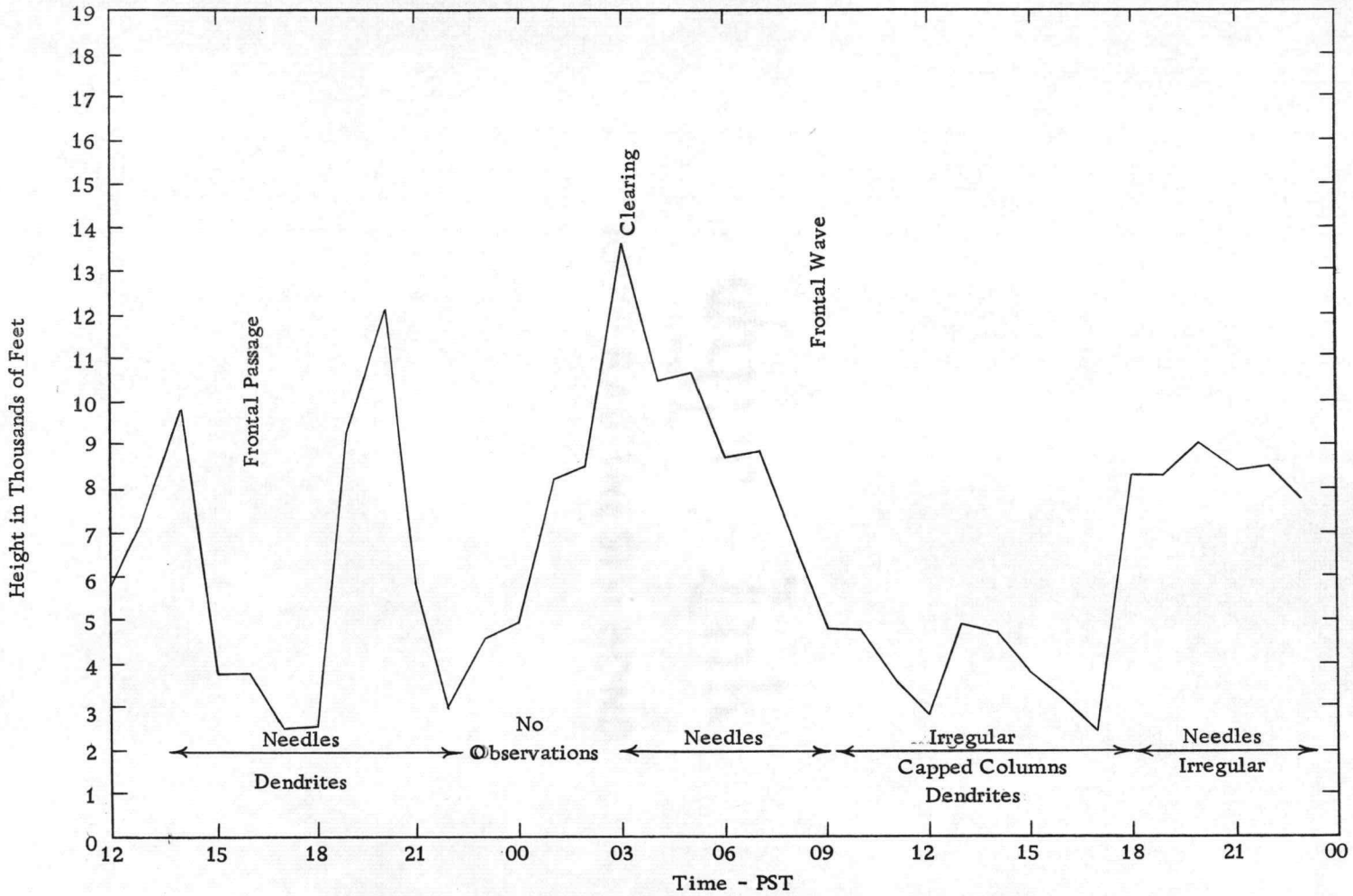

Figure 16. Mean height of overcast for Eugene, Salem, and Redmond, and predominant crystal types associated with various overcast heights, 1330 PST 19 January to 2240 PST 20 January 1967.

The crystals appearing during low overcast conditions were not as heavily rimed as the crystals appearing during high overcast conditions.

The preceding operation was carried out for the February storm (Figure 17), except that cloud data from Redmond were not considered. On the basis of the reports from Salem and Eugene (U. S. W. B., Surface Observations), the low overcast conditions were associated with crystals covering the greater part of the crystal spectrum. The lowest overcast accompanying the frontal passage over the valley stations occurred between 0200 PST and 0500 PST on the 15th. The front did not reach the Cascades until 0400 PST. Commencing with 0500 PST and the higher overcasts, needles and graupel predominated.

In comparing Figures 16 and 17, it appears that 5000 feet ceilings mark the change from supersaturation crystal types such as needles and graupel to crystal types from higher altitudes. In other words, with ceilings above 5000 feet, needles and graupellike forms predominate, and with ceilings less than 5000 feet, all crystal types are encountered. The lowest ceilings are associated with the greatest range in crystal groups.

With high ceilings, the rimed needles and graupellike forms are a product of orographic lifting, and the overcast conditions above the crest of the Cascades are not influenced markedly by orographic factors to the same extent as the airmass below the crestline.

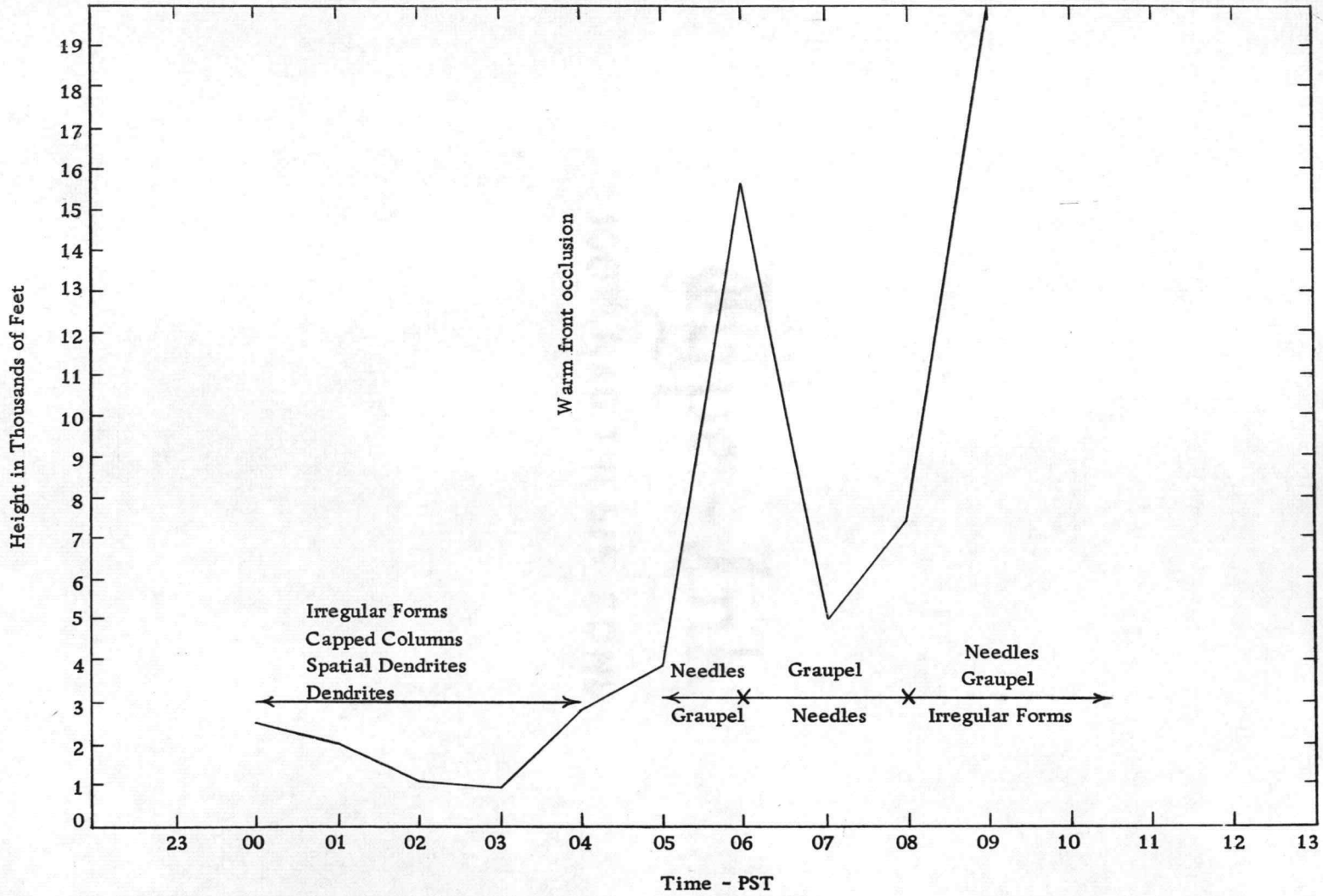

Figure 17. Mean height of overcast for Salem and Eugene, and predominant crystal types associated with various overcast heights for Santiam Pass, 0000 PST to 1030 PST, 15 February, 1967.

CONCLUSIONS

The three atmospheric disturbances examined in this study prevent drawing definite conclusions based solely on data acquired, as more cases are needed to draw definite conclusions on crystal trends. Conclusions can be drawn, however, when results from this study are related to empirical work and to studies carried out in other geographic areas. The following conclusions are made:

1. Crystal trends can definitely be related to synoptic developments and give insight on storm development and precipitation cloudiness that is not available from twice daily radiosonde flights, as a crystal analysis reveals not only general trends in synoptic development, but also small scale phenomena. The January storm had needle crystals fall during the period of time when orographic factors prevailed as drying aloft had caused a discontinuance of upper level crystal types. With the onset of convective activity, crystal types from all levels were observed periodically indicating deep multilayered cloudiness or cellular cloudiness that was not apparent on the radiosonde reports or on the time-height cross sectional analyses. Wave formation was noted as high level crystal types appeared prior to the Salem radiosonde sounding which indicated that layers of relative humidity greater than 100 percent were encountered at high altitudes. Riming of the crystals indicated the presence of supercooled

layers of cloud droplets and the riming of one crystal type and the lack of riming on another facilitated the location of supercooled layers of cloud droplets in the atmosphere. Graupellike forms noted in February indicated the presence of a deep layer of supercooled cloud droplets. The March crystal trend revealed drying at middle levels (lack of caps on cold crystal types) long before the Salem radiosonde flight revealed drying at intermediate levels.

2. For general surveys, it appears that crystal sampling is unnecessary at intervals closer than 15 minutes and hourly sampling provides satisfactory results as crystal fluctuations do not occur rapidly except in the case of frontal passages. The January storm did not exhibit notable fluctuations in crystal types until post-frontal convective activity was encountered. In February, crystal trends were uniform or gradually changed with the exception of the frontal passage for which the crystal sequence changed markedly in a span of a few minutes. For March, crystal trend changes were gradual and could have been detected with hourly crystal samples.

3. The crystal trend noted with the warm front occlusion commenced with higher crystal types (capped bullets and capped columns), crystal types associated with overrunning (spatial dendrites), and dendrites. With the frontal passage, warmer crystal forms were encountered such as graupel and needles. After the frontal passage, toward the end of the storm, a decrease of higher crystal types was

noted prior to the disappearance of lower types. The lower types were felt to be types associated with orographic lifting.

Precipitation from the cold front occlusion exhibited a trend from warmer crystal types (dendrites and needles) to those of high levels (capped columns and irregular forms) after frontal passage. Post-frontal orographic and convective activity complicated the crystal trend. Occasionally crystals from all levels were observed simultaneously, indicating deep or multilayered effects.

4. There appeared to be a relationship between cloud ceilings and crystal types for the cases involving frontal situations. Low ceilings over the valley stations were associated with crystal forms from higher altitudes and higher ceilings were associated with conditions during which riming and needles predominated. Orographic influences probably caused the precipitation over the mountains during periods of high cloudiness when lifting was confined to or affected the lower levels only.

5. Direct photography utilizing transmitted light and camera attachments facilitating macrophotography provided an adequate method of recording representative records of crystal samples for analyses. Colored slides of snow crystal samples allowed low power microscopic analysis which appeared to be superior to analyses based on interpretation from photographic prints. Photographic interpretation from prints would be enhanced if suitable enlargements were

made, but the expense would be prohibitive.

For analyses of slides by microscope, slide records of X 0.68 to X 1 appeared to be most satisfactory and for analyses from prints, macrophotography with crystal magnifications of X 4 to X 12 yielded best results.

RECOMMENDATIONS FOR FUTHER RESEARCH

Several results have emerged through this study: (1) Adaptation of principals used in micro-photography and shadow photography to a mass crystal sampling method utilizing a camera, closeup attachments and transmitted light, (2) the verification of studies in differing geographic areas, and (3) the introduction of a possible relationship between cloud ceilings and crystal types. Further crystal studies in the Northwest should include:

1. The determination of crystal generation levels and locations using radar techniques to better determine saturation levels and the relationship of various crystal groups to echo intensity.

2. Information to better determine precipitation structure associated with cellular clouds compared to deep multilayered clouds as determined by radar observation and related to crystal sequence.

3. Study in an area that is proximate to, and down wind from a radiosonde sounding station and an accompanied increase in the number of soundings during sampling periods.

4. Study the effects of the Cascades on orographic precipitation with respect to the heights that cloud layers are affected in crossing the mountains and crystal forms to be expected as the result of orographic influence.

5. Improvement of sampling technique by utilizing stereophotography in order to utilize stereoanalysis of spatial crystal forms.

BIBLIOGRAPHY

American Meteorological Society. 1957. Meteorological research reviews, summaries of progress from 1951-1955. Boston. 283 p. (Meteorological Monographs. Vol. 3, no. 19)

aufm Kampe, H. J., H. K. Weickmann and J. J. Kelly. 1951. The influence of temperature on the shape of ice crystals growing at water saturation. Journal of Meteorology 8:168-174.

Battan, L. J. 1962. Cloud physics and cloud seeding. Garden City, New York, Doubleday. 144 p.

Bentley, W. A. and W. J. Humphreys. 1931. Snow crystals. New York, McGraw-Hill. 227 p.

Bergeron, Tor. n. d. On the low-level redistribution of atmospheric water caused by orography. In: Proceedings of the International Conference on Cloud Physics, Tokyo and Sapporo, 1965. Sup. p. 96-100. (Unpublished)

Braham, Roscoe R., Jr. n. d. The aerial observation of snow and rain-clouds. In: Proceedings of the International Conference on Cloud Physics. Tokyo and Sapporo. 1965. p. 492-501. (unpublished)

Braham, Roscoe R., Jr. and Paul Spyers-Duran. 1966. Cirrus crystals in clear air. April 1965-April 1966. 77 numb. leaves. (University of Chicago, Department of the Geophysical Sciences, Cloud Physics Laboratory. Report to The National Science Foundation on work performed under Grant NSF-GP 3779)

Byers, Horace Robert. 1965. Elements of cloud physics. Chicago, University of Chicago. 191 p.

Gold, L. W. and B. A. Power. 1954. Dependence of the forms of natural snow crystals on meteorological conditions. Journal of Meteorology 11:35-42.

Grunow, Johannes and Dieter Huefner. 1959. Observations and analysis of snow crystals for proving the suitability as aerological sonde. 77 numb. leaves. (Deutsher Wetterdienst Meteorological observatory, Hohenpeissenberg, Oberbayern. Final report to U. S. Dept. of Army, Chief of Research and Development, European Office, on Contract no. DA-91-508-EUC-286, Jan. 15, 1958-Jan. 15, 1959. ASTIA Document no. 217431)

Grunow, Johannes. 1960. Observations and analysis of snow crystals for proving suitability as aerological sonde. II. Special studies on the sequence of snow crystal types, on hoar frost crystals. 80 numb. leaves. (Deutscher Wetterdienst Meteorological Observatory, Hohenpeissenberg, Oberbayern. Final report to U. S. Dept. of Army, European Research Office, on Contract no. DA-91-591-EUC-1030, Jan. 16, 1959-Jan. 15, 1960)

Hallett, J. 1956. Replica technique for the study of snow crystals. Weather 11:40-41.

Hallett, J. 1965. Field and laboratory observations of ice crystal growth from the vapor. Journal of the Atmospheric Sciences 22:64-69.

Hallett, J. and B. J. Mason. 1958. The influence of temperature and supersaturation on the habit of ice crystals grown from the vapour. Proceedings of the Royal Society, ser. A, 247:440-453.

Haltiner, George J. and Frank L. Martin. 1957. Dynamical and physical meteorology. New York, McGraw-Hill. 470 p.

Higuchi, Keiji. 1956. A new method for the simultaneous observation of shape and size of a large number of falling snow particles. Journal of Meteorology 13:274-278.

Houghton, H. G. 1950. A preliminary quantitative estimate of precipitation mechanisms. Journal of Meteology 7:363-367.

Kobayashi, T. 1961. The growth of snow crystals at low supersaturations. Philosophical Magazine, ser. 8, 6:1363-1370.

Koenig, L. Randall. n. d. Ice-forming processes in relatively warm clouds. In: Proceedings of the International Conference on Cloud Physics, Tokyo and Sapporo, 1965. p. 242-246. (Unpublished)

Kuettner, J. P., R. Honkala and R. J. Boucher. 1956. Results of ice crystal observations during the passage of cyclones. 25 numb. leaves. (Milton, Massachusetts. Final report to U. S. Army, Signal Corps Engineering Laboratories on Contract no. DA-36-039 SC-64671, May 15, 1955-May 14, 1956)

Kuettner, J. P., L. Aldaz and R. J. Boucher. 1958. A study of precipitation systems by means of snow crystals, synoptic and radar analyses. 53 numb. leaves. (Gorham, New Hampshire. Final report to U. S. Army, Signal Corps Engineering Laboratories, on Contract no. DA-36-039 SC-73153, Nov. 15, 1956-June 30, 1958)

Langmuir, I. 1948. The production of rain by a chain reaction in cumulus clouds at temperatures above freezing. Journal of Meteorology 5:175-192.

Magono, Choji. N. D. The snowfall in the winter monsoon season of Japan. In: Proceedings of the International Conference on Cloud Physics, Tokyo and Sapporo, 1965. p. 502-511.

Magono, Choji and Tasawa Seiichi. n. d. Observations of snow clouds by means of "snow crystal sondes." In: Proceedings of the International Conference on Cloud Physics, Tokyo and Sapporo, 1965. p. 231-235. (Unpublished)

Magono, Choji, et al. 1959. Preliminary investigation on the growth of natural snow crystals by the use of observation points distributed vertically. Journal of the Faculty of Science, Hokkaido University, ser. 7, 1:195-211.

_____ 1960. Investigation on the growth of natural snow crystals by the use of observation points distributed vertically. Journal of the Faculty of Science, Hokkaido University, ser. 7, 1:195-211.

_____ 1962. Investigation on the growth of natural snow crystals by the use of observation points distributed vertically. III. Journal of the Faculty of Science, Hokkaido University, ser. 7, 1:373-391.

_____ 1963. Investigation on the growth and distribution of natural snow crystals. IV. Journal of the Faculty of Science, Hokkaido University, ser. 7, 2:49-78.

_____ 1964. An observation of snow crystals and their mother cloud. V. Journal of the Faculty of Science, Hokkaido University, ser. 7, 7:123-148.

Marshall, J. S. and K. L. S. Gunn. 1957. A first experiment on snow crystal growth. In: Artificial stimulation of rain: Proceedings of the First Conference on the Physics of Cloud and Precipitation Particles, ed. by Helmut Weickmann. Woods Hole, Mass., 1955. New York, Pergamon. p. 340-347.

Mason, B. J. 1950. The formation of ice crystals and snowflakes. In: Centenary proceedings. London, Royal Meteorological Society. p. 51-58.

_____ 1951. Snow crystals, natural and artificial. Endeavor 10:205-212.

_____ 1957. The physics of clouds. Oxford, Oxford University. 481 p.

_____ 1958. The growth of ice crystals from the vapour and the melt. Advances in Physics 7:235-253.

_____ 1962. Clouds, rain and rainmaking. Cambridge, Cambridge University. 145 p.

_____ n. d. The nucleation and growth of ice crystals. In: Proceedings of the International Conference on Cloud Physics, Tokyo and Sapporo, 1965. p. 467-480. (Unpublished)

Nakaya, Ukichiro. 1951. The formation of ice crystals. In: Compendium of meteorology, ed. by Thomas F. Malone. Boston, American Meteorological Society. p. 207-220.

_____ 1954. Snow crystals: natural and artificial. Cambridge, Harvard University. 510 p.

_____ 1957. Physical investigations of snowflakes. In: Artificial stimulation of rain: Proceedings of the First Conference on the Physics of Cloud and Precipitation Particles, Woods Hole, Mass., 1955. New York, Pergamon. p. 327-331.

Nakaya, Ukichiro and Keiji Higuchi. 1960. Horizontal distribution of snow crystals during the snowfall. In: Physics of precipitation ed. by Helmut Weickmann. p. 118-129. (American Geophysical Union. Geophysical Monograph no. 5)

Petterssen, Sverre. 1956. Weather analysis and forecasting. Vol. 2. 2d ed. New York, McGraw-Hill. 266 p.

Power, Bernard A. 1962. Relationship between density of newly fallen snow and form of snow crystals. Nature 193:1171.

Power, Bernard A., P. W. Summers and J. d'Avignon. 1964. Snow crystal forms and riming effects as related to snowfall density and general storm conditions. Journal of the Atmospheric Sciences 21:300-305.

Schaefer, Vincent J. 1956. The preparation of snow crystal replicas. Weatherwise 9:132-135.

_____ 1962. The vapor method for making replicas of liquid and solid aerosols. Journal of Applied Meteorology 1:413-418.

_____ n. d. Studies of cirrus type clouds at ground level. In: Proceedings of the International Conference on Cloud Physics, Tokyo and Sapporo, 1965. p. 414-418. (Unpublished)

Shaw, D. and B. J. Mason. 1955. The growth of ice crystals from the vapour. Philosophical Magazine, ser. 7, 46:249-262.

Smith, R. I. and Johannsen. 1965. Resin vapour replication technique for snow crystals and biological specimens. Nature 205:1204-1205.

Strong, C. L. 1966. On preserving the shapes of snow crystals by catching snowflakes in dissolved plastic. Scientific American 214(3):120-126.

U. S. Federal Aviation Administration. 1967. Surface weather observations, Redmond, Oregon, Jan.-Mar.

U. S. Weather Bureau. 1947-1967. Climatological data. Oregon. Vols. 53-73.

_____. 1967. Adiabatic chart. Salem, Oregon. Jan.-Mar. (WBAN 31A)

_____ 1967. Facsimile charts. Washington, D. C., National Meteorological Center. Jan.-Mar.

_____ 1967. Pacific Northwest weather satellite summary. Seattle, Washington. Jan.-Mar. (Teletype circuit)

_____ 1967. Surface weather observations. Eugene, Oregon. Jan.-Mar. (WBAN 10)

_____ 1967. Surface weather observations. Salem, Oregon. Jan.-Mar. (WBAN 10)

_____ 1967. Weather Bureau Forecast Center (FP3). Seattle, Washington. Jan.-Mar. (Teletype circuit)

Weickmann, Helmut. 1957. The snow crystal as aerological sonde. In: Artificial stimulation of rain: Proceedings of the First Conference on the Physics of Cloud and Precipitation Particles, Woods Hole, Mass., 1955. New York, Pergamon. p. 315-326.

APPENDICES

APPENDIX A

CLIMATIC DATA FOR SANTIAM PASS

Table 8. Climatological data for Santiam Pass for years in which records were kept. (U.S.W.B., Climatological Data, Oregon, 1947-1966)

Date		Temperature Data (°F)			Precipitation Data (in inches)	
		Mean	Ave. Max.	Ave. Min.	Total PPN	Total Snow Fall
Dec.	1947	29.6				41.5
	1948	20.5				
	1949	22.7				29.0
	1950	35.0				
	1951	26.4m				
	1952					
	1953					
	1954	28.9m				
	1955					
	1963	33.4	41.1	25.6	6.70	32.3
	1964	25.8	30.9	20.6	34.72	177.8
	1965	27.8m	34.8m	20.7	12.77	116.9
	1966	30.8	35.7	25.8	13.30	59.0
Jan.	1947					
	1948	27.2				69.0
	1949	17.6				33.5
	1950	14.4				128.5
	1951	24.0				107.0
	1952	25.4				53.0
	1953	34.3m				
	1954	26.0	40.8m	27.8m		
	1955	29.7m	38.1m	21.2m		
	1963					
	1964	27.4	32.8	22.0	23.09	227.3
	1965	30.3	35.7	24.8	19.29	121.6
	1966	28.3m	34.6m	22.0m	18.66	147.6
	1967	29.8m	34.7m	24.8m	19.26	134.5
Feb.	1947	36.2				29.0+
	1948	25.0			14.73	141.0
	1949	25.4				113.0
	1950	26.3				36.0
	1951	30.3				19.0
	1952	29.7	37.2	18.5		53.0
	1953	33.0	41.8	24.1		
	1954	39.1	45.6	32.5		
	1955	26.3	35.5	17.1		
	1963					
	1964	30.7	39.9	21.4	3.26	31.3
	1965	31.9	40.1	23.7	6.41	41.4
	1966	28.3	35.2	21.3	6.15	60.4
	1967	32.5	40.5	24.5	4.88	45.5

Table 8. (Continued)

Date		Temperature Data (°F)			Precipitation Data (in inches)	
		Mean	Ave. Max.	Ave. Min.	Total PPN	Total Snow Fall
March	1947	35.6				79.5
	1948	28.4				100.5
	1949	43.3				33.5
	1950	27.4				77.0
	1951	35.3				107.0
	1952	29.5	38.3	21.1		65.0
	1953	29.4	39.8	18.9		
	1954		45.6	32.5		
	1955					
	1963					
	1964	29.9	37.3	22.4	12.22	125.9
	1965	33.7m	43.4m	23.9m	2.32	21.0
	1966	32.8	42.4	23.1	13.44	114.3
	1967	29.3m	37.0m	21.5m	9.71	81.4

Table 9. Temperature and precipitation data for Santiam Pass, January 1967 (U. S. W. B., Climatological data. Oregon 1967).

Date	Temperature °F Maximum	Minimum	Precipitation (inches)
1	31	25	.77
2	32	23	.10
3	33	30	1.12
4	38	25	.44
5	26	17	1.08
6	28	18	.88
7	29	20	
8	38	25	
9	40	25	
10	48	30	
11	38	30	.73
12	32	27	.43
13	37	30	1.03
14	44	33	.08
15	48	28	.46
16	31	25	.28
17	38	19	
18			
19	40	30	.86
20	32	26	2.38
21	29	22	1.28
22	26	19	.27
23	30	15	..03
24	26	18	.49
25	30	23	.33
26	37	25	1.80
27	41	35	1.63
28	38	31	1.56
29	39	29	.67
30	30	17	.36
31	31	25	.20

Additional Data for Month	
Temperature Data	
Average Max.	34.7m °F
Average Min.	24.8m °F
Average	29.8m °F
Highest Temp.	48.0 °F
Lowest Temp.	15.0 °F
Days Max. < 32°F	15
Days Min. < 32°F	29
Precipitation Data	
Total ppn.	19.26 in.
Greatest day	2.38 in.
Total snow	134.5 in.
Max. snow depth Jan. 26	96.0 in.
Days ppn. ⩾ .10 in.	23
Days ppn. ⩾ .50 in.	13
Days ppn. ⩾ 1.0 in.	8

Table 10. Temperature and precipitation data for Santiam Pass, February 1967 (U. S. W. B., Climatological data. Oregon 1967).

Date	Temperature °F Maximum	Minimum	Precipitation (inches)
1	32	26	.24
2	34	28	.07
3	43	27	
4	41	33	.06
5	39	22	
6	46	19	
7	42	27	
8	46	24	
9	39	31	.02
10	38	29	
11	36	27	.14
12	44	31	
13	39	22	.94
14	26	22	.39
15	28	22	1.18
16	32	22	.57
17	35	29	.63
18	36	22	.41
19	31	21	.06
20	47	8	
21	45	24	
22	49	27	
23	53	20	
24	45	26	
25	40	28	.12
26	46	16	T
27	54	25	
28	48	29	.05
29			
30			
31			

Additional Data for Month	
Temperature Data	
Average Max.	40.5 °F
Average Min.	24.5°F
Average	32.5°F
Highest Temp.	54 °F
Lowest Temp.	8 °F
Days Max. < 32°F	5
Days Min. < 32°F	27
Precipitation Data	
Total ppn.	4.88 in.
Greatest day	1.18 in.
Total snow	45.5 in.
Max. snow depth Feb. 16	106 in.
Days ppn. ≥ .10 in.	9
Days ppn. ≥ .50 in.	4
Days ppn. ≥ 1.0 in.	1

Table 11. Temperature and precipitation data for Santiam Pass, March 1967 (U.S.W.B., Climatological data. Oregon 1967).

Date	Temperature °F Maximun	Minimum	Precipitation (inches)
1	33	26	.82
2	30	20	.56
3	31	13	
4	39	13	
5	47	15	
6	48	27	
7	48	18	
8	42	26	
9	35	24	1.10
10	26	20	1.12
11	30	16	.05
12	28	4	.04
13	33	18	.14
14	34	18	.10
15	44	28	T
16	43	32	..16
17	38	28	.57
18	35	25	.79
19	37	16	.16
20			
21	43	29	1.04
22	51	33	.09
23	40	28	.94
24	33	23	.46
25	35	23	.06
26	37	24	.11
27	38	26	
28	34	24	.25
29	28	19	.37
30	32	20	.71
31	37	9	.05

Additional Data for Month	
Temperature Data	
Average Max.	37.0m °F
Average Min.	21.5m °F
Average	29.3m °F
Highest Temp.	51.0 °F
Lowest Temp.	4.0 °F
Days Max. < 32°F	7
Days Min. < 32°F	30
Precipitation Data	
Total ppn.	9.71 in.
Greatest day	1.12 in.
Total snow	81.4 in.
Max. snow depth Mar. 30	113.0 in.

APPENDIX B

LOCATION MAPS

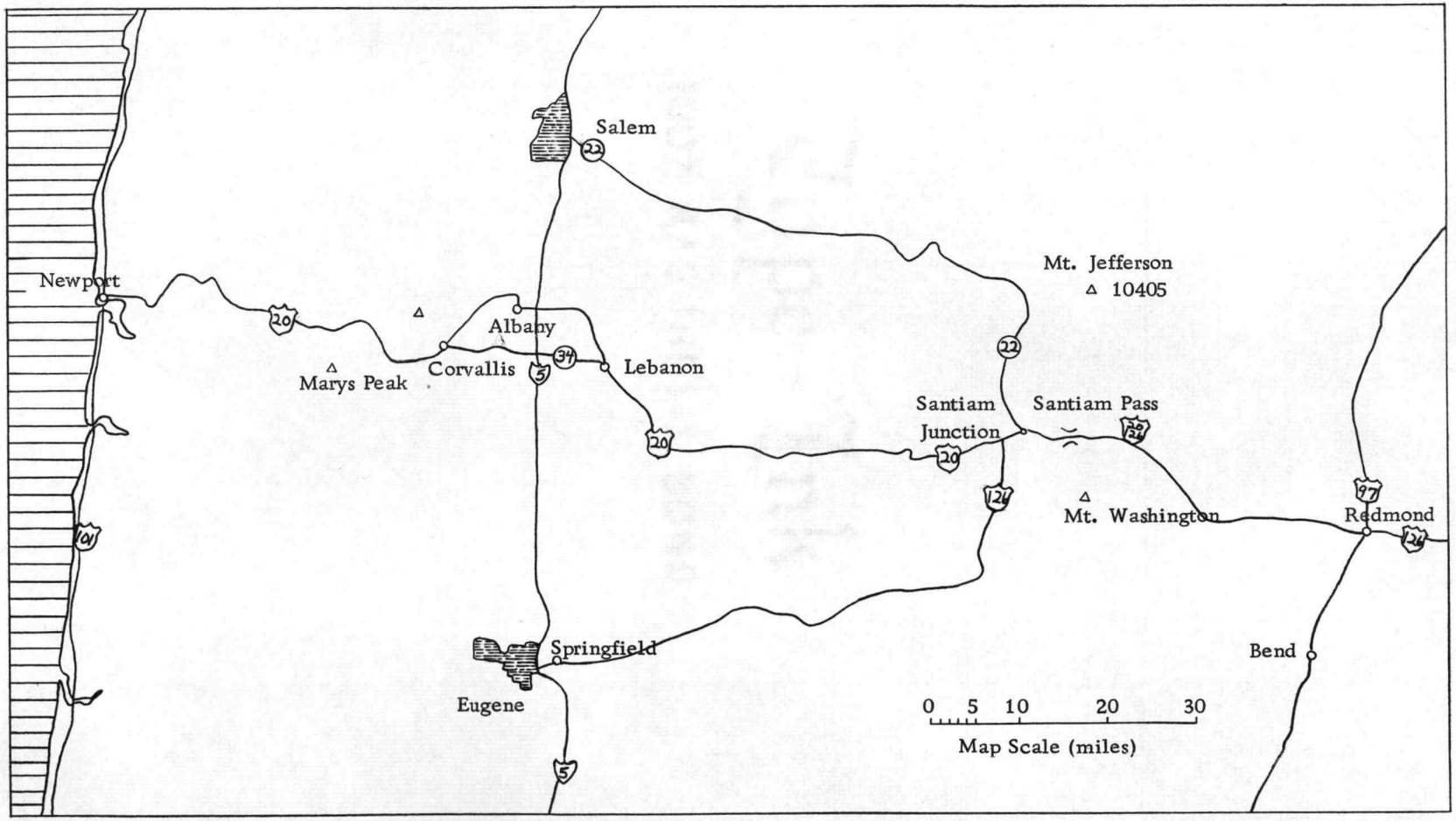

Figure 18. Highway map of western portion of Central Oregon.

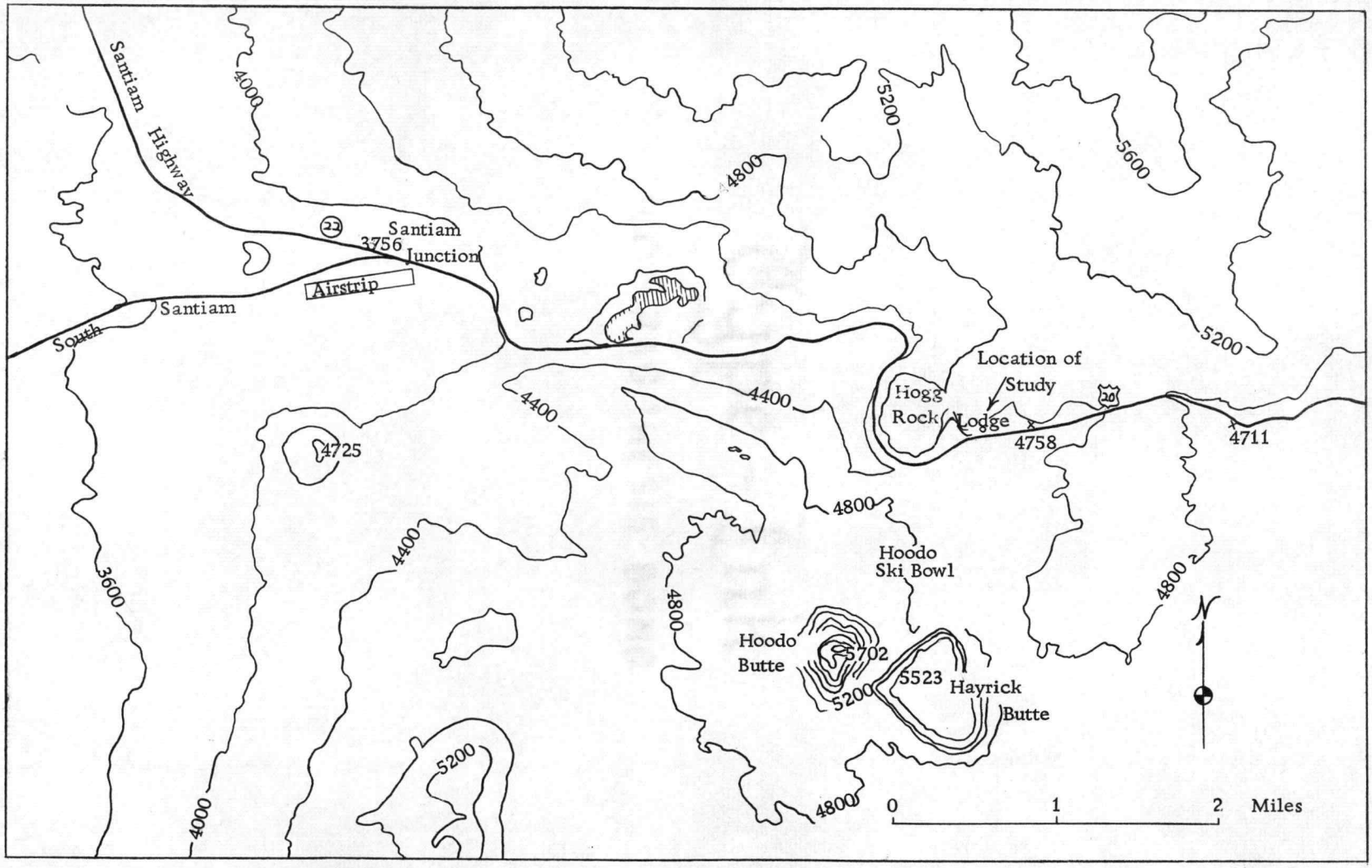

Figure 19. Topographic map of immediate sampling area.

APPENDIX C

SYNOPTIC MAPS

January, 0400 on the 9th through 0400 on the 21st, 1967

February, 2200 on the 14th through 1600 on the 15th, 1967

March, 1600 on the 9th through 1600 on the 10th, 1967

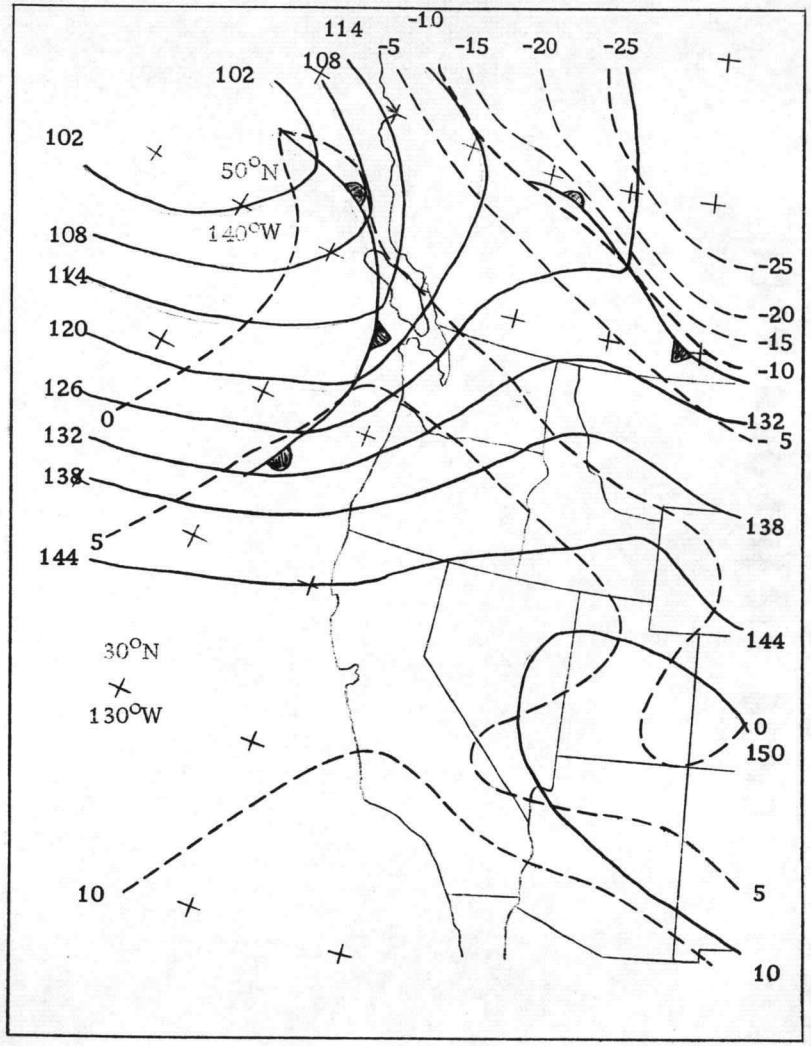

Figure 20. 850 millabar analysis 0400 PST 19 January, 1967.

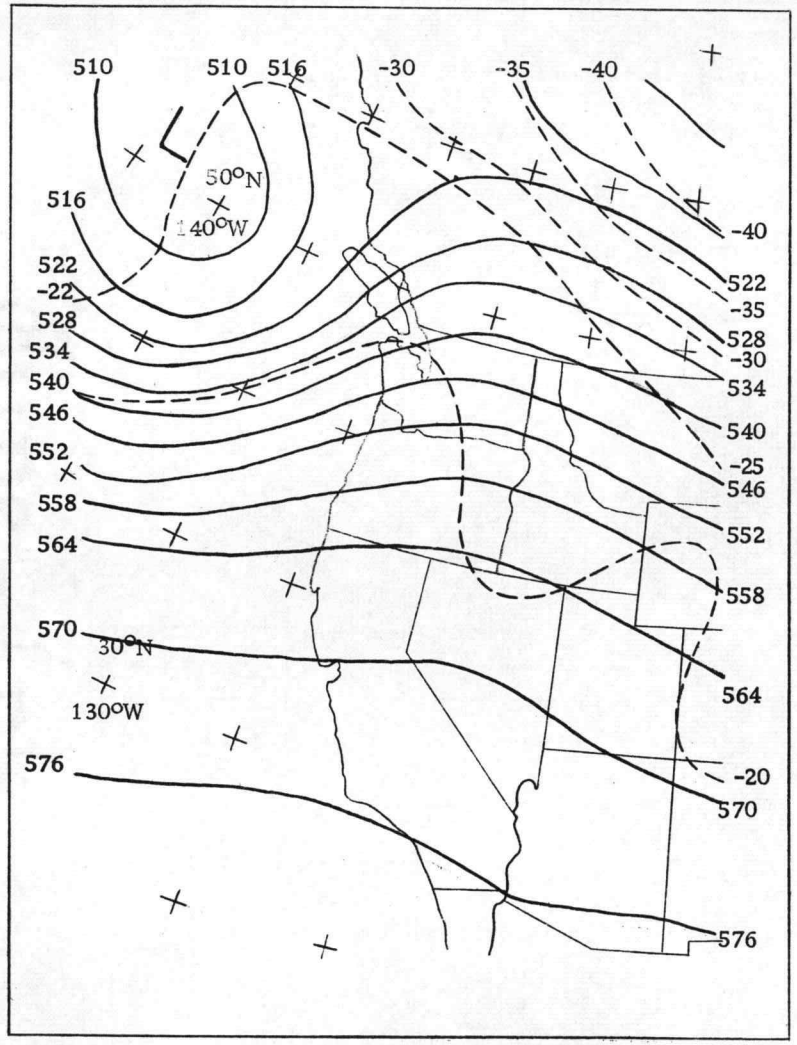

Figure 21. 500 millabar analysis 0400 PST 19 January, 1967

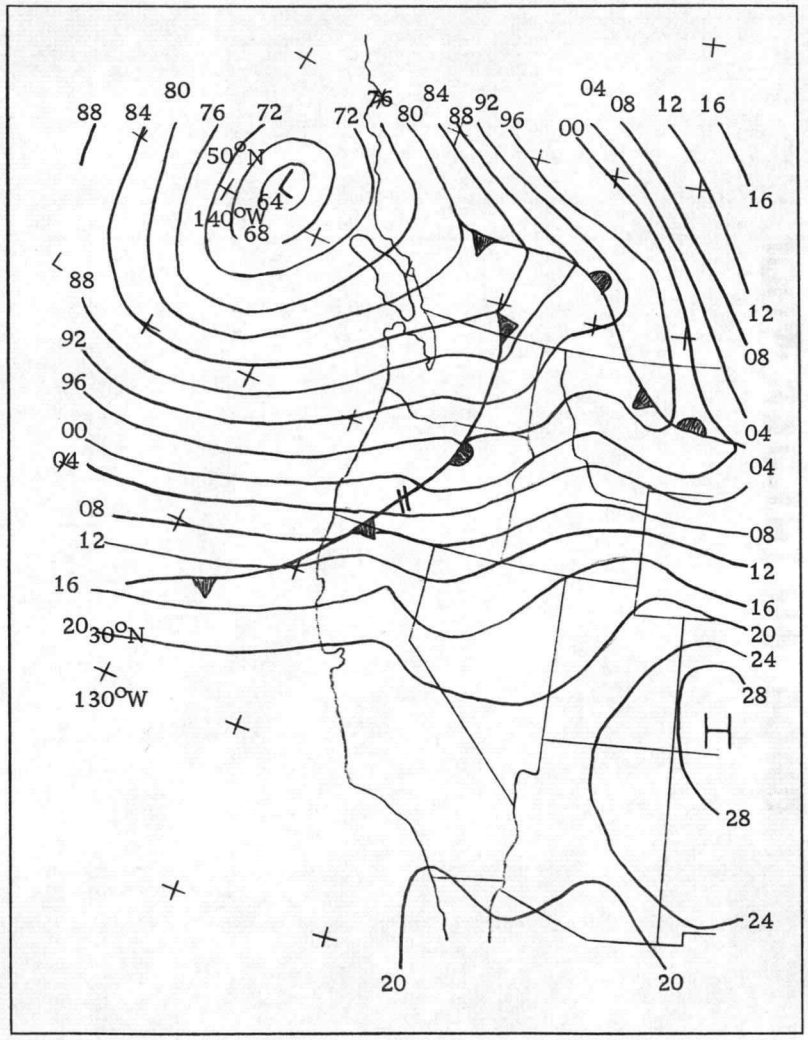

Figure 22. Surface analysis 1300 PST 19 January, 1967.

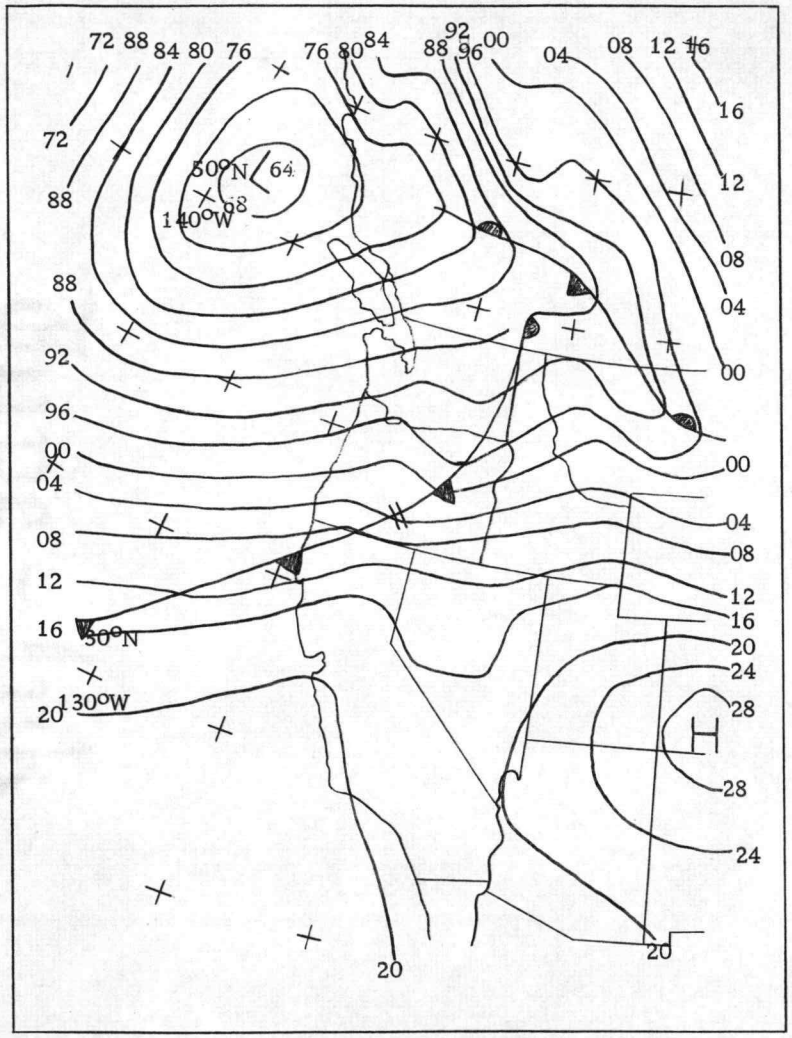

Figure 23. Surface analysis 1600 PST 19 January, 1967.

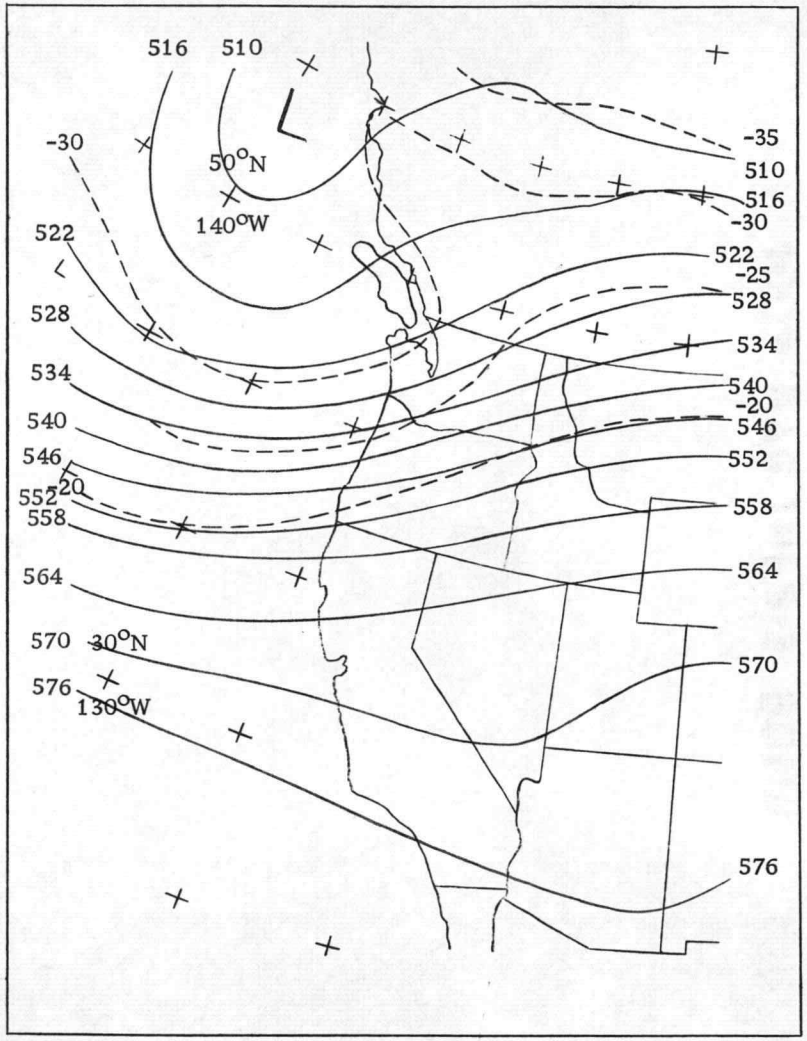

Figure 24. 500 millabar analysis 1600 PST 19 January, 1967.

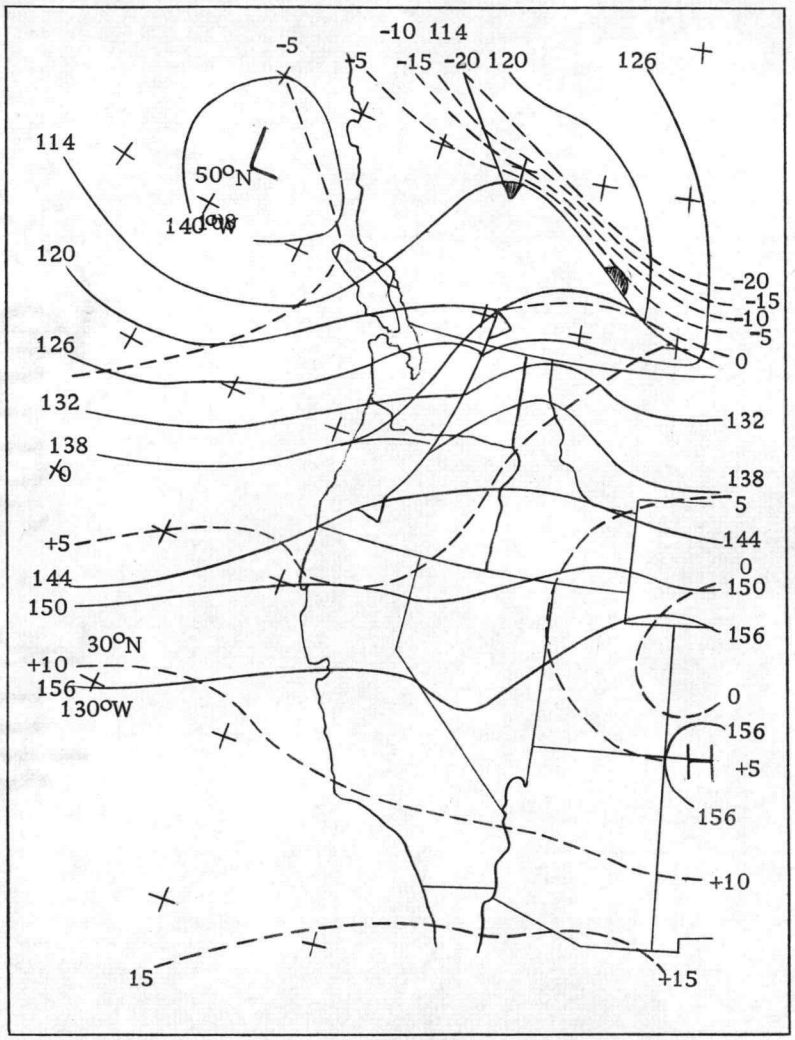

Figure 25. 850 millabar analysis 1600 PST 19 January, 1967.

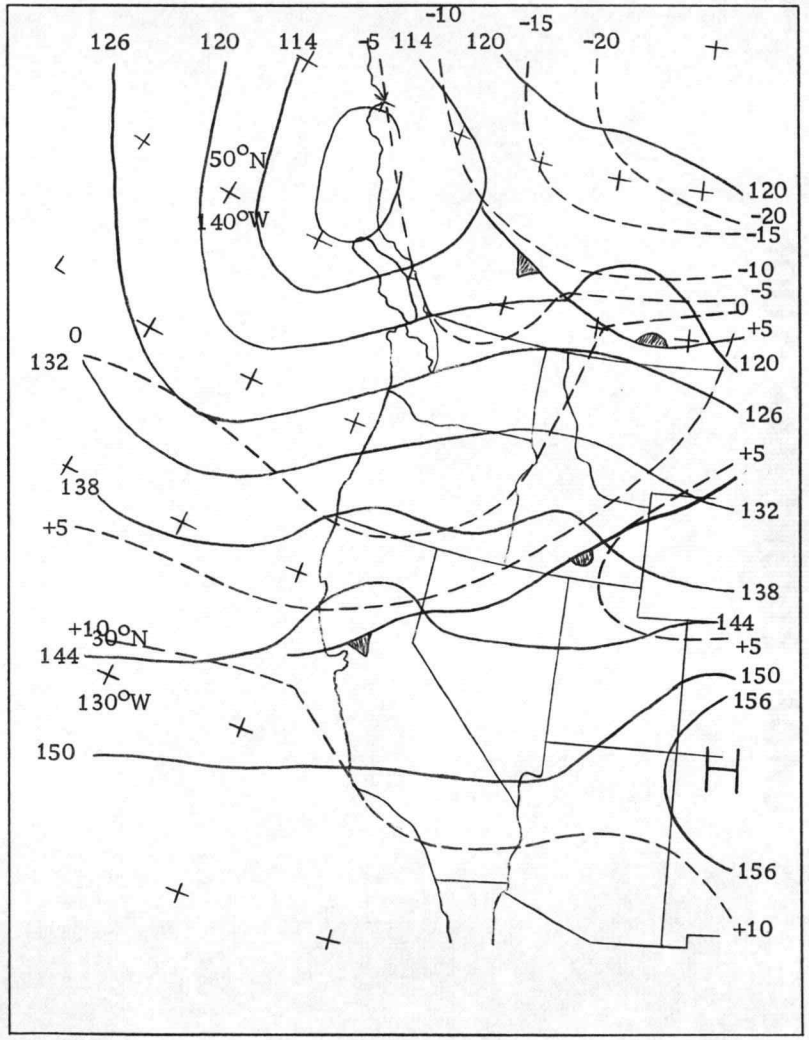

Figure 26. 850 millabar analysis 0400 PST 20 January, 1967.

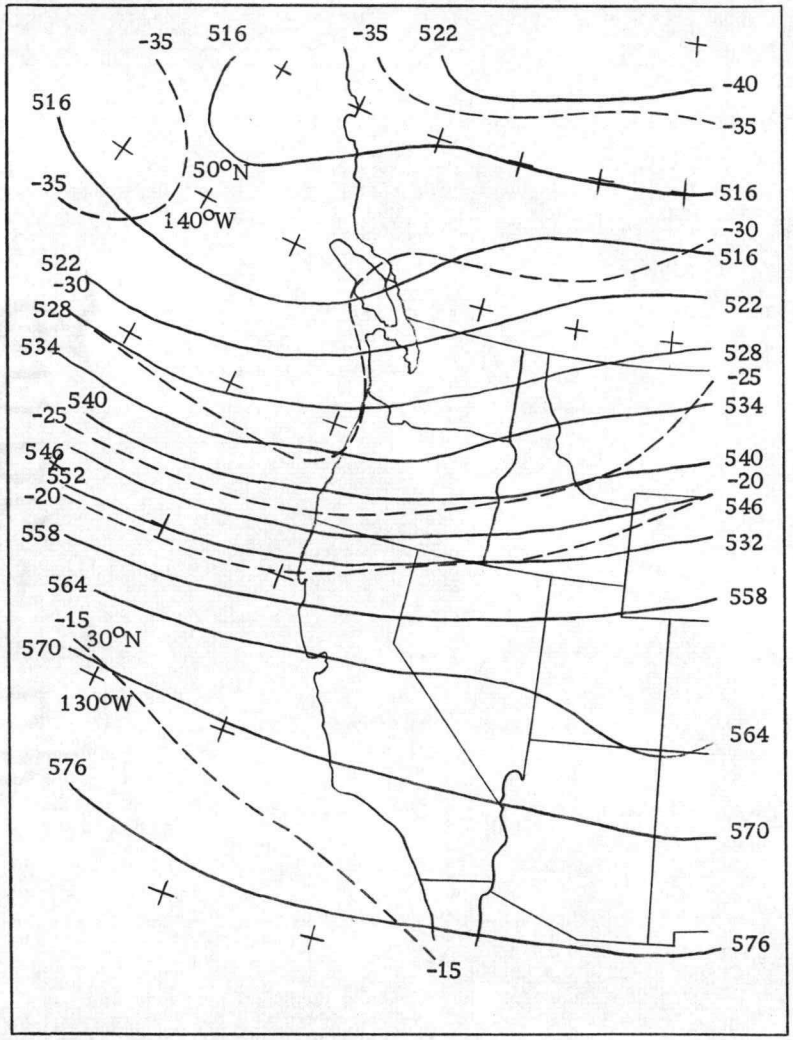

Figure 27. 500 millabar analysis 0400 PST 20 January, 1967.

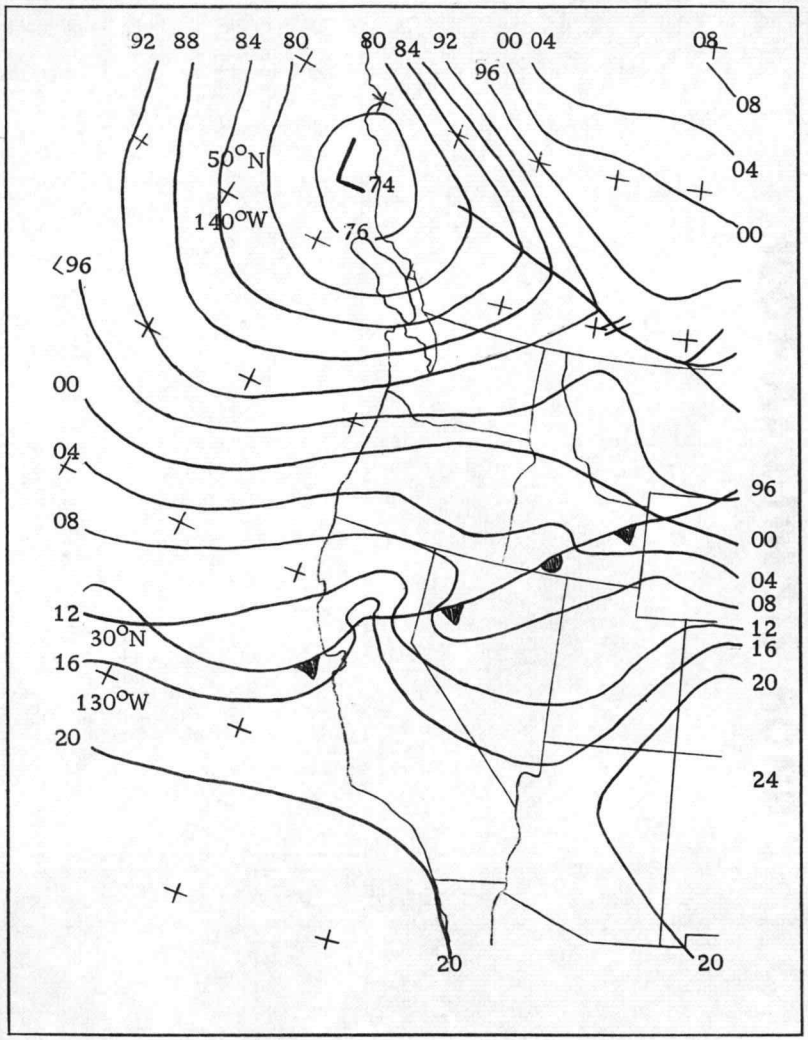

Figure 28. Surface analysis 0400 PST 20 January, 1967.

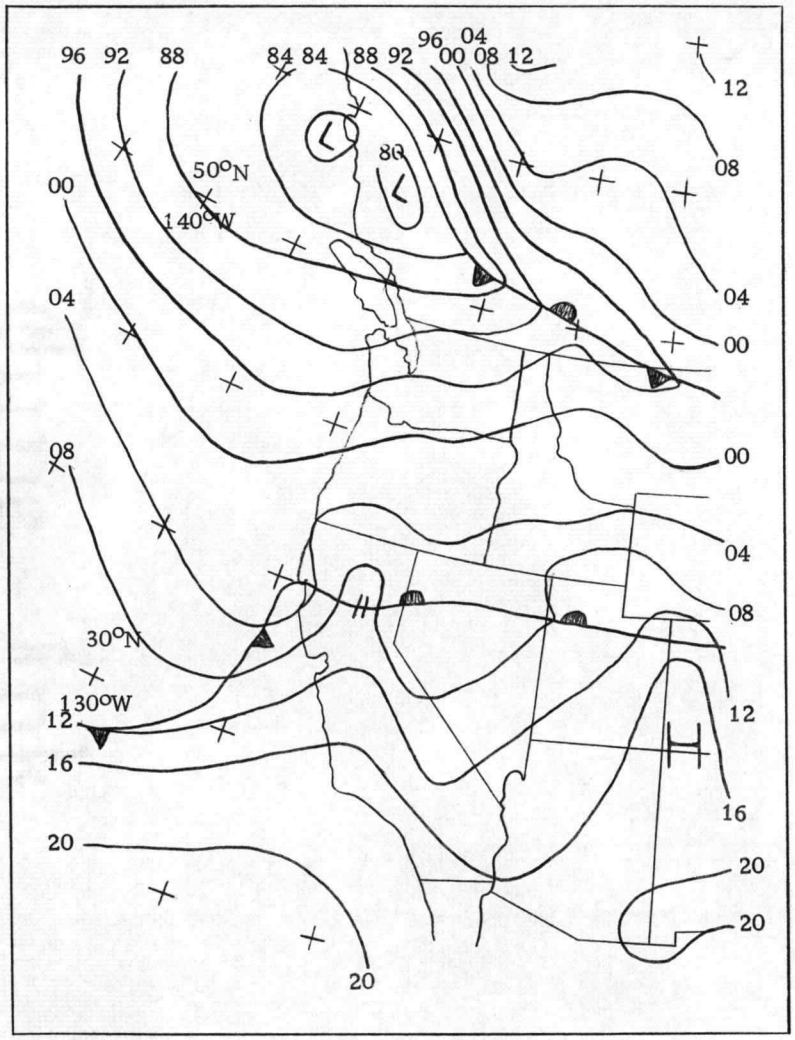

Figure 29. Surface analysis 1600 PST 20 January, 1967.

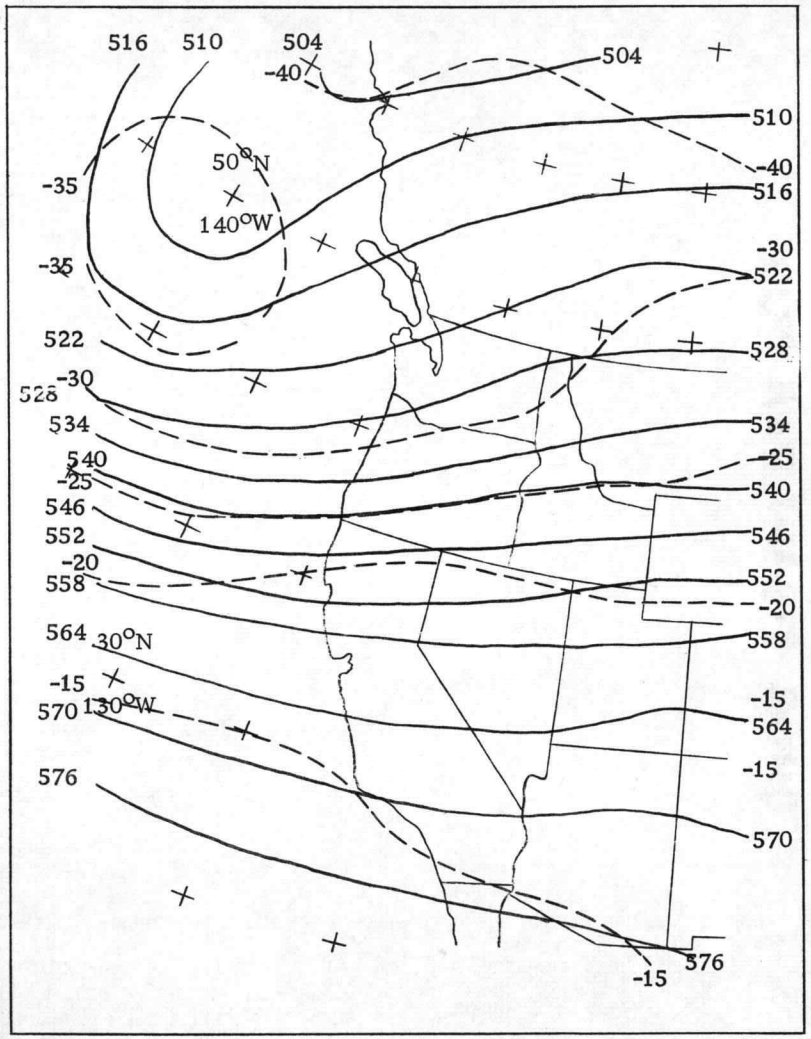

Figure 30. 500 millabar analysis 1600 PST 20 January, 1967.

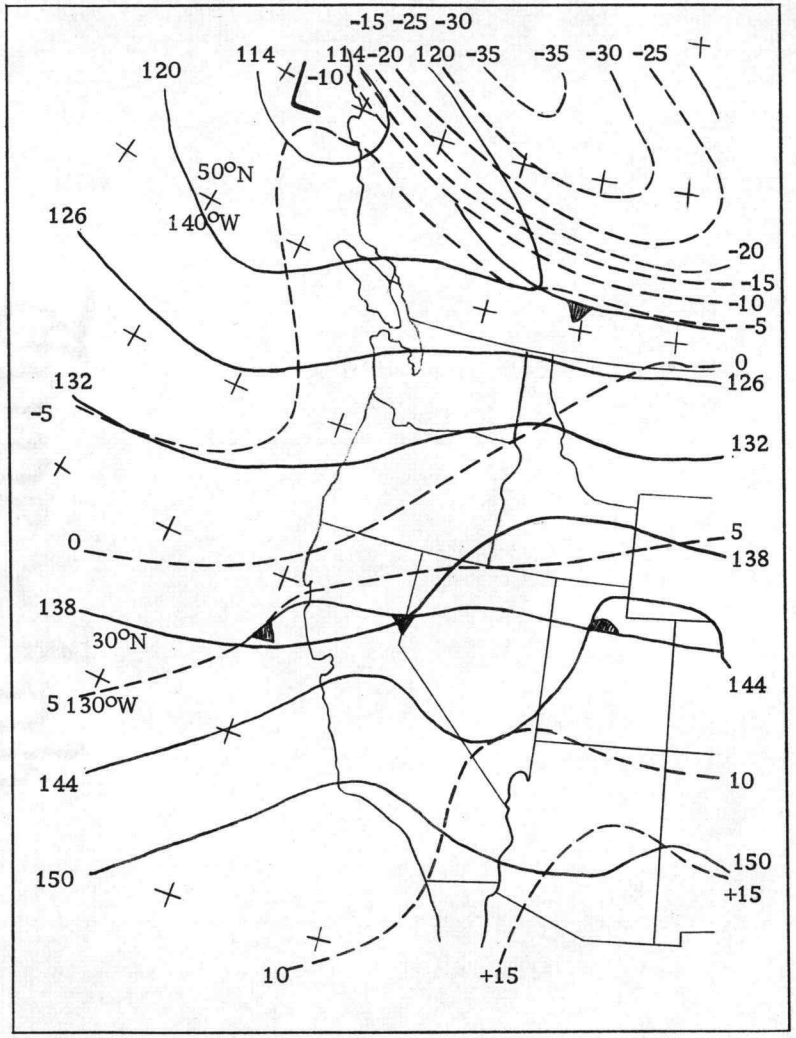

Figure 31. 850 millabar analysis 1600 PST 20 January, 1967.

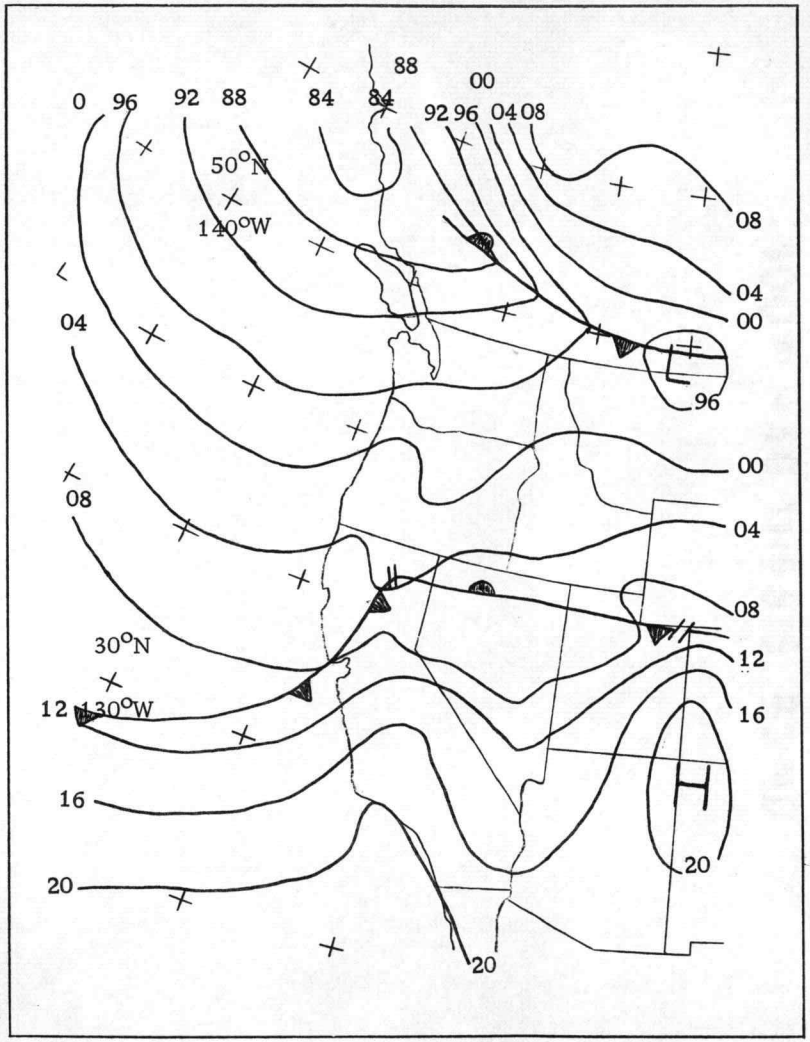

Figure 32. Surface analysis 2200 PST 21 January, 1967.

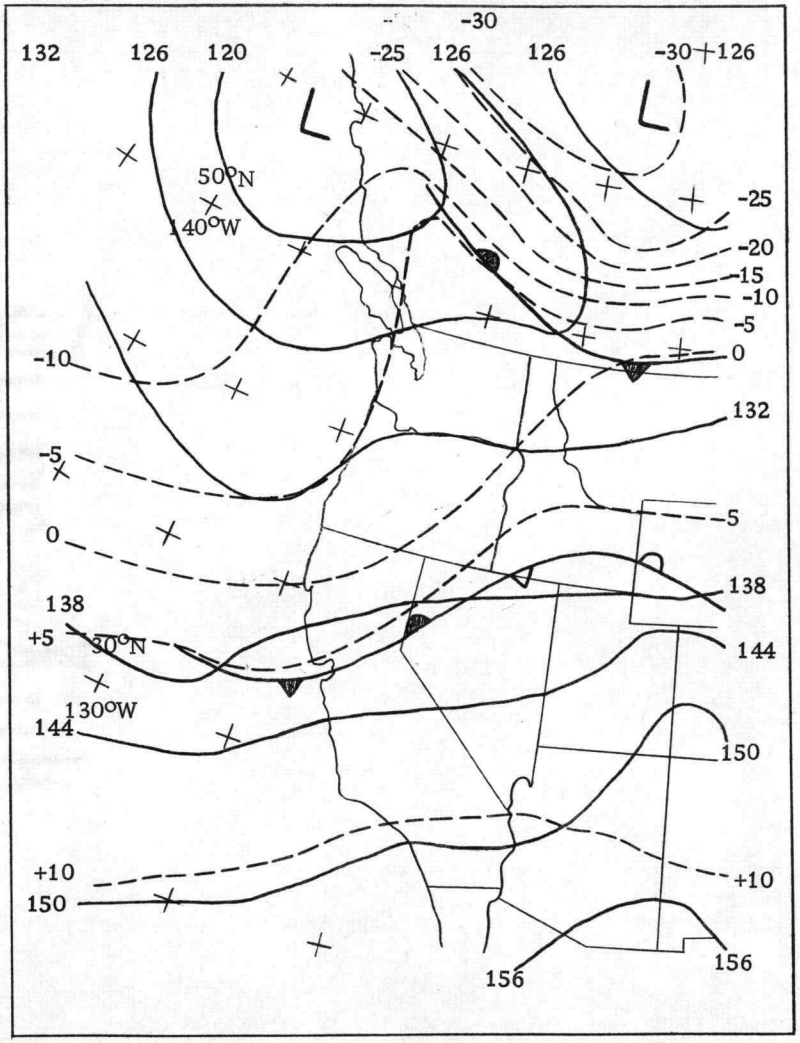

Figure 33. 850 millabar analysis 0400 PST 21 January, 1967.

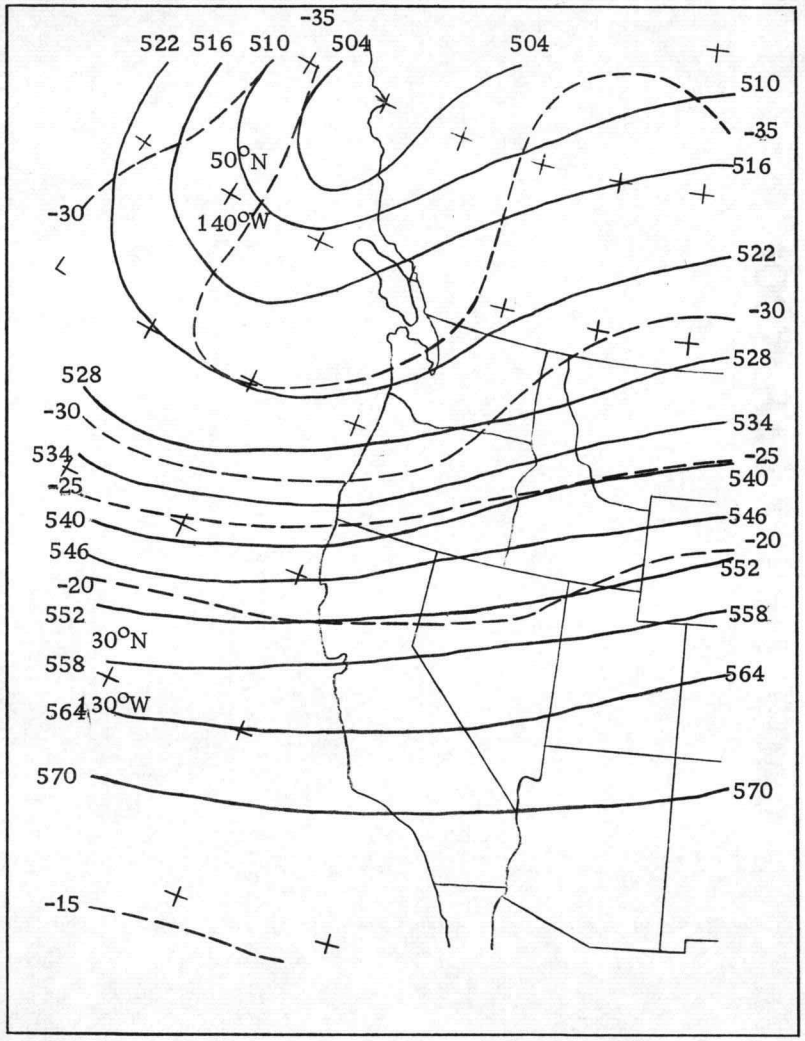

Figure 34. 500 millabar 0400 PST 21 January, 1967.

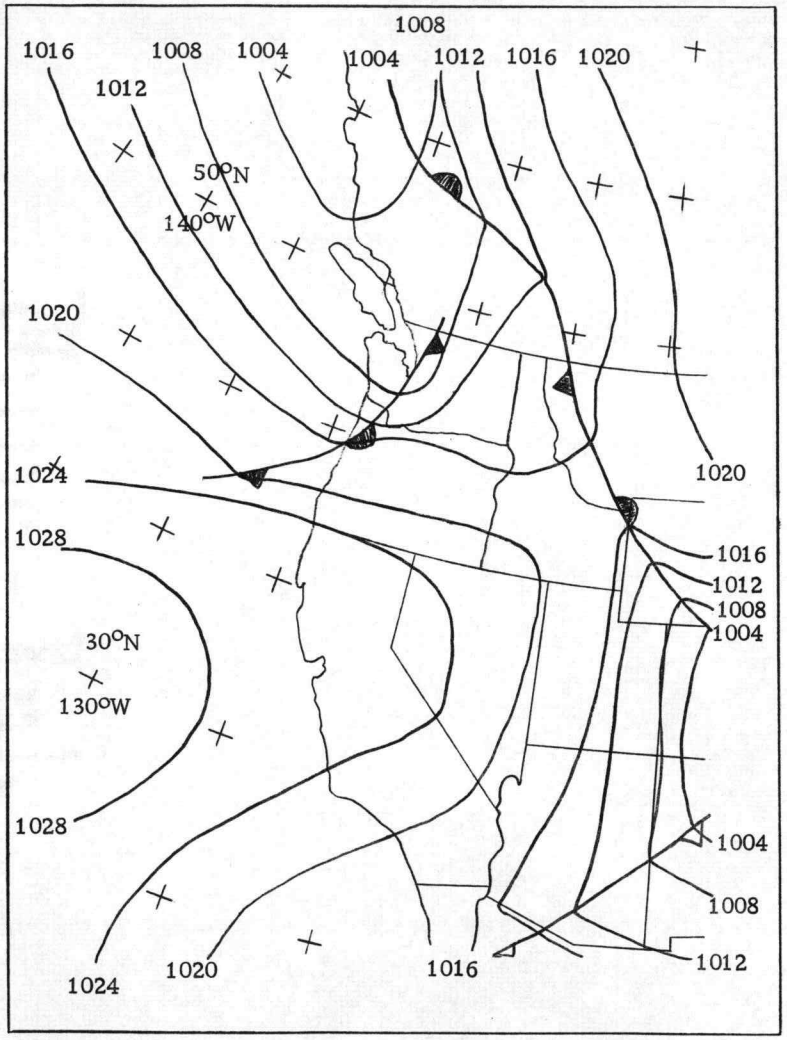

Figure 35. Surface analysis 2200 PST 14 February, 1967.

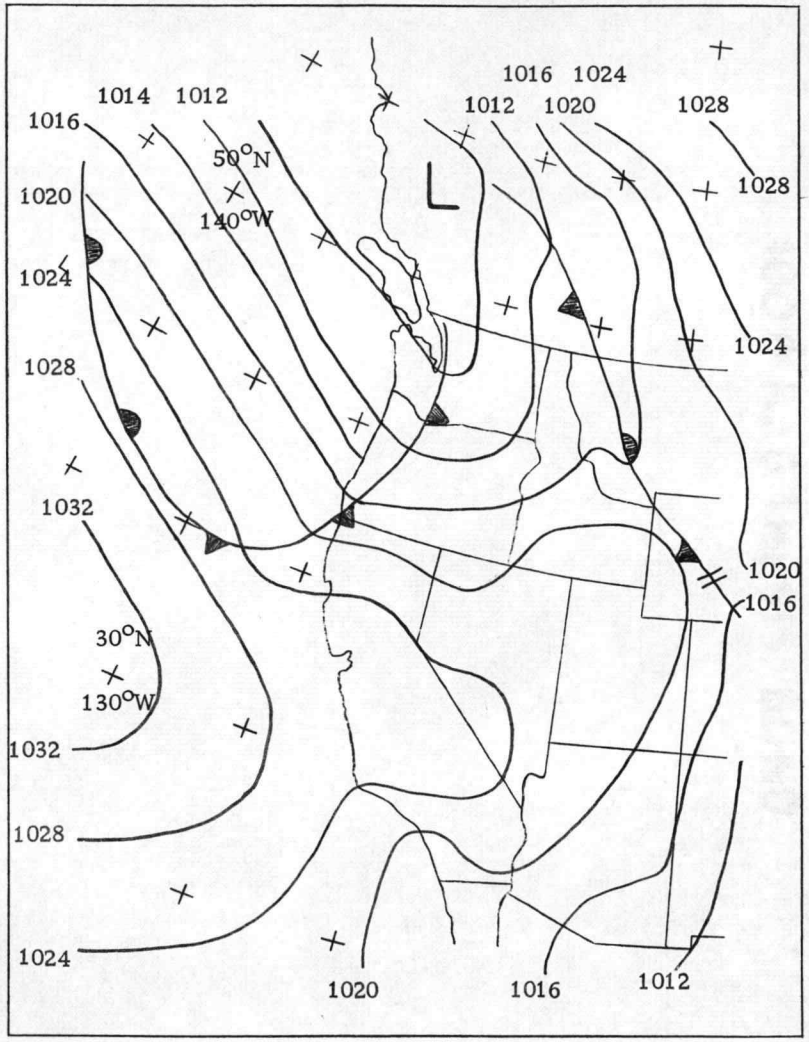

Figure 36. Surface analysis, 0400 PST 15 February, 1967.

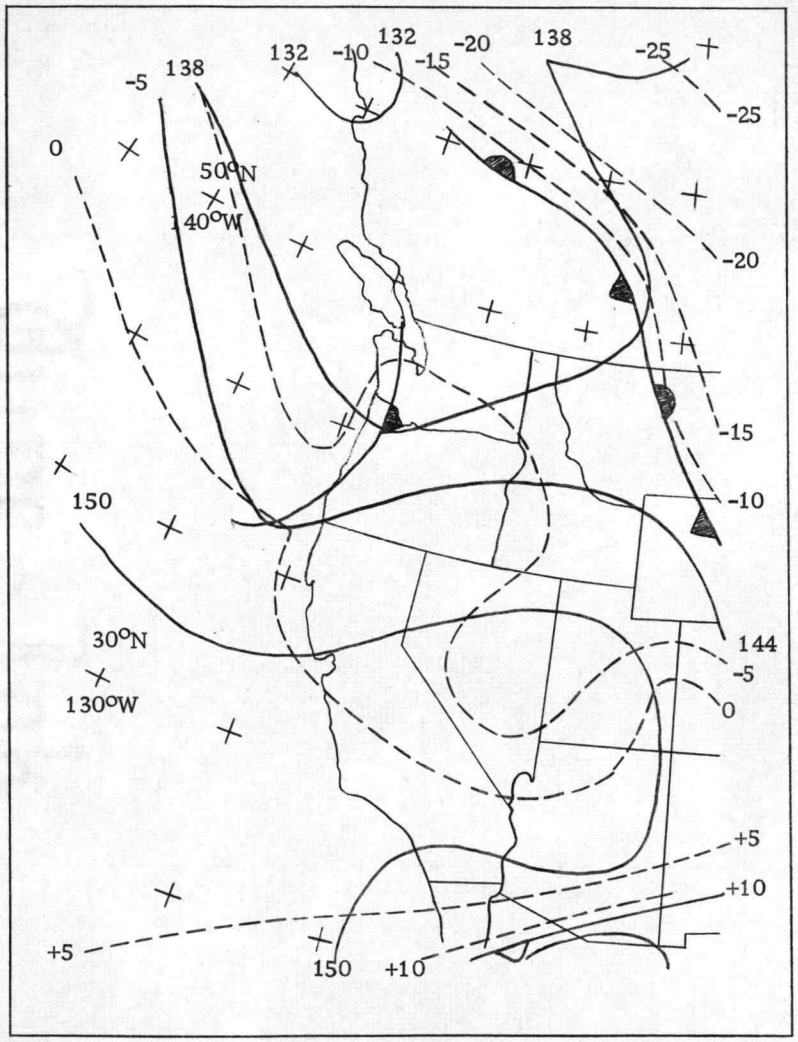

Figure 37. 850 millibar analysis, 0400 PST 15 February, 1967.

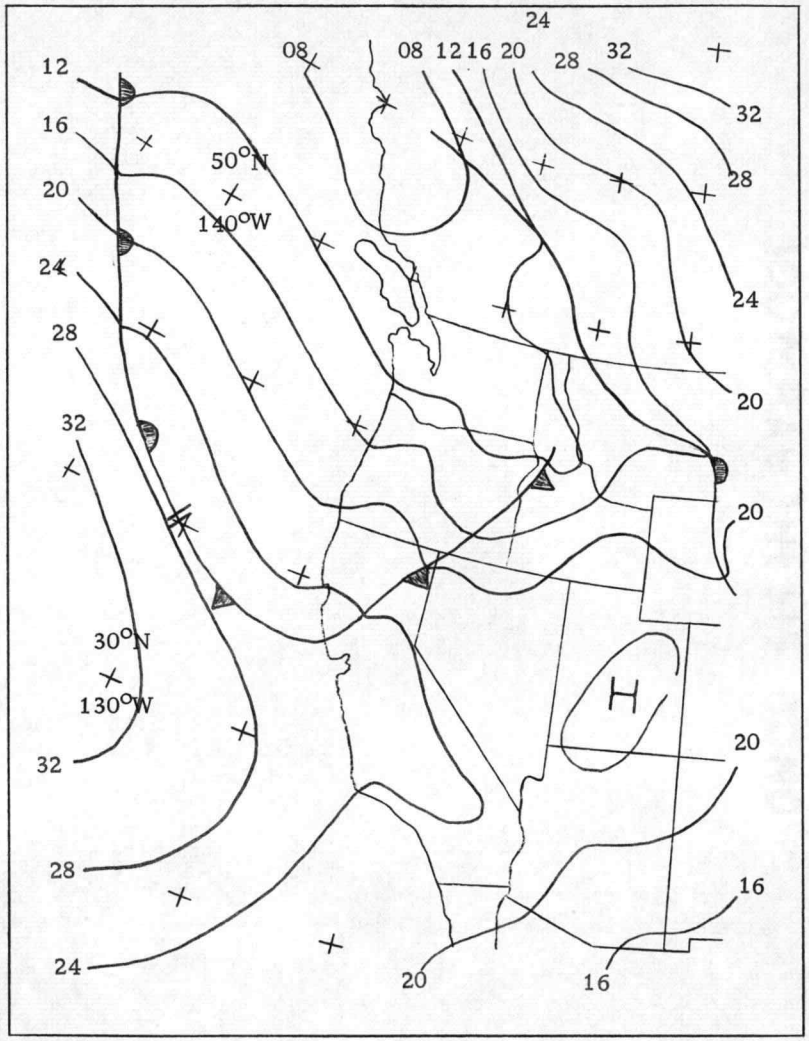

Figure 38. Surface analysis, 1000 PST 15 February, 1967.

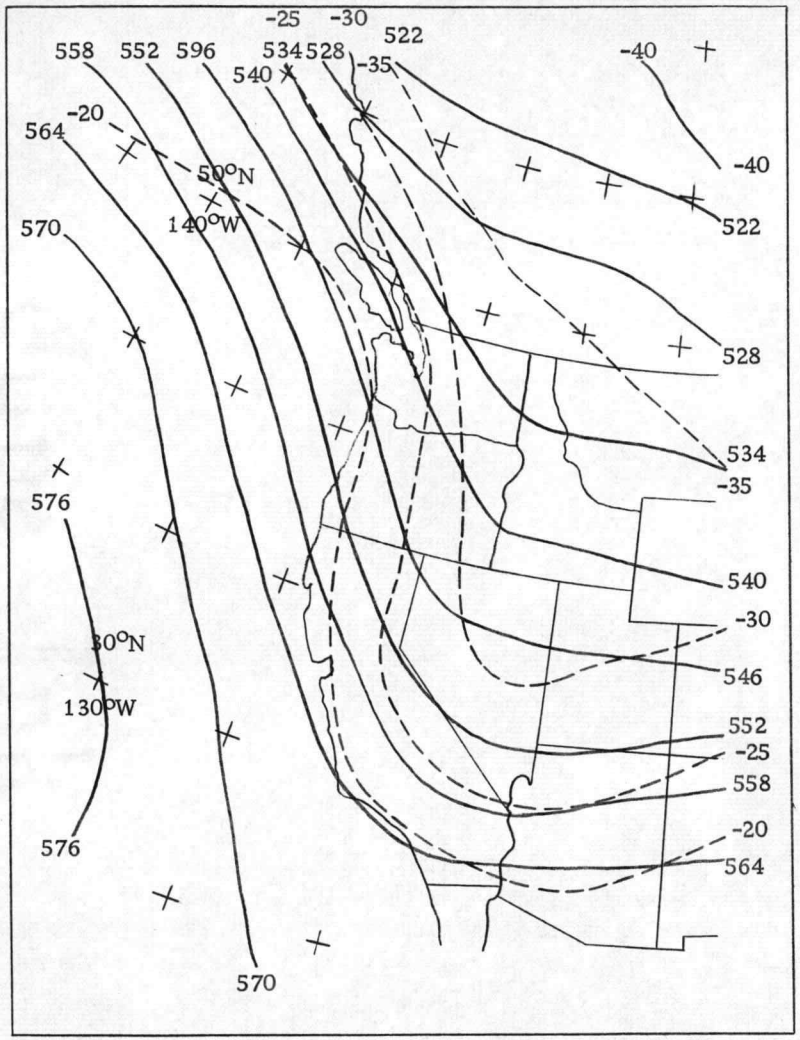

Figure 39. 500 millibar analysis, 1600 PST 15 February 1967.

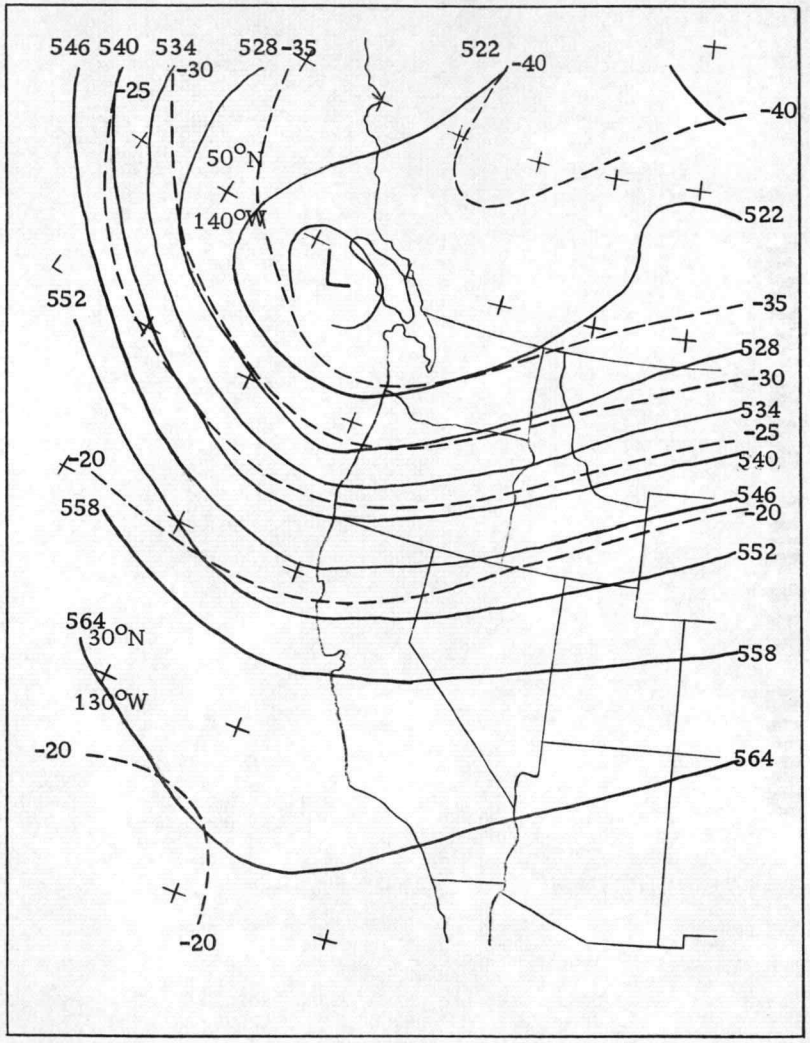

Figure 40. 500 millibar analysis, 1600 PST 9 March, 1967.

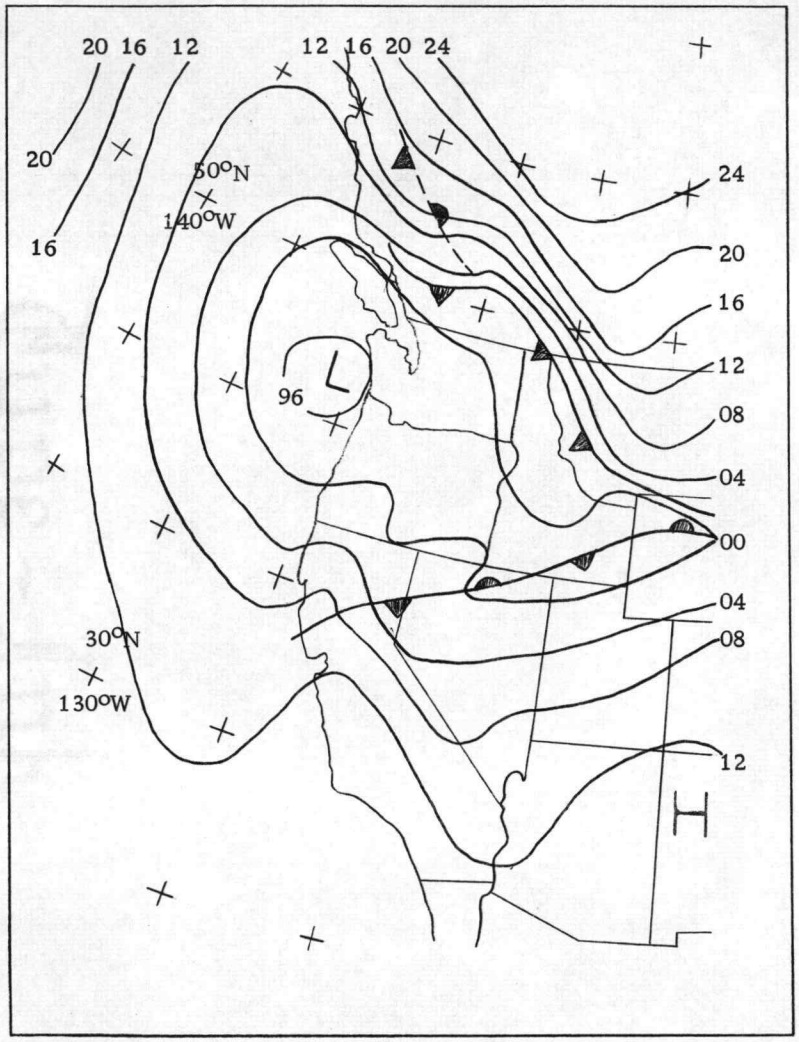

Figure 41. Surface analysis, 2200 PST 9 March, 1967.

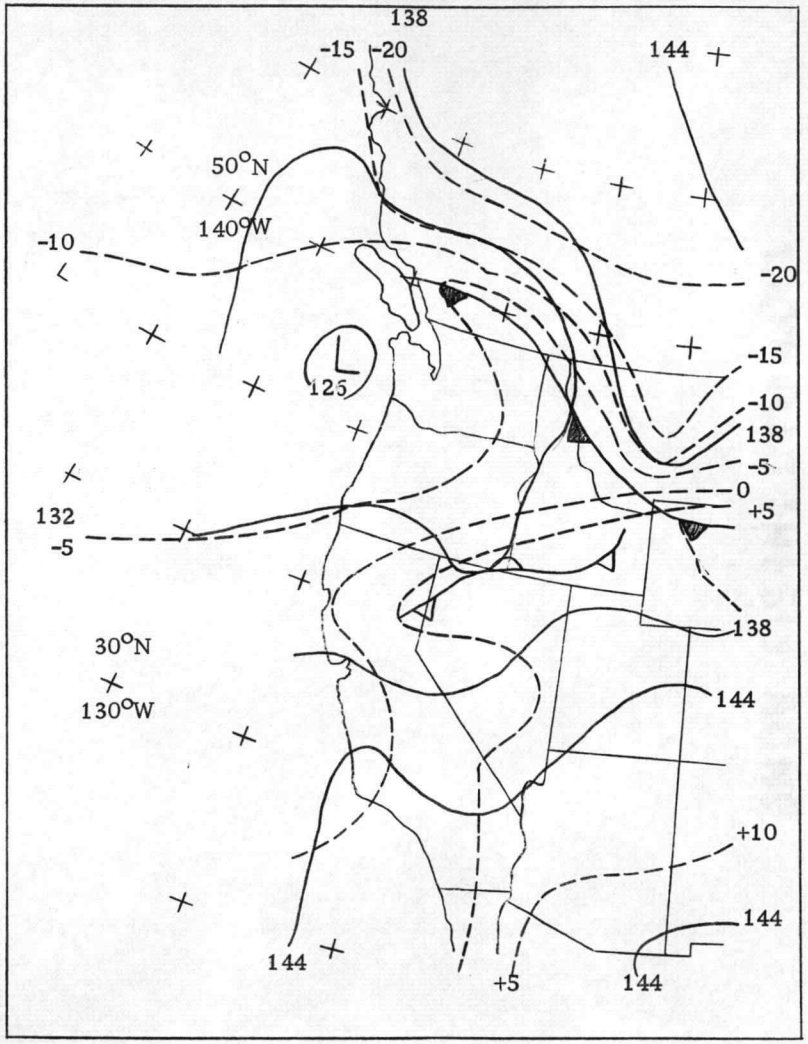

Figure 42. 850 millibar analysis, 0400 PST 10 March, 1967.

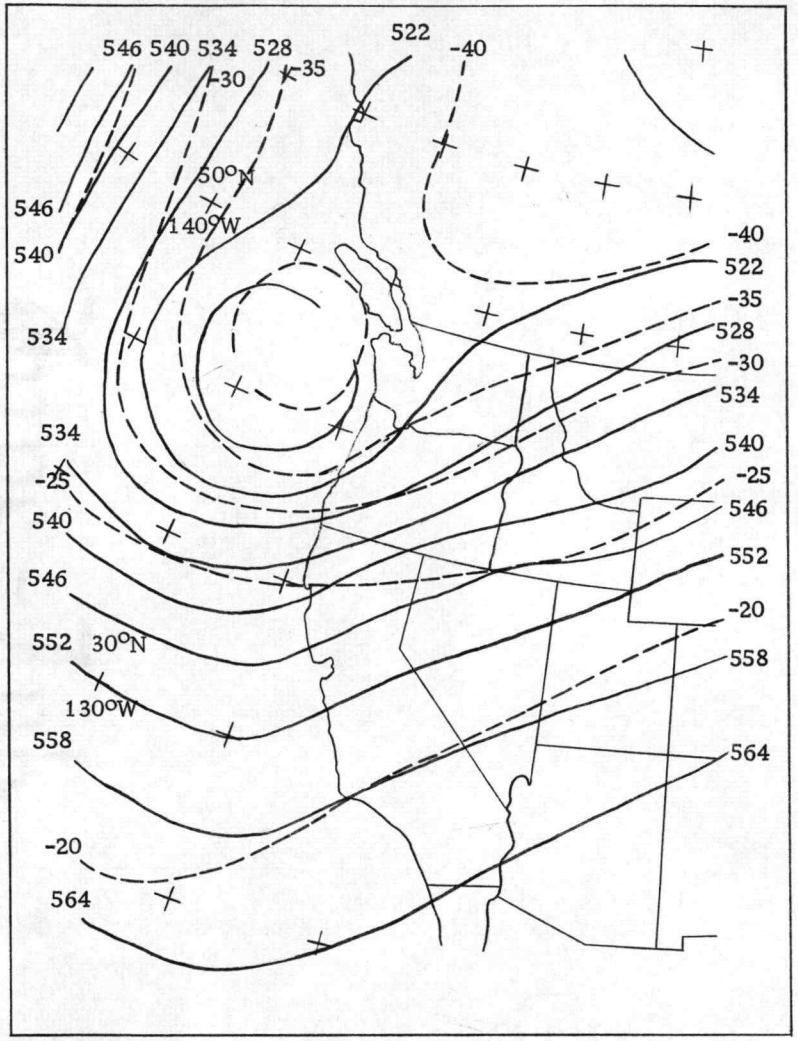

Figure 43. 500 millibar analysis, 0400 PST 10 March, 1967.

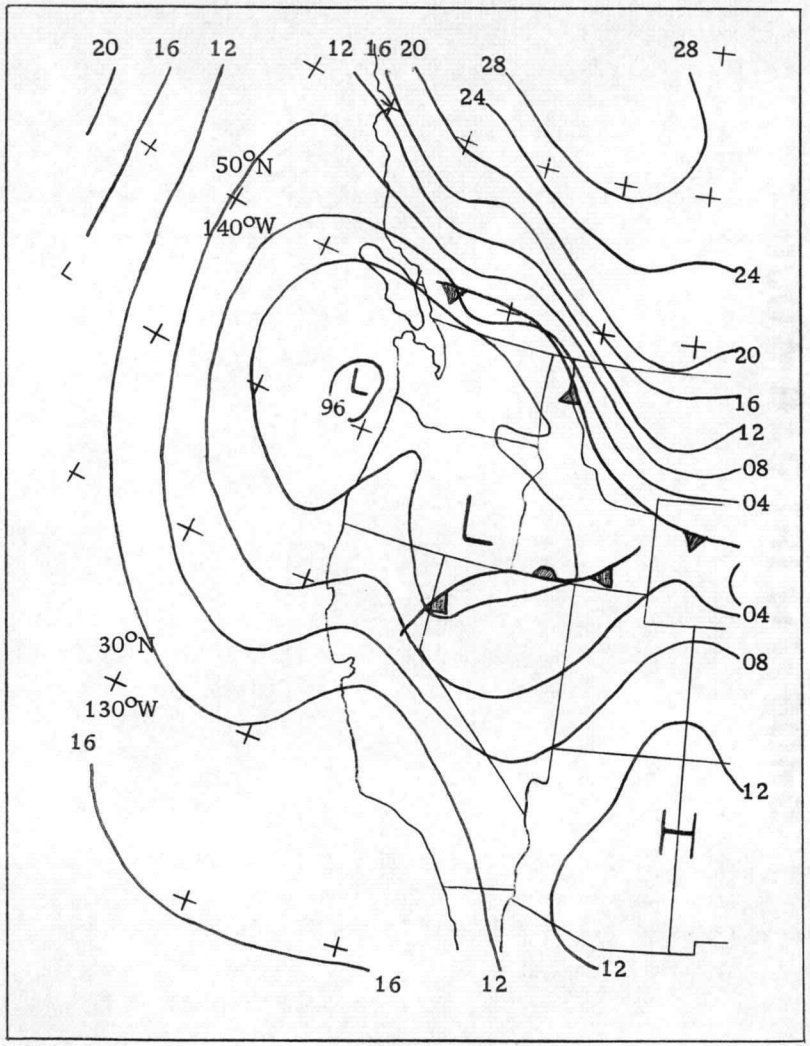

Figure 44. Surface analysis, 0400 PST 10 March, 1967.

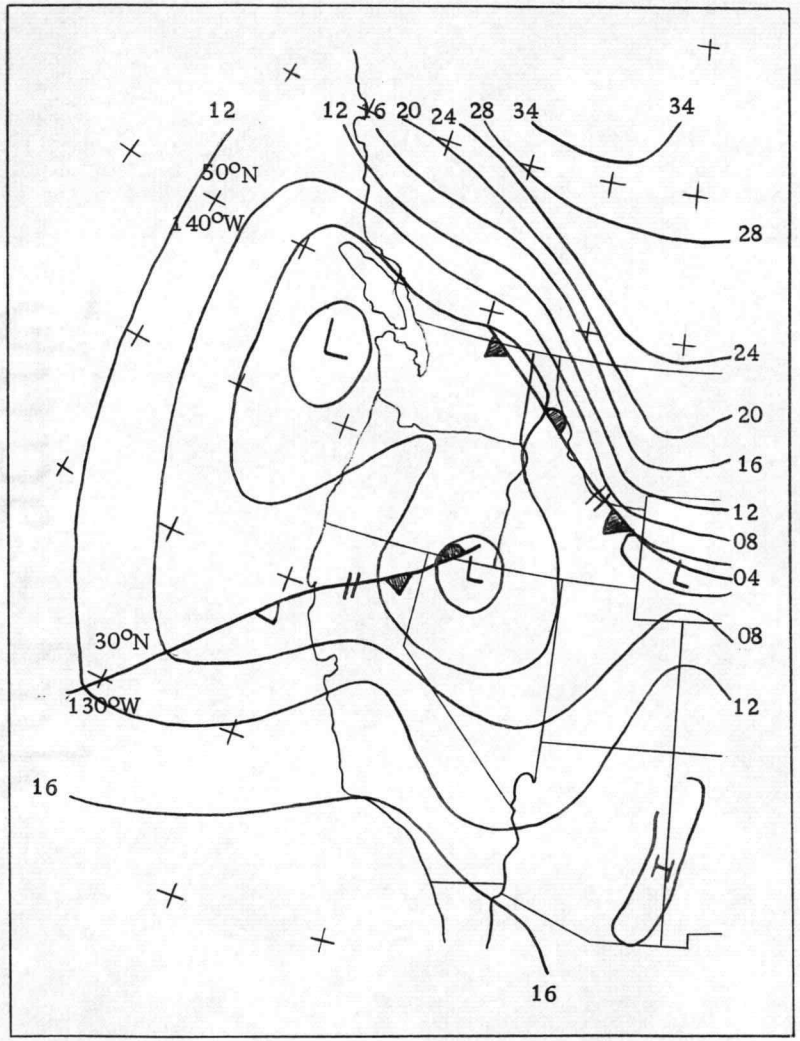

Figure 45. Surface analysis, 1300 PST 10 March, 1967.

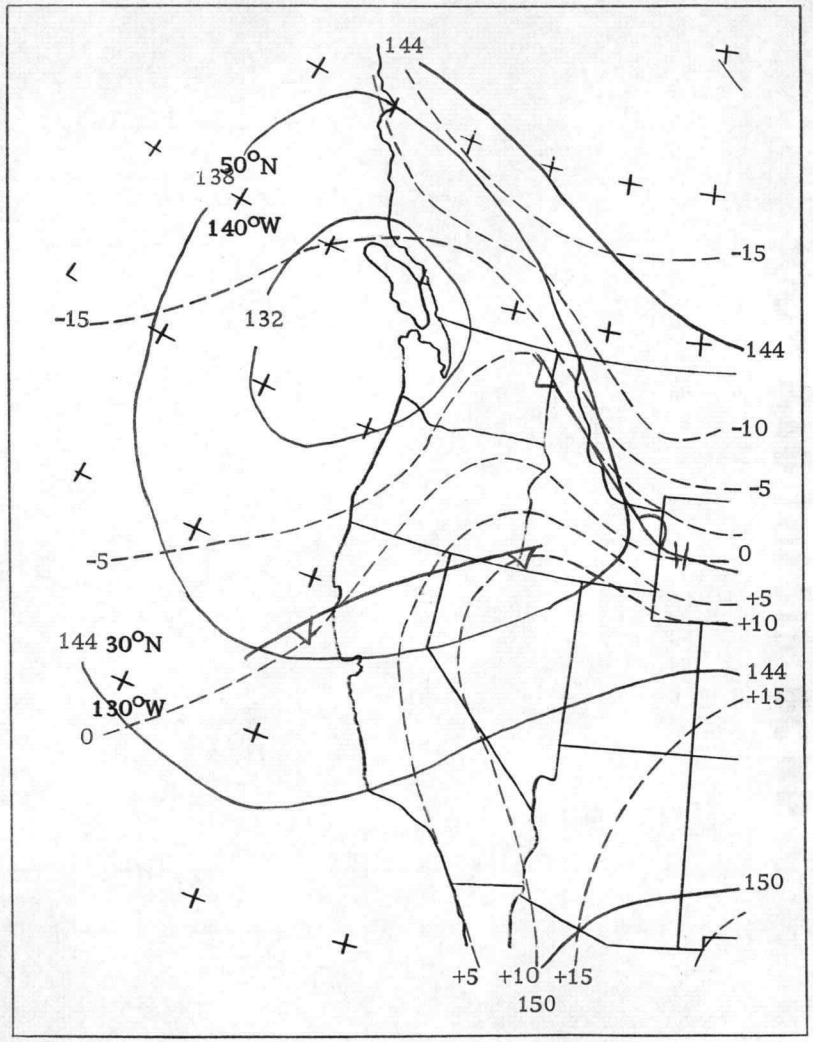

Figure 46. 850 millibar analysis, 1600 PST 10 March, 1967.

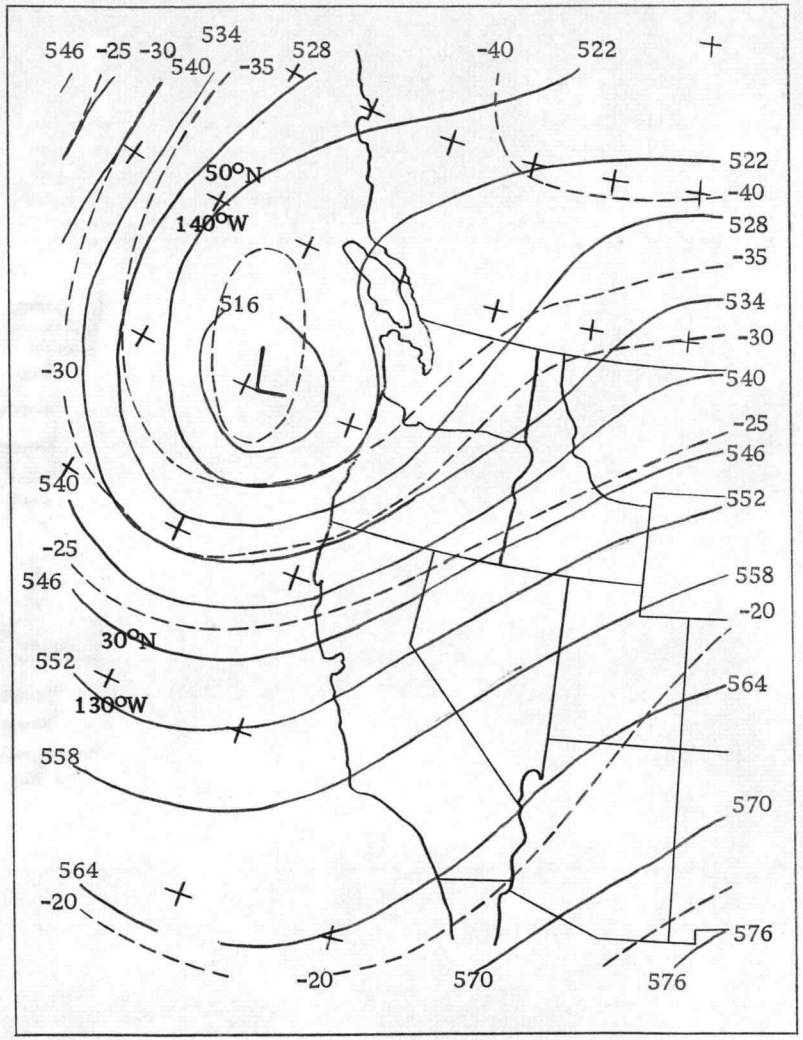

Figure 47. 500 millibar analysis, 1600 PST 10 March, 1967.

APPENDIX D

SALEM RADIOSONDE DATA

January 19-21 from 0400 through 0400, 1967

February 14-15, from 1600 through 1600, 1967

March 9-10, 1600 through 1600, 1967

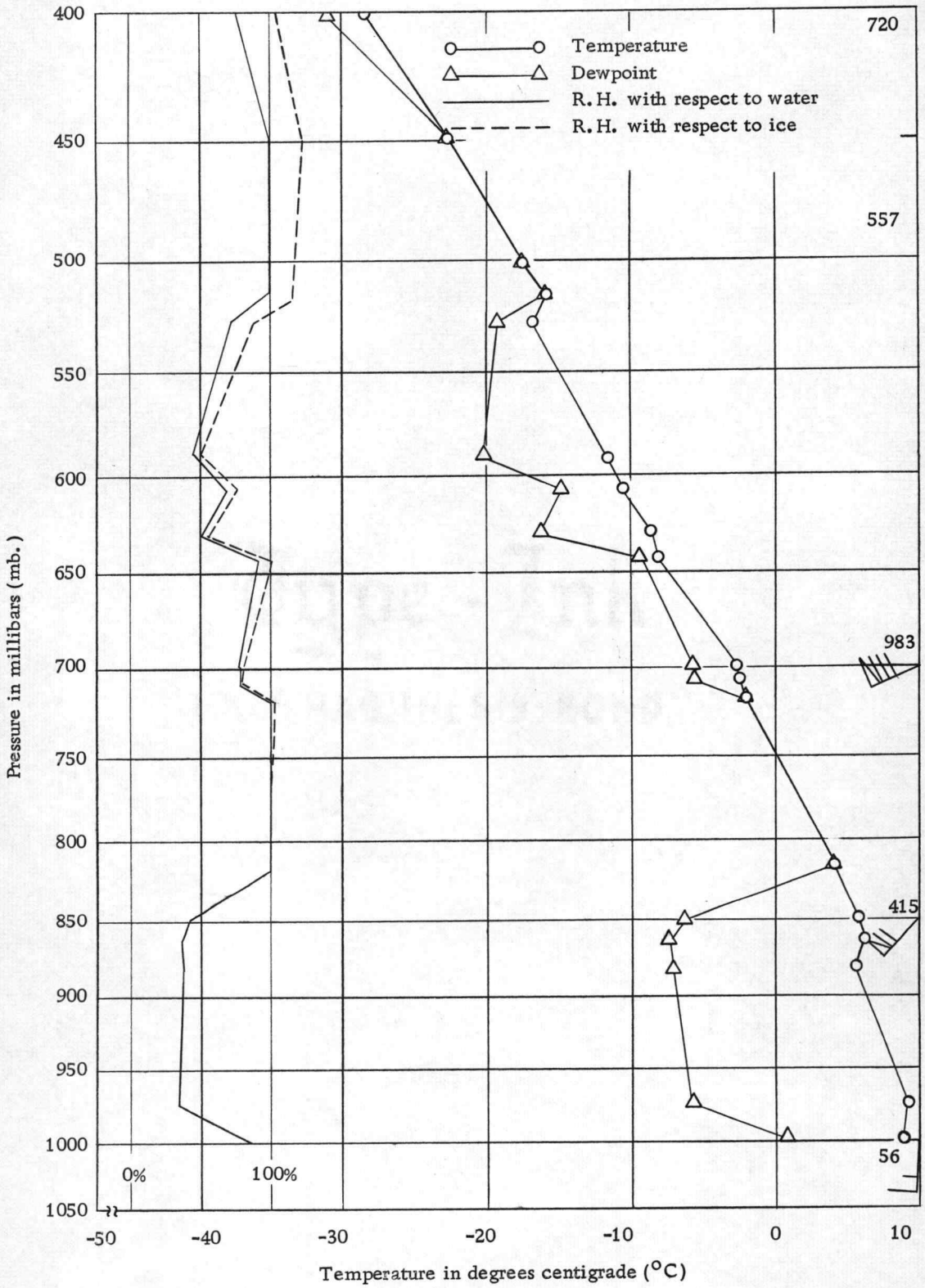

Figure 48. Salem radiosonde sounding, 0400 PST, 19 January, 1967.

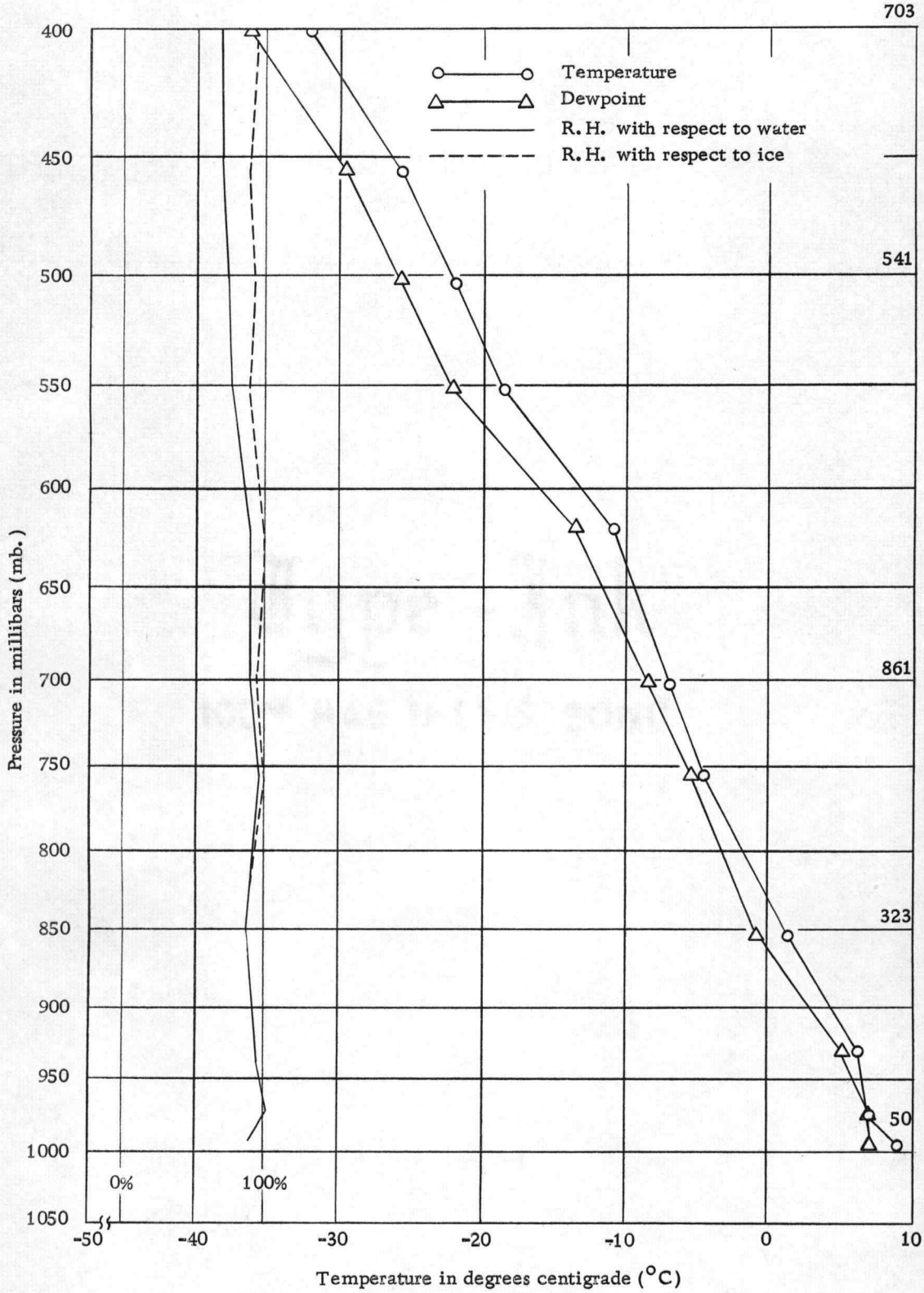

Figure 49. Salem radiosonde sounding, 1600 PST, 19 January, 1967.

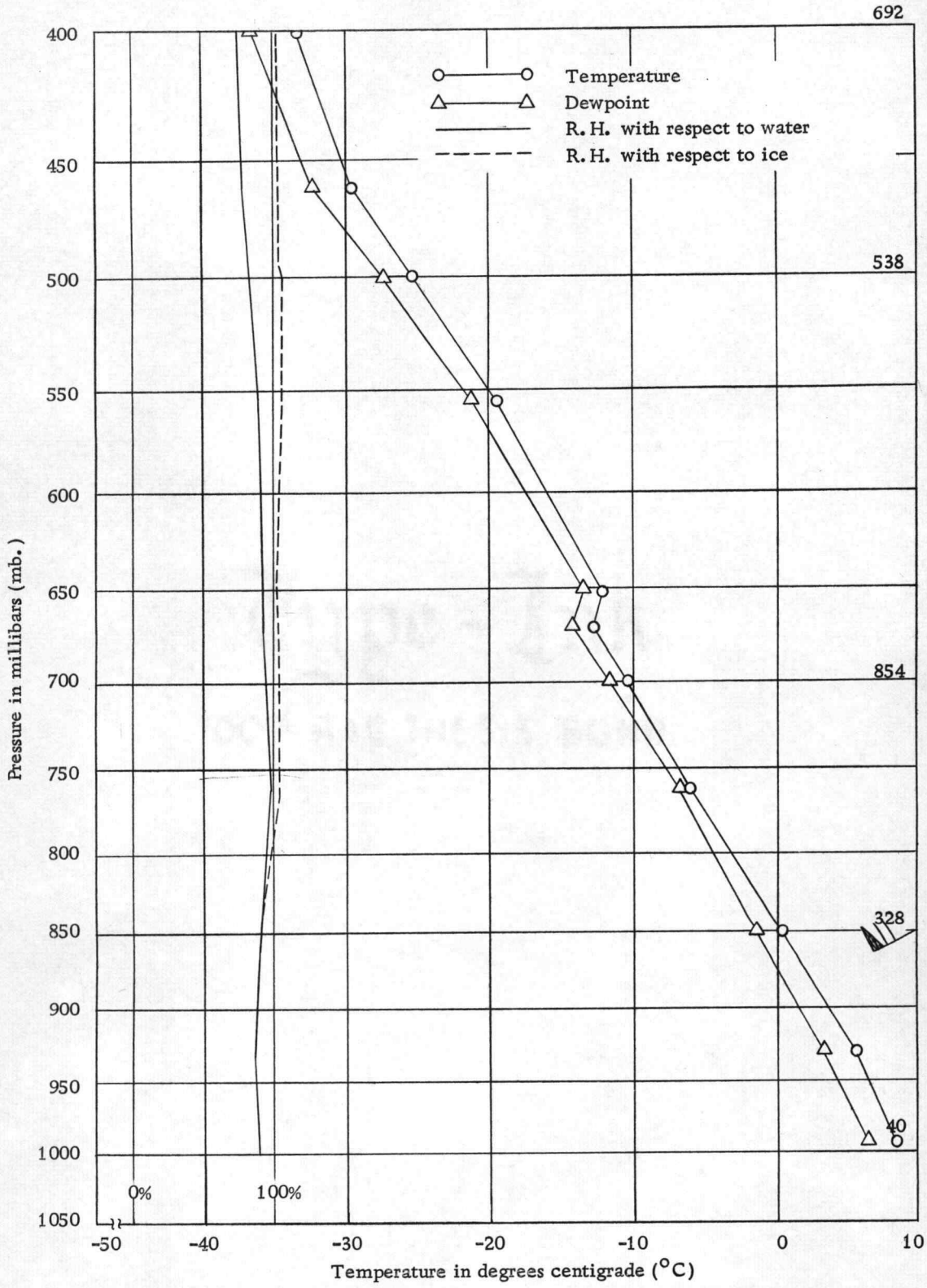

Figure 50. Salem radiosonde sounding, 1900 PST, 19 January, 1967.

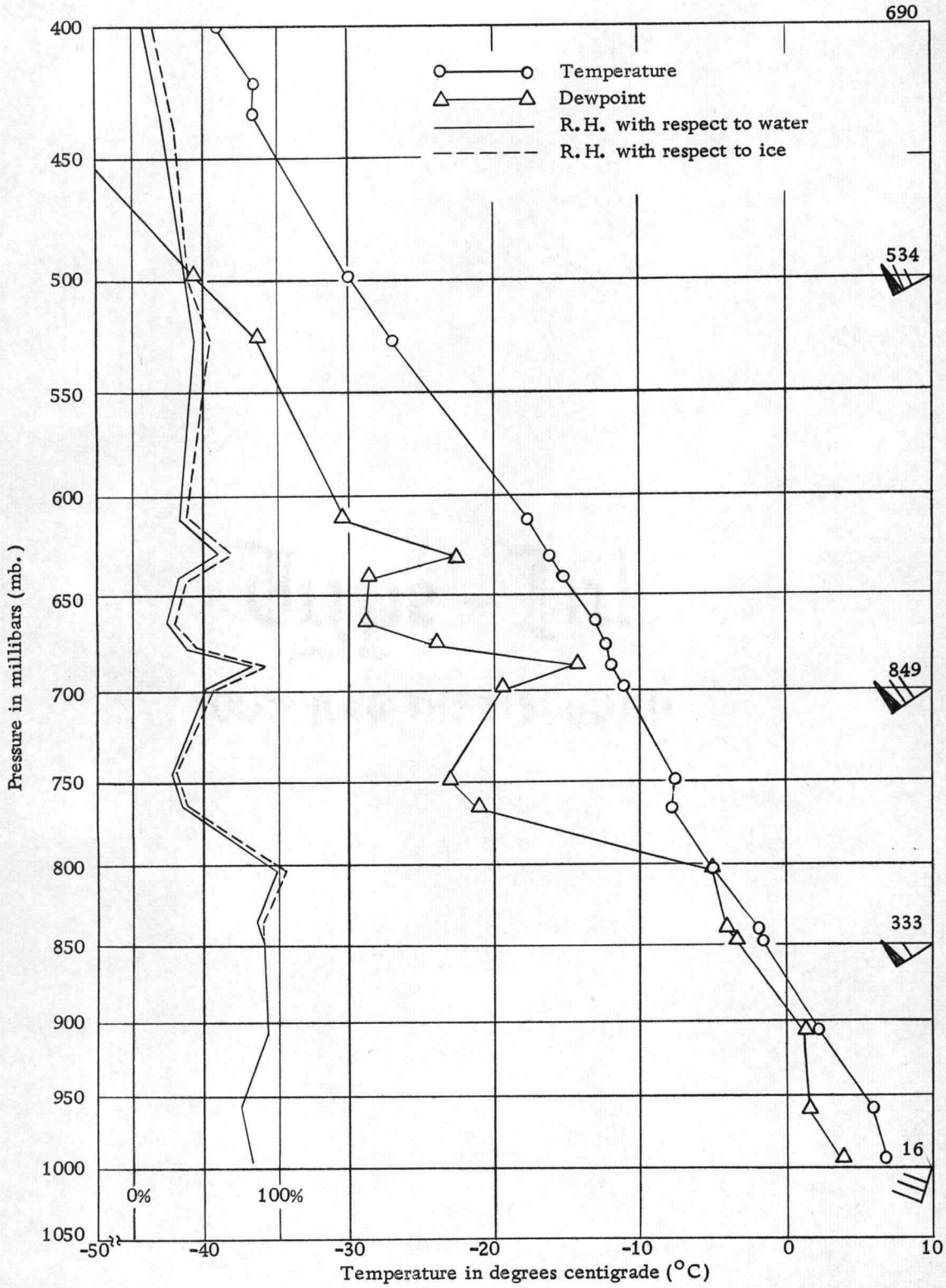

Figure 51. Salem radiosonde sounding, 0400 PST, 20 Januray, 1967.

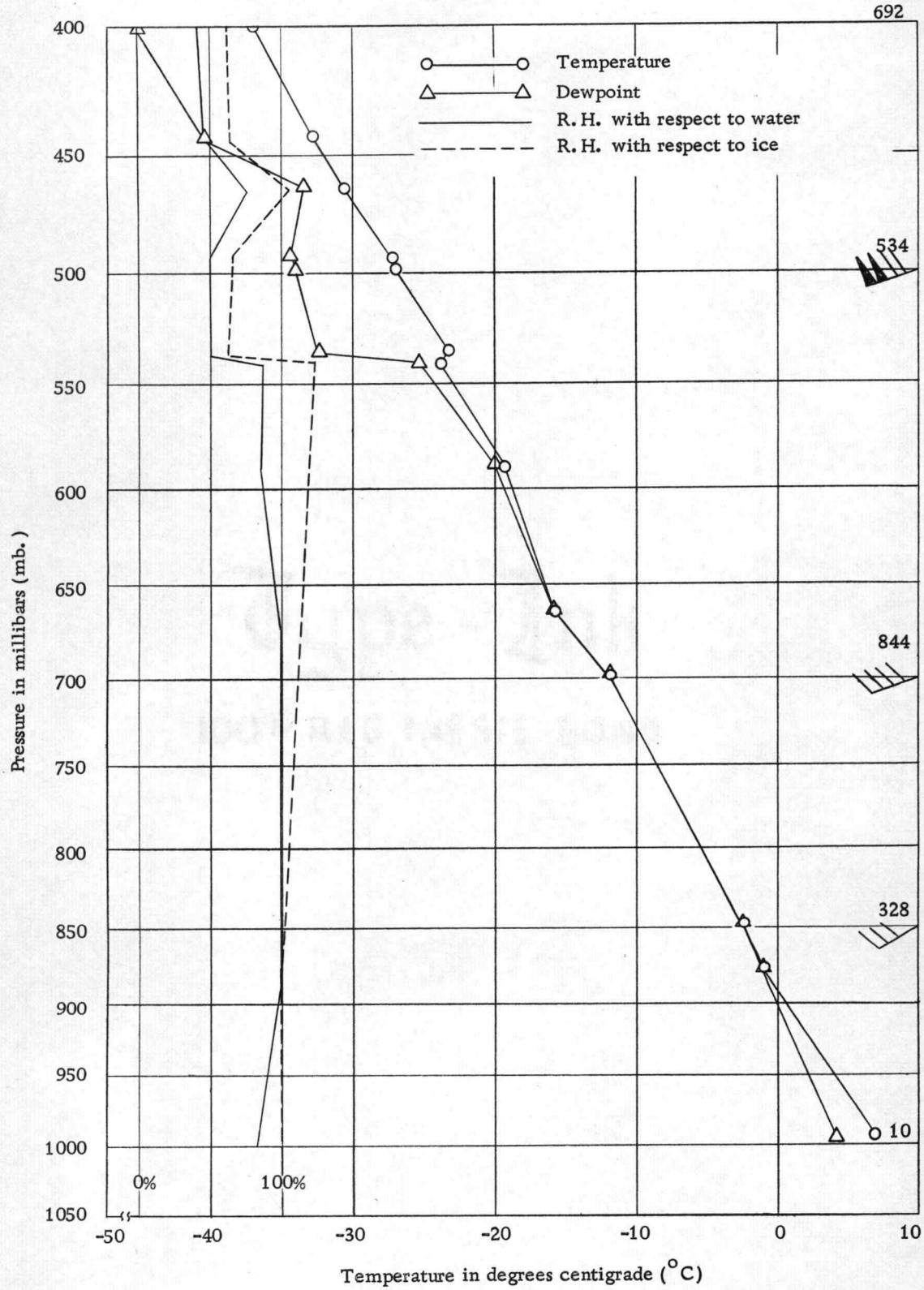

Figure 52. Salem radiosonde sounding, 1600 PST, 20 January, 1967.

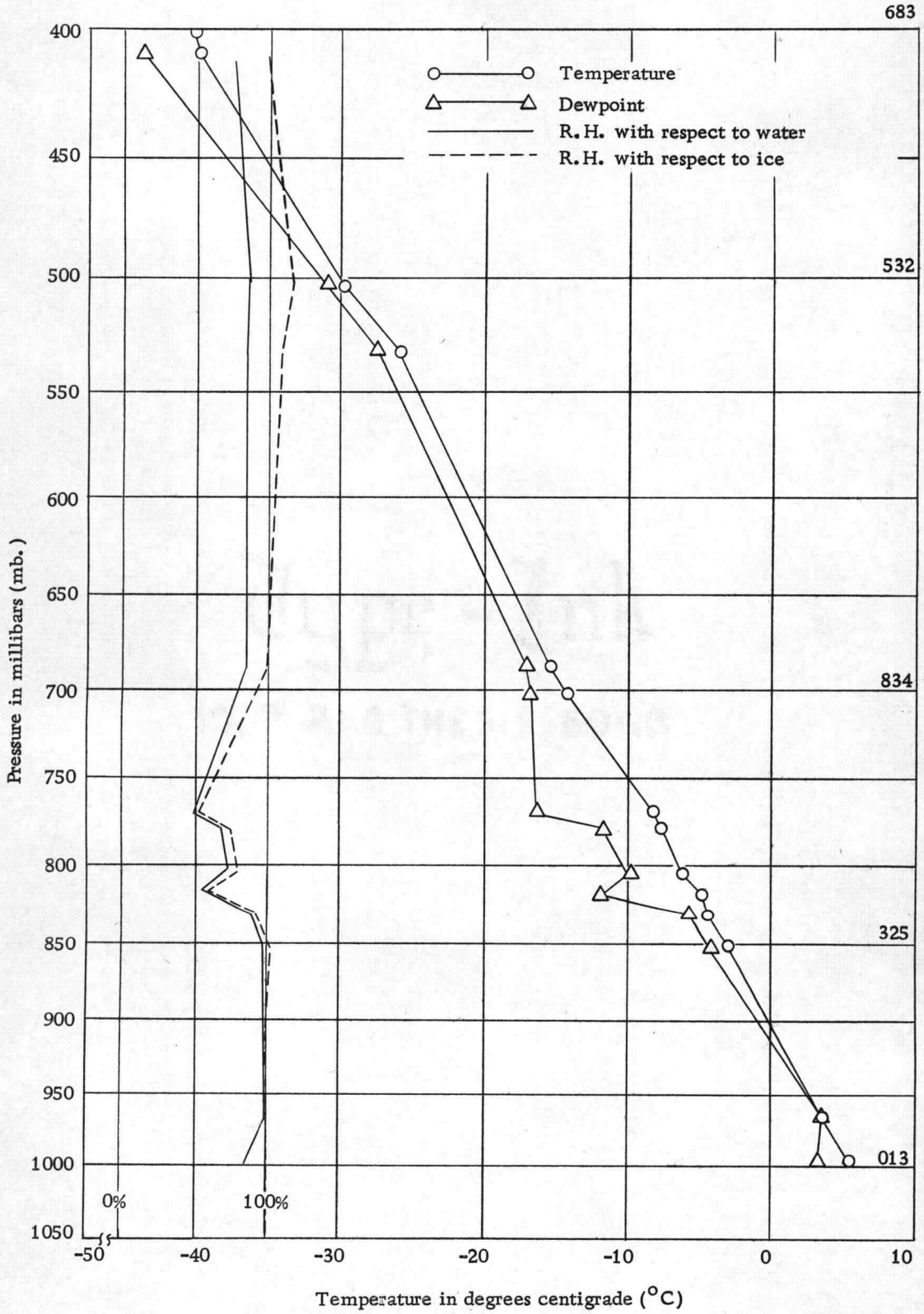

Figure 53. Salem radiosonde sounding, 0400 PST, 21 January, 1967.

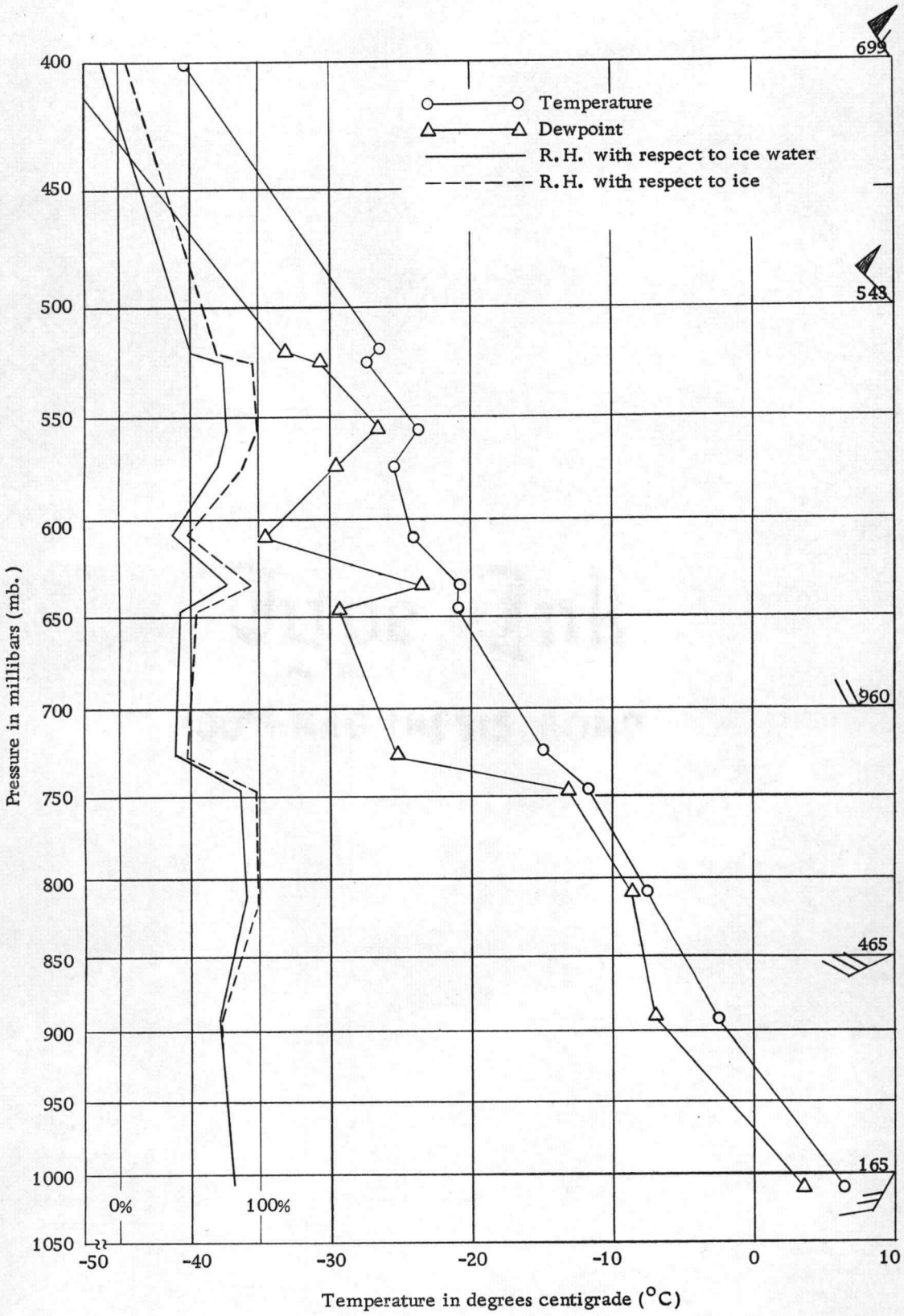

Figure 54. Salem radiosonde sounding, 1600 PST, 14 February, 1967.

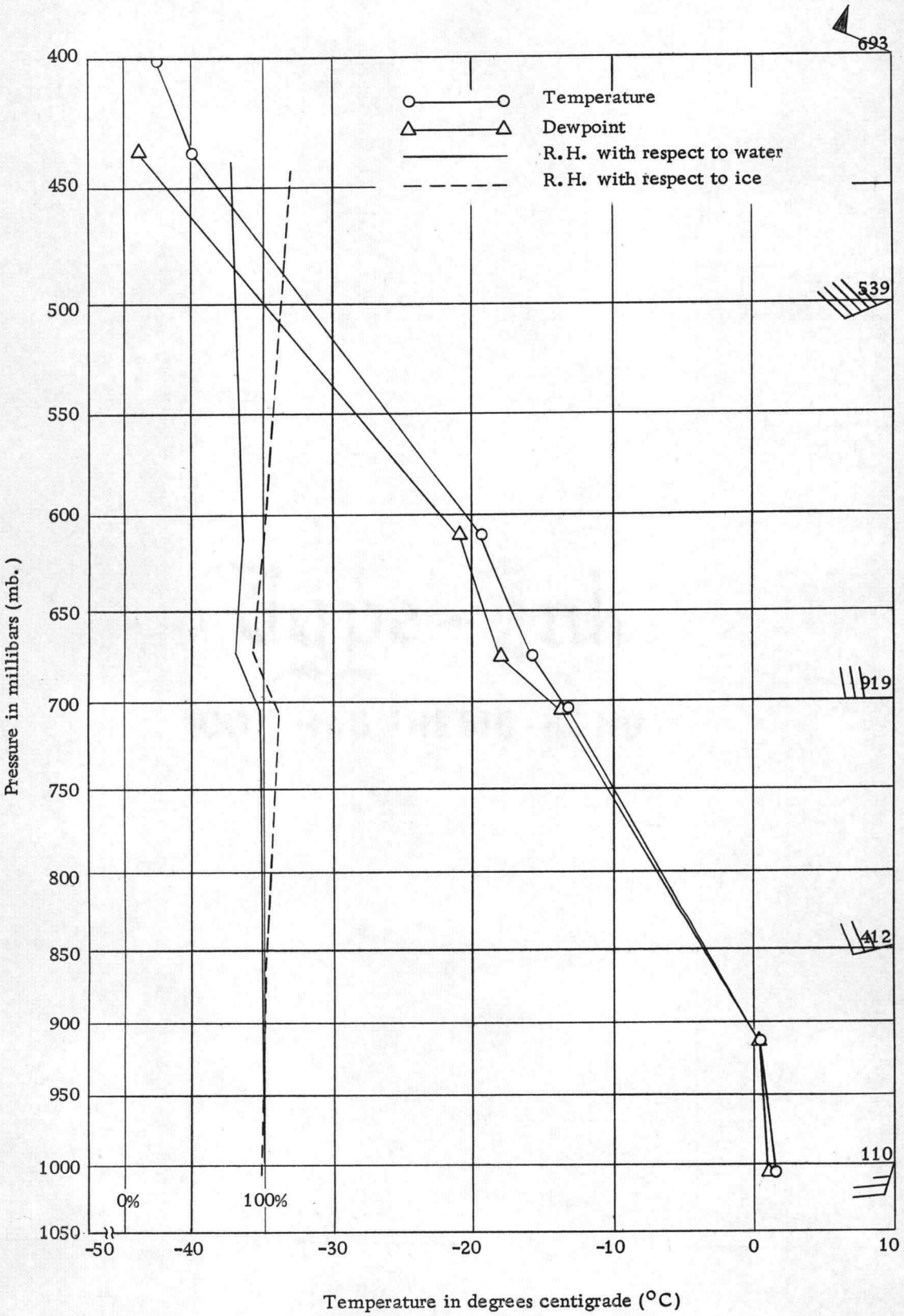

Figure 55. Salem radiosonde sounding, 0400 PST, 15 February 1967.

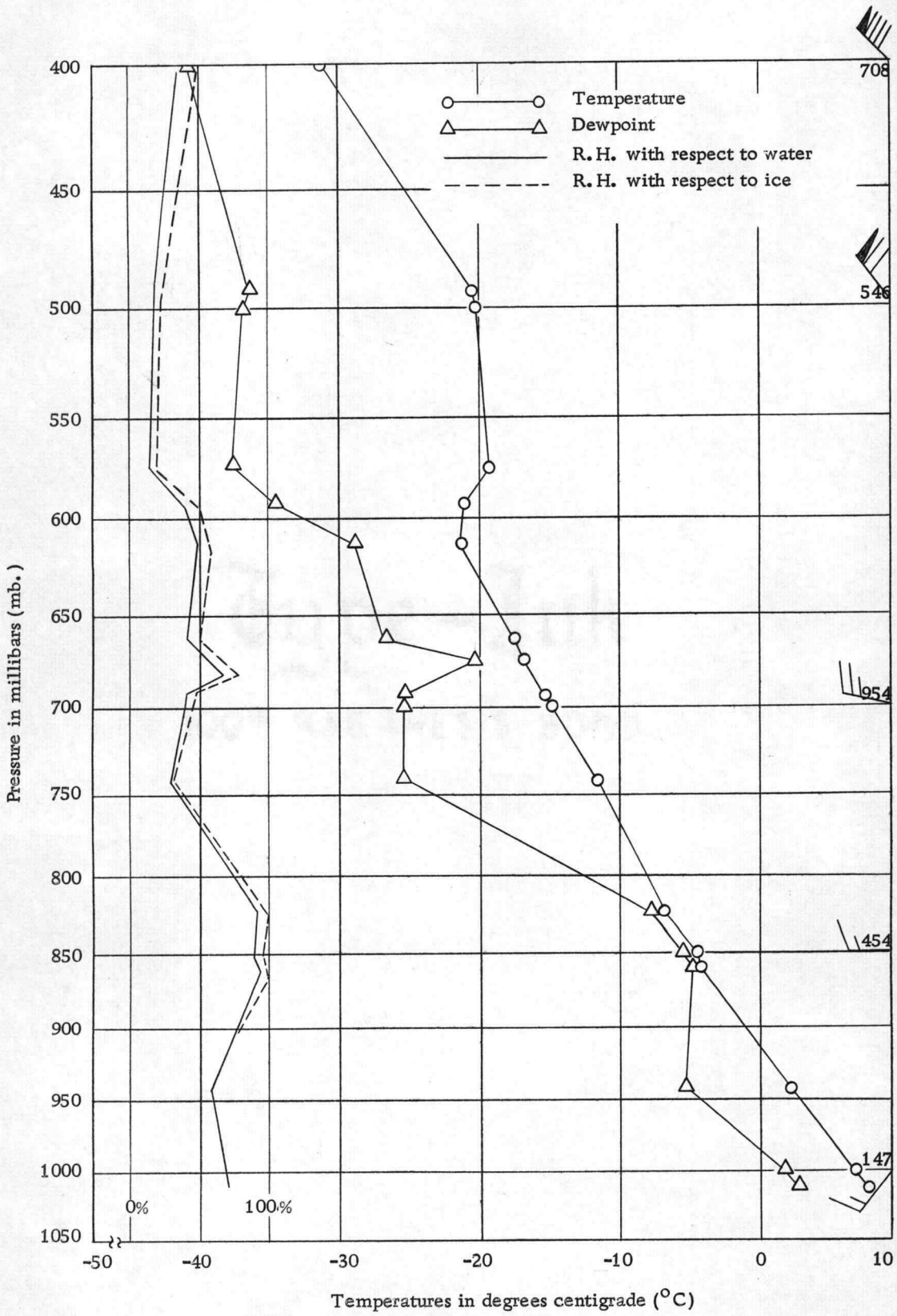

Figure 56. Salem radiosonde sounding, 1600 PST, 15 February, 1967.

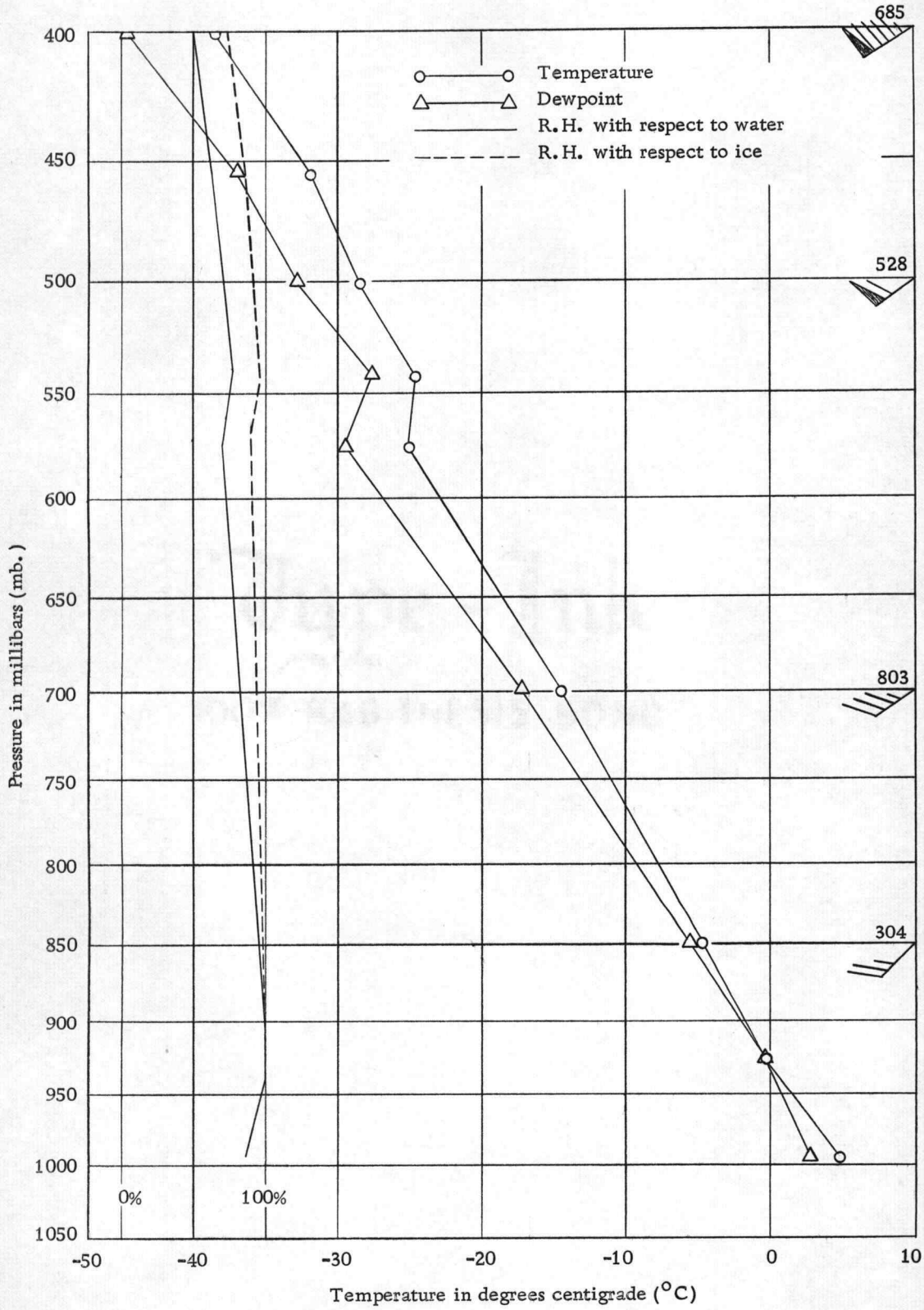

Figure 57. Salem radiosonde sounding, 1600 PST, 9 March, 1967.

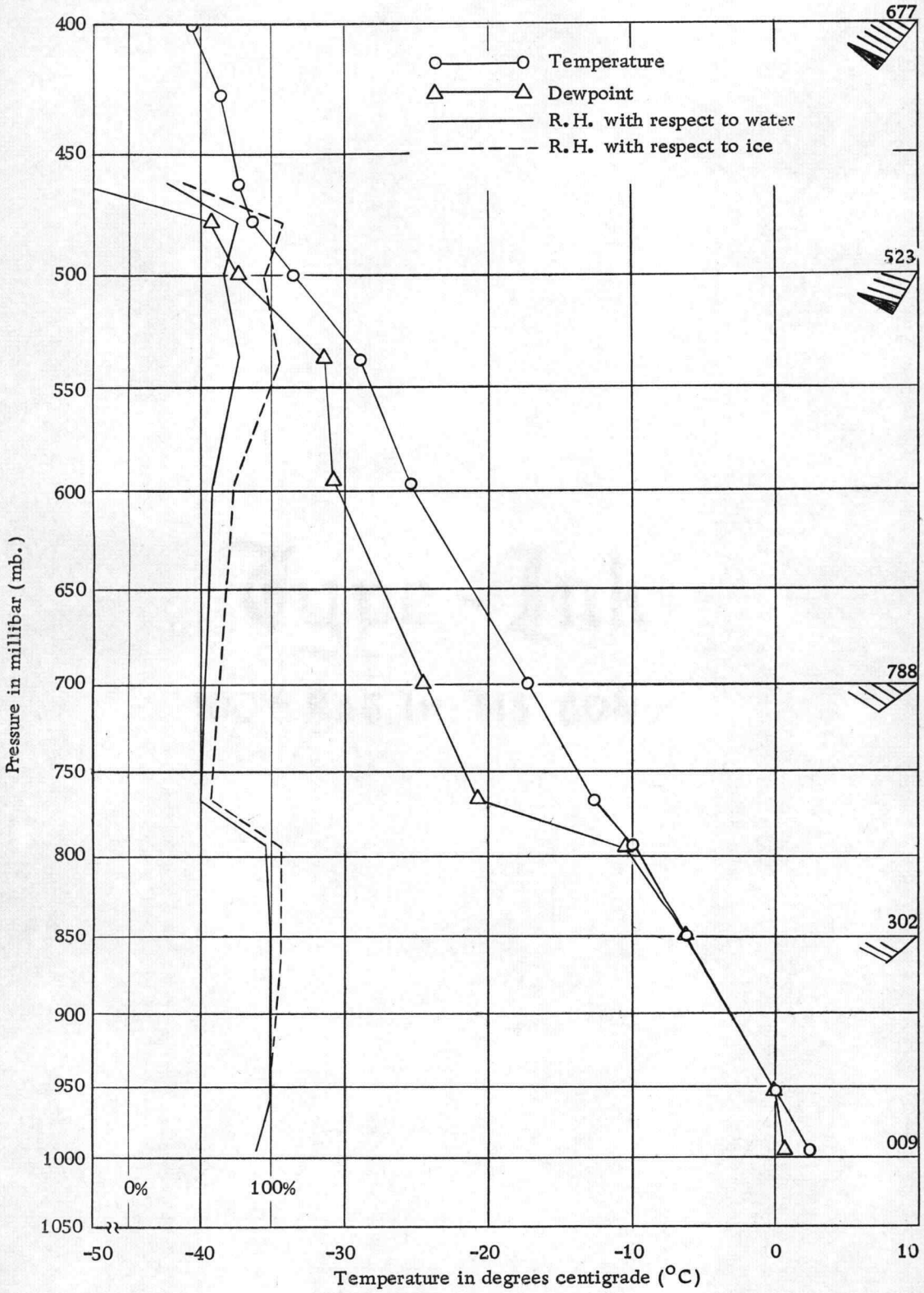

Figure 58. Salem radiosonde sounding, 0400 PST, 10 March, 1967.

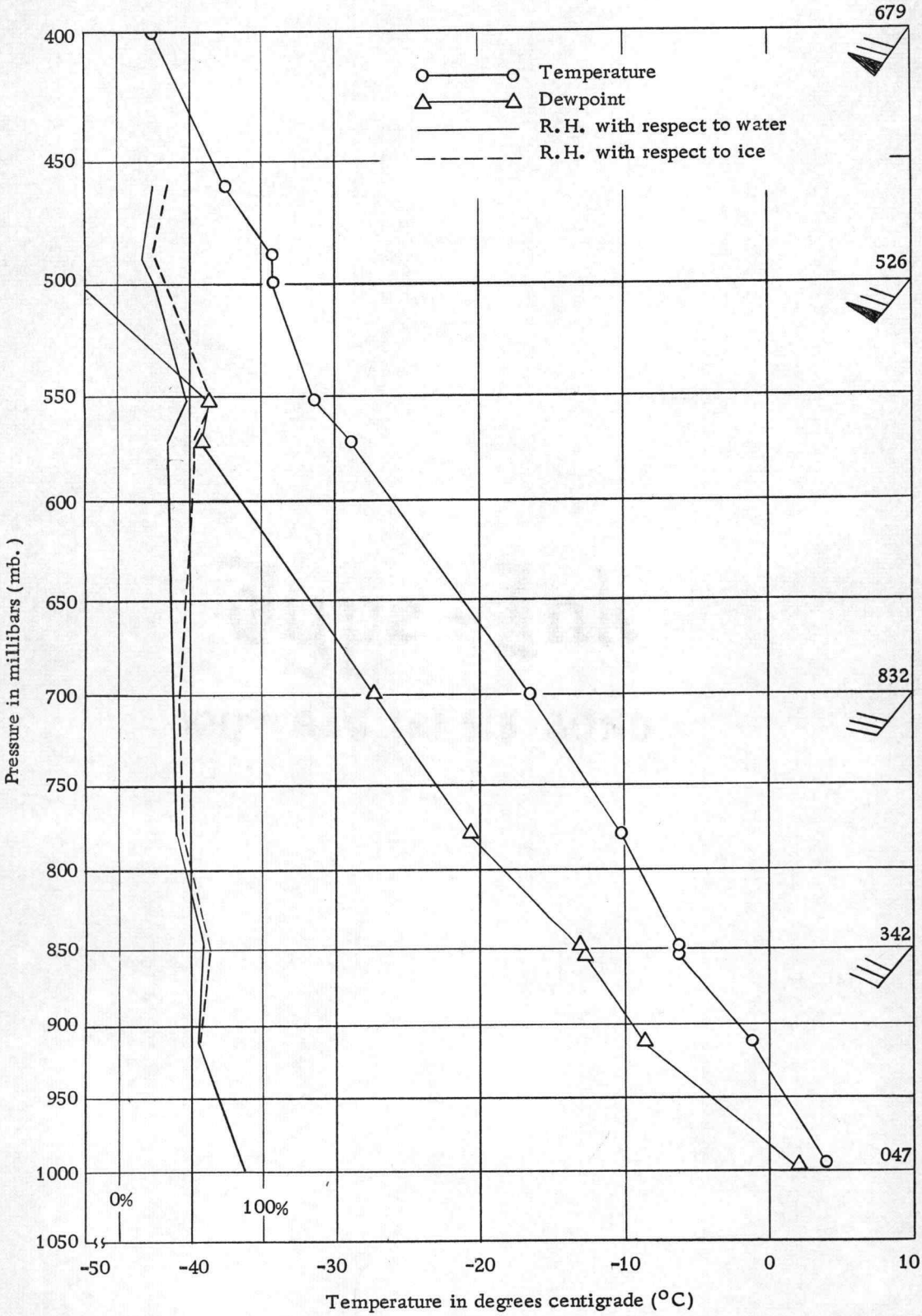

Figure 59. Salem radiosonde sounding, 1600 PST, 10 March, 1967.

APPENDIX E

GENERAL SURVEY OF CRYSTAL TYPES

Table 12. General survey of crystal types as a function of time versus predominant temperature of formation, and percentage of each crystal type appearing for 19-20 January 1967.

Time - PST	Exposure time in sec	Squares counted out of 35	Crystals counted	Surface temperature °C	Riming	Miscellaneous Crystal Types					Temperature Range °C: -5 to -10			-10 to -15			-15 to -20					-20 to -25			-25 to -30			-30 to -55
								P1i	I3	I1		C1b	C1c	CP1c	P1a	P1d	CP1b	P1c	P1e	P3b	P1b	CP1a	S	CP3	P1a	C2b	C1c	C1b
						R3a	R3b	CP2a/N1b	CP1b/N1b	I2	N1a	N1b	N2			P4d	CP2b	P3a	P5b	P1g	P1f	CP2a						C2a
1330				+1.0														x										
												x	x															
1400				- .3												x												
												x	x															
1500				- .4												x				x								
											x	x	x															
1540				- .4														x										
						x					x	x	x															
1630				0												x												
												x	x															
2040																x			x									
												x	x															
2100																												
																					x							
2200				-0.6																								
												x	x						x		x							
2240				-0.3	r											x												
												x	x								x							
0350	10	15	282	-1.7	r																							
										29	32	55	13															
0505	30	20	77	-1.7																								
										2		65	4															
0608	15	13	270	-2.2	r											x												
											27	70	3															
0625					r																							
											x	x	x															
0700	30	15	153	-1.7												x												
											6	62	37															
0800	10	15	121	-1.7	r											1												
										74		23	2															
0820					r			x																				
											x	x	x						x		x							
0850	10	15	244	-1.9	r											4		1						1	4	1		6
										21		49	9															3
0955	10	15	220	-1.9						16						3		x					2	23	39	2		x
												1						4					10					
1035				-2.2																		x		x	x	x		
												x											x					
1130																						x	x			x		x
																		x					x					
1205	10	20	229	-2.2	r											10				x								
										10		57	7			x		15										1
1305	5	12	5	-1.9												60												
												40																
1315	5	20	60	-1.9					10									9					3	8	2			3
							2	10				3						25					13					
1340				-1.9												x		x					x	x	x			
																		x					x					
1515				-2.2														x				x	x	x				
																		x					x					
1535	10	15	215	-2.2						12						6		5				1	1	4	26	6		1
												x				1		36					1					x
1600				-2.2												x		x							x	x		
																		x					x					
1615	10	16	182	-2.2												8		5					1	45	30			
																		9					2					
1740	10	15	268	-2.2												x		1					4	39	36	7		
																		3					10					
1835					r														x				x					
						x	x				x	x	x									x						
1848				-1.9					x				x															
												x	x															
1930	10	10	202	-1.7	r-				19																			
												64	14										2					
2115	10	15	220	-1.7					25	28																		
												39	8															
2220	10	11	275	-1.9	r				2							8		2							13	1		
										14		50	3					6					1					
2250				-1.9																			x		x			x
												x	x										x					

Table 13. General survey of crystal types as a function of time versus predominant temperature of formation, and percentage of each crystal type for 15 February 1967.

Time - PST	Exposure time in sec	Squares counted out of 35	Crystals counted	Surface temperature °C	Riming	Miscellaneous Crystal Types						Temperature Range °C: -5 to -10						-10 to -15						-15 to -20						-20 to -25			-25 to -30		-30 to -55	
							I3	I1				C1b	C1c		CP1c	P1a	P1d		CP1b	P1c	P1e	P3b	P1b		CP1a	S	CP3	P1a		C2b	C1c	C1a	C1b
						R3a	R3b	I2	N1a	N1b	N2						P4d		CP2b	P4b	P5b	P1g	P1f		CP2a								C2a
0010	10		109	-4.2			15										3		5							6	15	1			1		1
0020	10	20	156	-4.2			4	9									5		20 1		18		1		10 1	1	16						
0030	10	35	32	-4.2				19									13		24		23				7	3	6						
0045	10	35	29	-4.3			7	14							6		3		16		13				34 4	17	10						
0100	10	15	237	-4.3	r--		5	3							x				17 3		14				17= x	5	14						2
0115	10	20	78	-4.7	r--		2	8									10		39 3		19		x			3	17						
0130	10	18	188	-4.7	r--		1	12									28		23 4		14		1		1	1	7						
0145	10	20	155	-4.7			5	15									1		20 2	25	30				x	8	7						
0200	10	25	148	-4.7			5	15									1		15 1	18	26				3	3	7	1					
0215	10	25	179	-5.0			4	5									2		20 5	15	30				1		6						1
0230	10	25	238	-5.0	r--		1	7									1		20 5	17	41				x	2	6						
0300	10	25	107	-4.7	r--		20	11									25 1		18		33	1			1 1	4	12				3		
0315	10	30	214	-4.7	r--		7	8									13		13 2		20				2	1	9				x		1
0330	10	18	211	-4.4	r		7	9									27 x		21 6		17				7	1	8						
0345	10	20	146	-4.4	r--		16	21									14 1		36		12		1		5 2	3	11				2		x
0400	10	20	214	-4.4			15	8									14 3		23 x		3				4	x	7						
0420	10		77	-4.4	r	2	1 39										5 3		54	1	3	x	1		1		5						
0430	10	25	126	-4.4	r--			20 28					5				6		1		22	4			1 1	2	19				6		
0500	20	30	120	-3.9	r		2						13				1		13		2		6		1			1			13		
0515	20	30	179	-3.9	r			46					39										2				3				5		
0530	15	20	205	-3.9	r+		14 17	31					45				2					3					10				x		
0545	8	20	238	-3.9	r+		10 8	20					36				5					4	4				17				1		
0600	8	20	239	-3.9	r		11 17	17					29				2					11	1				42				6		
0605	8	15	181	-3.9	r		8	8					17	3								4	x		1		30						
0630	5	15	270	-3.9	r		13 13	13					23				3		12						x		6						
0645	10	20	206	-3.9	r		27 7	28					14				x		8				x				5						
0700	10	20	124	-3.9	r		22 18	34					21				6		x			5	5				1						
0715	10	20	156	-3.9	r		6 19	43 1					14	2			2 6		3			2	3				2						
0730	10	20	147	-3.9	r		24 10	31					5	1			3 1		6	1			1 2				2						
0745	5	20	176	-3.9	r		20 8	49 5					14	1			1 2		1			1					8				1		
0800	20	30	151	-3.6	r		34 1	17 15					5				x		5			1			3						1		
0830	10	20	136	-3.6	r+		38 20			x	45						1										5				4		
0900	10	20	135	-3.3	r		8 18	17 11					19				1			4	4	1	1 1		15		4	1			3		
0910	10	25	130	-3.3	r		12 15	6 3					40	2			2		1	x		1	1								6		
1000	10	15	157	-3.1	r		3 19	13 19					50	5			1			1		2				3	4				1		
1030	10	20	236	-2.8	r		x 4	24 4 18					14 45	1 4					7 3		6				2 1		1				20		

Table 14. General survey of crystal types as a function of time versus predominant temperature of formation, and percentage of each crystal type for 9-10 March 1967.

Time - PST	Exposure time in sec	Squares counted out of 35	Crystals counted	Surface temperature °C	Riming	Miscellaneous Crystal Types			Temperature Range °C: -5 to -10			-10 to -15				-15 to -20					-20 to -25				-25 to -30		-30 to -55	
									Crystal Types																			
						P1i	I3	I2 / I1	N1a	N1b	C1b / C1c	N2	CP1c / P4d	P1a	P1d	CP1b / CP2b	P1c	P3a	P1e / P5b	P3b / P1g	P1b / P1f	CP1a / CP2a	S	CP3	P1a	C2b	C1c	C1a	C1b / C2a
2330	10		65	-3.3			22	9							6	2							5	5			6		2
2340	20	35	134	-3.1			16	15							8 19	35 2	1							14	2			1	1
2350	20	30	138	-2.8			11	20					1		6 15	20 13				1		3	6	7			1		1
0000	10	15	244	-2.8			8	6							4 7	19 3						1 x	32	20			3		2
0010	10	20	171	-2.8	r--		13	7					1		1 8	16 1						2 2	33	15			6		1
0020	20	20	133	-2.8	r		17	2							1 13	10 7				1	1	2	13	16	1		9		
0030	10	20	168	-2.8	r		15	1 5			1		1		11 15	13 2				1	2	2	10	8	2		17		
0045	10	16	182	-3.3	r		14	3					2		4 8	19 2						1	9	12	1		11		
0100	10	16	252	-3.3	r--		10	9					x		x 12	33 7	4		2	2	1 x		10	12			4	x	x
0115	20		282	-3.3	r--	1	17	x 15					x		1 8	24	1		4		2 4	1	6	9	x		8		1
0130	10		224	-3.3			8	3					1		1 2	29 7	1		x		x x	1	1	11			10		2
0135	10	17	223	-3.3	r--	1	10	1 7					x		x 3	36 3	x		4	4	5 1	3 x	5	9	x		11	2	1 1
0145	10	16	225	-3.1	r--	1	8	12					1		4	29 2	1	1 1		2	3 x	x	3	8			9		1 1
0200	10	15	371	-3.1	r-		13	x 3					x		1 3	41 3	x		1	1 x	4	x	9	11			12	1	1 1
0215	5	11	279	-3.3	r--		13	5					x		3	39 4		x	x 1	1 1	2 1	1 1	2	10			6	1	2 2
0245	10	4	245	-3.3		1	x	3			1		x		2	42 1	1	x	2	2	2 1	1	8	7			14	1	2 3
0300	10	6	262	-3.3	r		2	3					1		1	55 1	1			x	2 5		8	5			8		1 18
0315	10	5	197	-3.3	r		2	1		x			2		1	21 6				x	18 x		3	1			9		9 4
0330	10	7	208	-3.3		1	3	1					1		3	63 3				1	4		7	1	1		13		4
0345	10	8	92	-3.3			4	11							8	54					7 9		10	2	2		6	1	1 2
0400	10	15	331	-3.3			2	11					1		2	16				1 x	26 3		19	3	2	1	9		2 6
0415	10	7	239	-3.6			1	6							3	10	1				22 6		21	2	3		2		9 8
0430	10	10	240	-3.6				3							1	10					28 15		13	1	1	1	5	1	9 12
0445	10	8	239	-3.9				4							1 2	1				x	41 6		18	x	1		4		4 3
0545	20	9	287	-3.6				2							x x	2				x	57 1		15	2	2	1	9		2 25
0600	20	11	293	-3.6				2							2	1					17 3		24		4		5		25 22
0615	10	9	282	-3.6				1							5	2					22 6		24	x	3		2		14 5
0630	10	10	297	-3.9			1	7							4	1 x					52 3		34	3	x		1		1 7
0645	10	7	250	-3.9			2	4							6	2 2				2	37 2		18	9	4		x		1 1
0700	10	7	247	-4.2		x	7	8							4	28 5			1	1	21		20	2					2 1
0715	20	10	275	-4.4				2								42			3	x 5	1		13	55	x		8		6
0730	20	10	254	-4.4											2						6 1		10	67	1		4		10 3
0745	10	12	212	-4.4				7													8 3		11	33	7		3		6 2
0800	20	10	254	-3.9			4	2							6	3				2	24		12	34	5				7
0815	10	10	273	-3.9				3							3	15					20 2		12	43	4				1
0830	10	11	163	-3.9				4							2	3					29 2		9	63	2				1
0900	10	6	204	-3.3				2								4					13		3	85	1		2		1
0915	10	17	198	-3.3				4							5	1					5		13	66			x		
0945	20	11	210	-4.4				5								7							x	67	1				5 9
1005	20	13	255	-3.9				1				3				x					3		8	80	2				15
1015	20	9	232	-3.9				2								1					4		10	84	x				1 x
1030	20	9	58	-3.9																	3		69	17	2				2
1100	20	20	170	-3.9				14															25	52					10 3
1130	20	20	162	-3.6				12															32	46	1		2		6 4
1230	20		234	-3.9											2	1	6				1		8	32	1		15		3 2
1300	20	20	144	-4.2				19 10								6					4		36	50					3
1330	20	20	116	-4.4				13													1		35	50					3
																													2

APPENDIX F

SNOW CRYSTAL PHOTOGRAPHS

Figure 60. Crystal sample (X 1.92) for 0405 PST, 20 Jan. 1967. a rimed needles.

Figure 61. Crystal sample (X 1.92) for 0850 PST, 20 Jan. 1967. a needles; b columns; c broad-branched dendrites; d spatial plates.

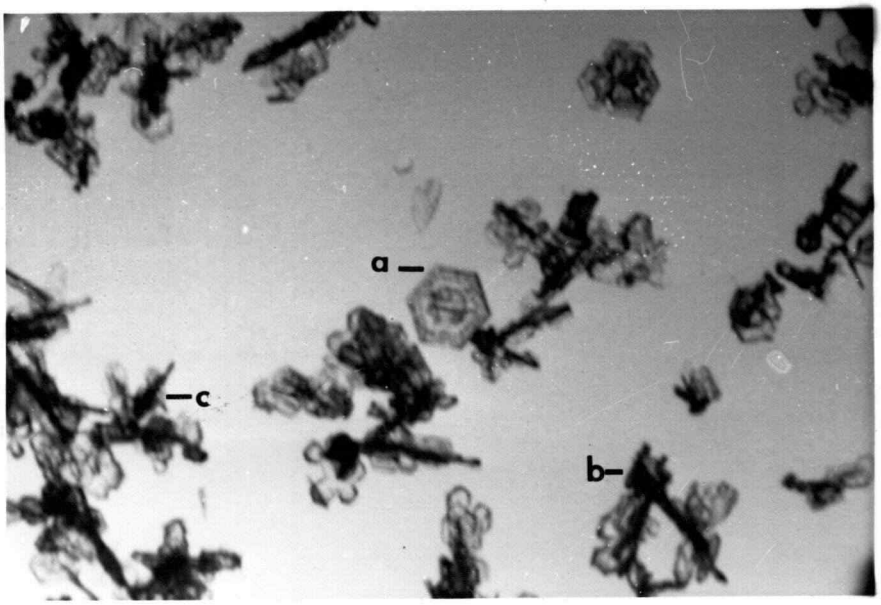

Figure 62. Crystal sample (X 12.16) for 0940 PST, 20 Jan. 1967. a plates; b spatial plates; c capped bullets.

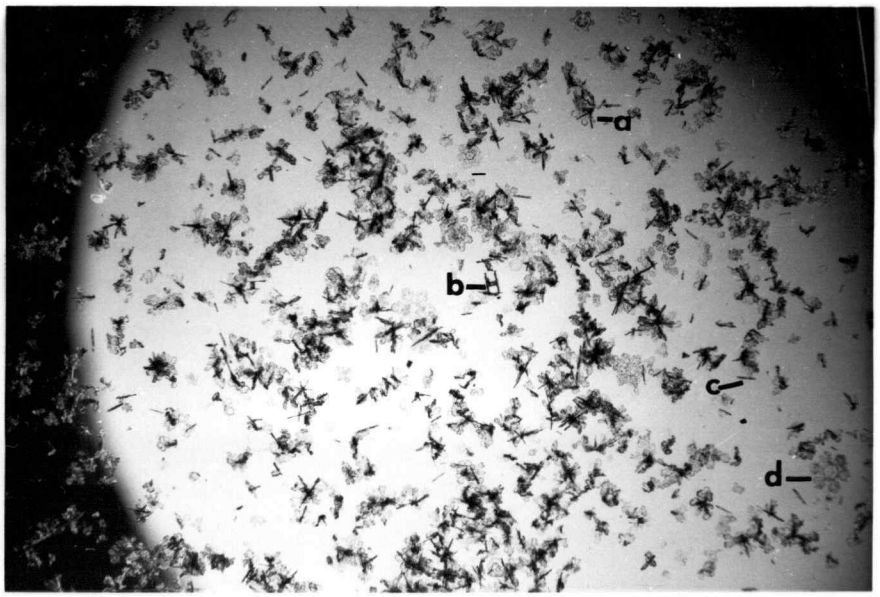

Figure 63. Crystal sample (X 1.92) for 1008 PST, 20 Jan. 1967. a spatial plates; b capped columns; c broad-branched dendrites; d needles.

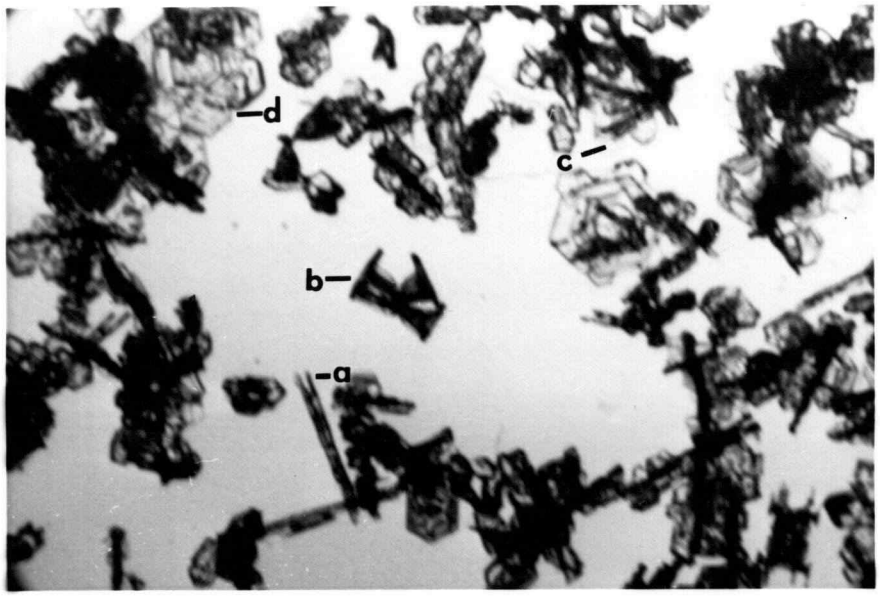

Figure 64. Crystal sample (X 12.16) for 1035 PST, 20 Jan. 1967. a needles; b capped bullets; c spatial plates; d sector plates.

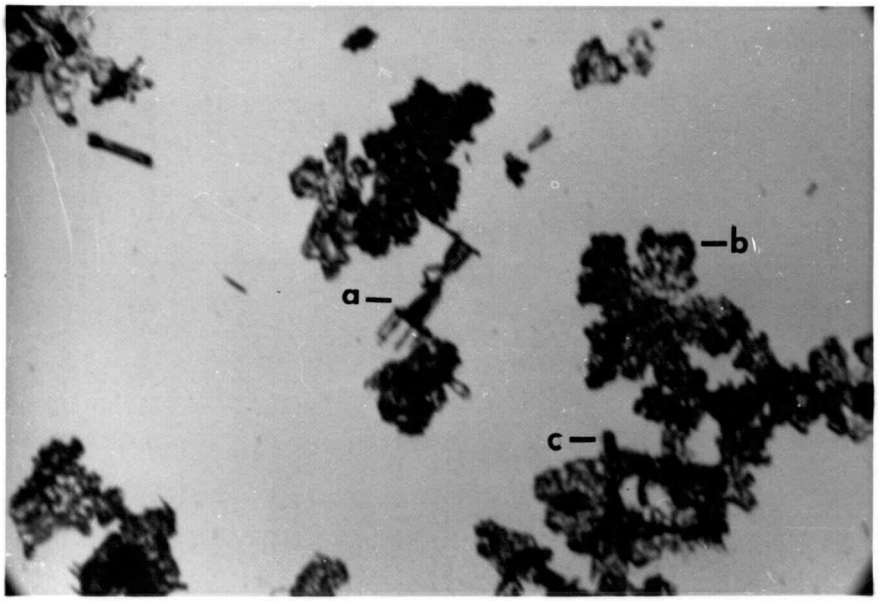

Figure 65. Crystal sample (X 12.16) for 1135 PST, 20 Jan. 1967. a capped column with needle extensions; b sector plates; c bullets.

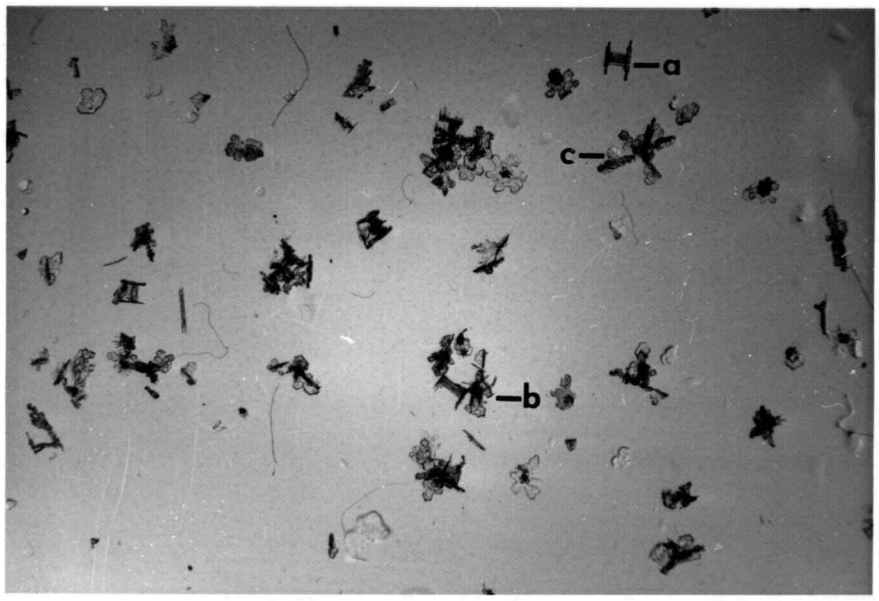

Figure 66. Crystal sample (X 3.84) for 1315 PST, 20 Jan. 1967. a capped columns; b needles; c spatial plates; d columns with side planes.

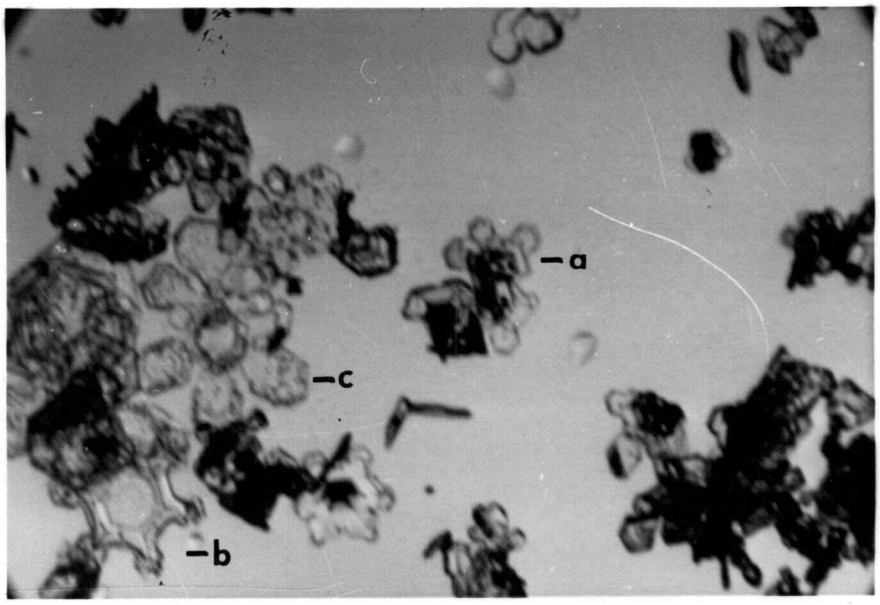

Figure 67. Crystal sample (X 12.16) for 1520 PST, 20 Jan. 1967. a bullets with plates and broad-branched dendrites; b plates; c sector plates.

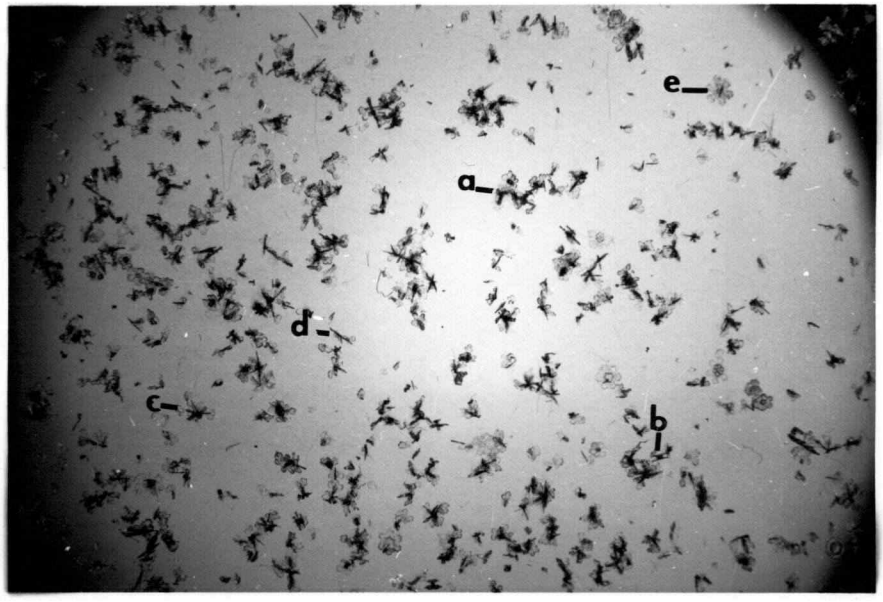

Figure 68. Crystal sample (X 1.92) for 1615 PST, 20 Jan. 1967. a capped bullets; b capped columns; c spatial plates; d columns with side planes; e broad-branched dendrites.

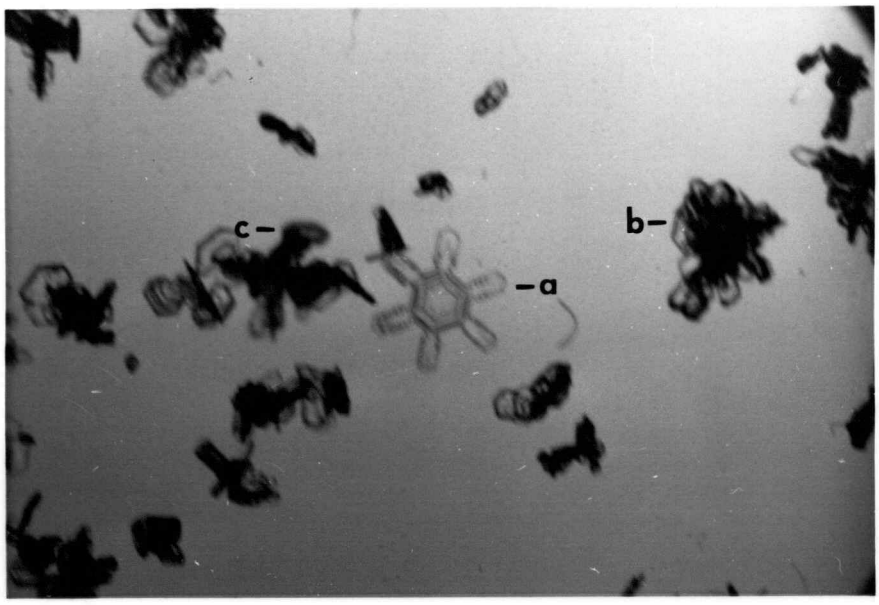

Figure 69. Crystal sample (X 12.16) for 1750 PST, 20 Jan. 1967. a plate with broad-branched extensions; b spatial plates; c bullets with caps.

Figure 70. Crystal sample (X 1.92) for 1930 PST, 20 Jan. 1967. a lightly rimed needles.

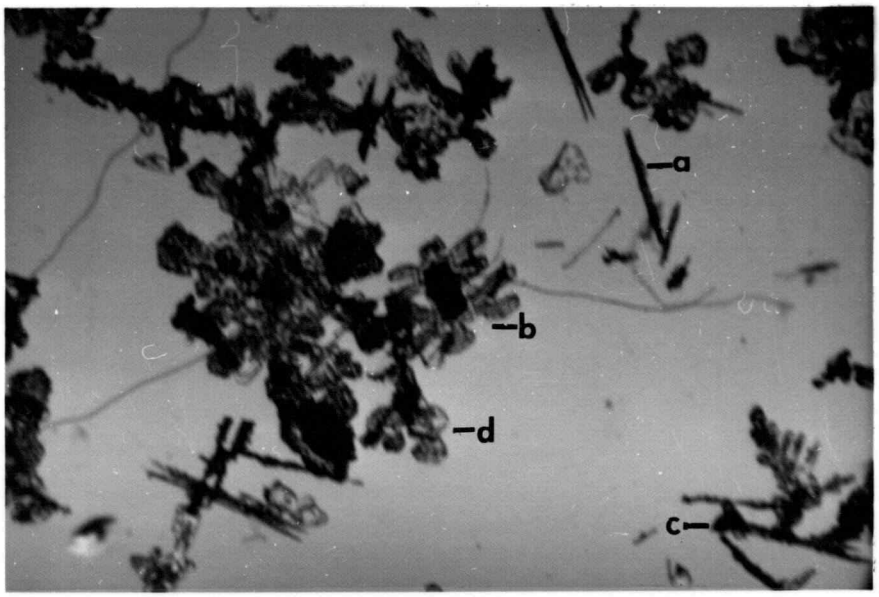

Figure 71. Crystal sample (X 12.16) for 2240 PST, 20 Jan. 1967. a rimed needles; b capped columns; c capped bullets; d spatial plates.

Figure 72. Crystal sample (X 3.84) for 0020 PST, 15 Feb. 1967. a capped columns; b capped bullets; c dendrites; d spatial dendrites; e spatial plates; f malformed dendrites.

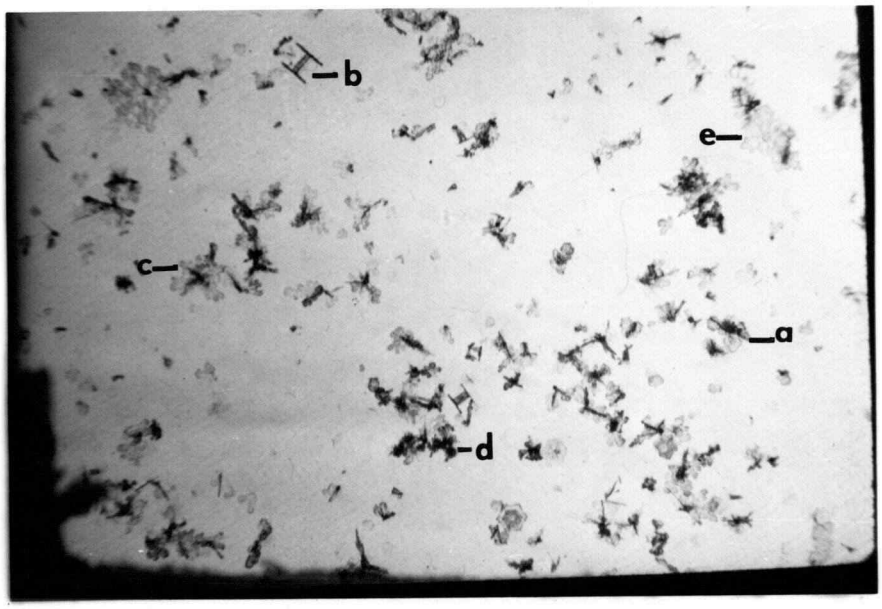

Figure 73. Crystal sample (X 3.2) for 0200 PST, 15 Feb. 1967. a spatial plates; b capped columns; c spatial dendrites; d capped bullets; e malformed sector plates.

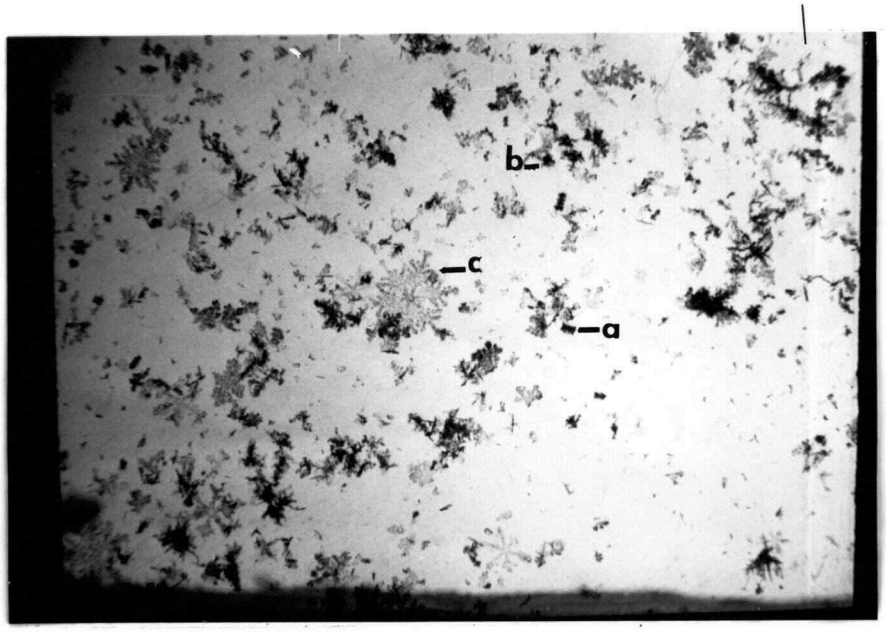

Figure 74. Crystal sample (X 2.24) for 0400 PST, 15 Feb. 1967. a capped column; b capped bullets; c dendrites; d spatial dendrites.

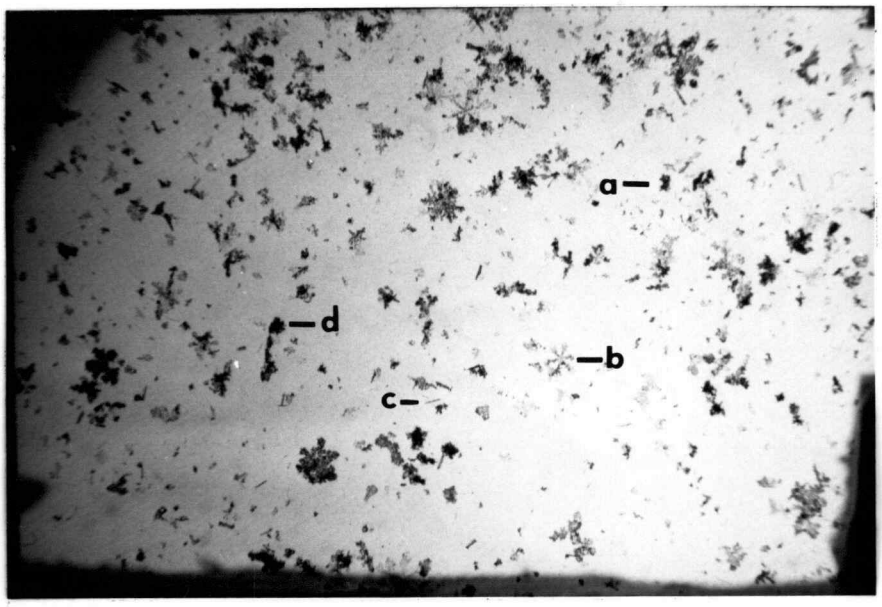

Figure 75. Crystal sample (X 2.24) for 0605 PST, 15 Feb. 1967. a capped bullets; b dendrites; c needles; d graupel-like snow.

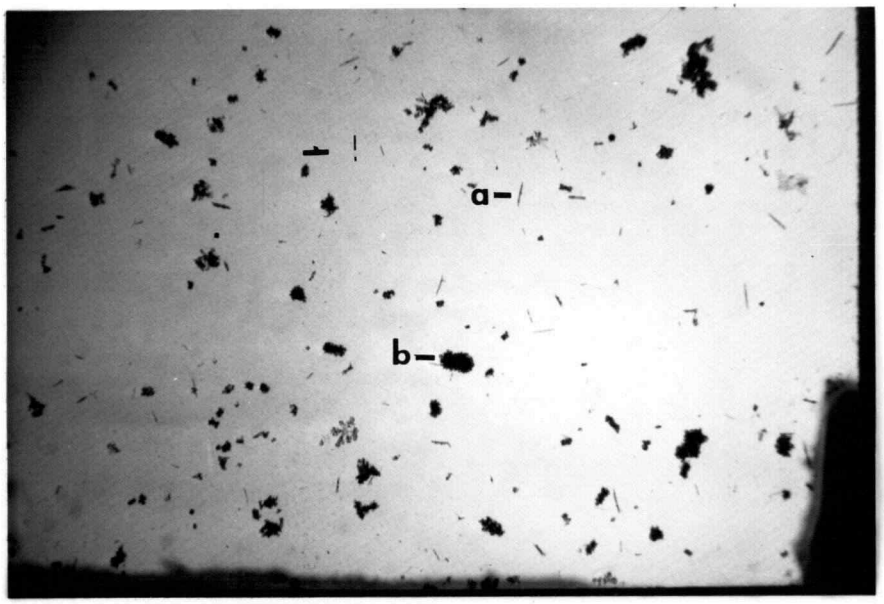

Figure 76. Crystal sample (X 2.24) for 0800 PST, 15 Feb. 1967. a needles; b graupel-like snow.

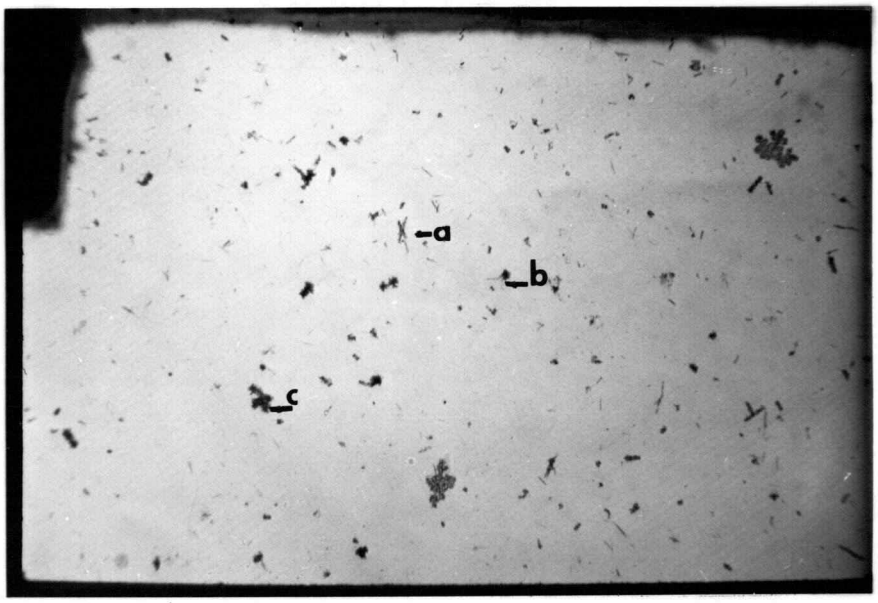

Figure 77. Crystal sample (X 2.24) for 1030 PST, 15 Feb. 1967. a needles; b capped bullets; c graupel-like snow.

Figure 78. Crystal sample (X 2.24) for 0000 PST, 10 Mar. 1967. a spatial plates; b capped bullets; c columns with side planes; d capped columns; e broad-branched dendrites.

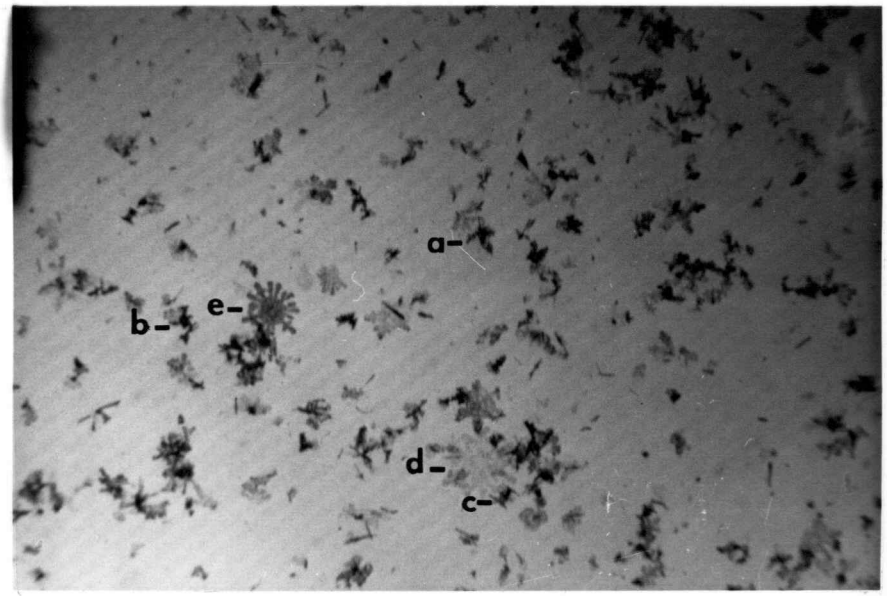

Figure 79. Crystal sample (X 2.56) for 0200 PST, 10 Mar. 1967. a spatial plates; b capped bullet; c capped columns; d dendrite; e 12-pointed dendrite; f broad-branched dendrite.

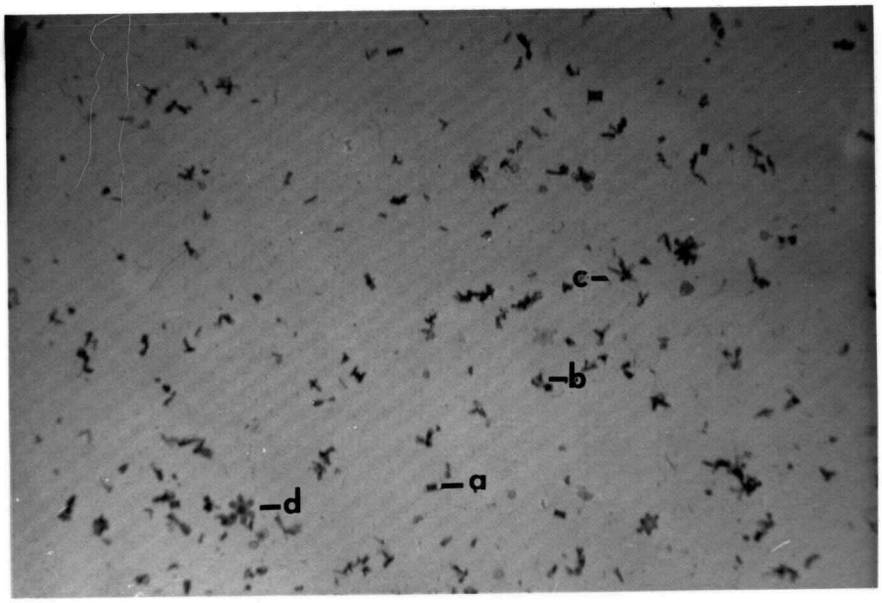

Figure 80. Crystal sample (X 2.56) for 0400 PST, 10 Mar. 1967. a columns; b capped bullets; c spatial plates; d broad-branched dendrites.

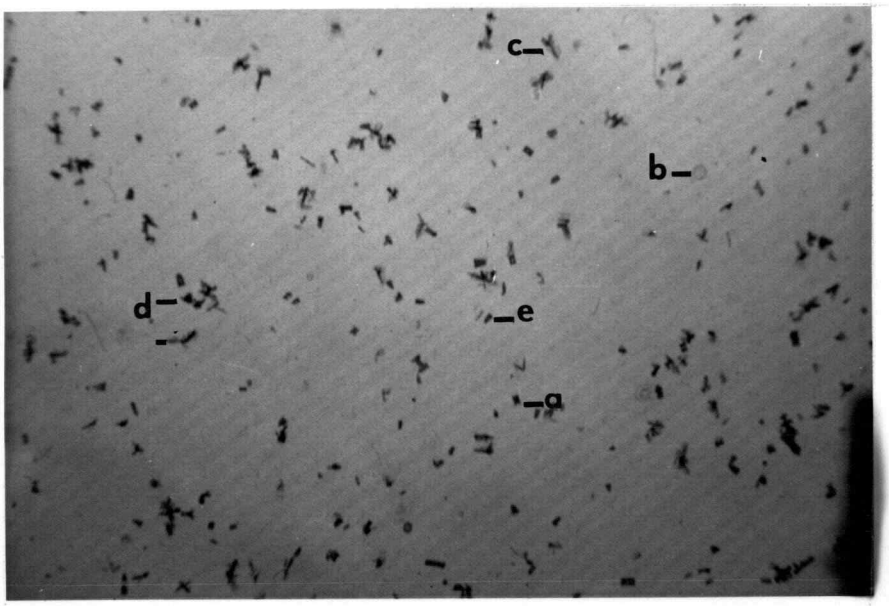

Figure 81. Crystal sample (X 2.56) for 0600 PST, 10 Mar. 1967. a columns; b pristine plates; c spatial plates; d capped bullets; e bullets.

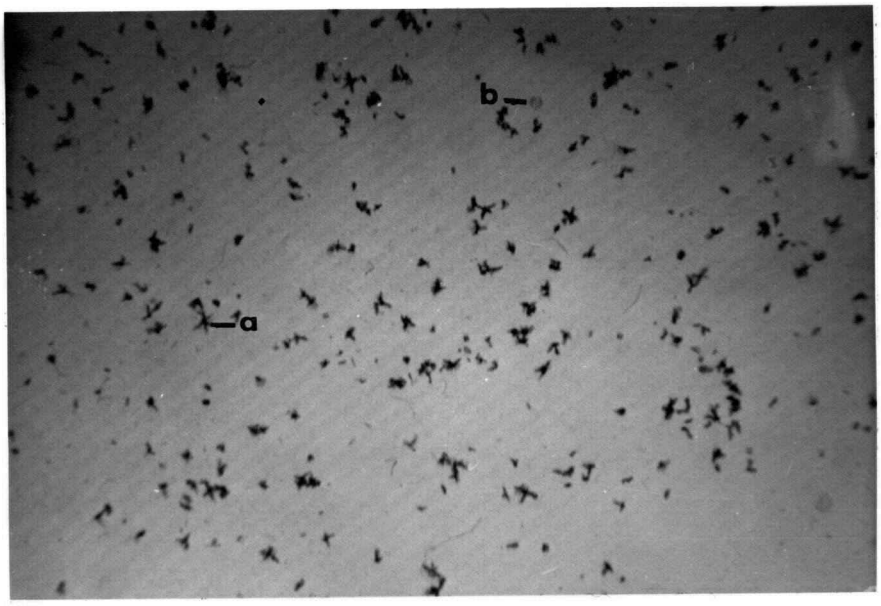

Figure 82. Crystal sample (X 2.56) for 1005 PST, 10 Mar. 1967. a spatial plates.

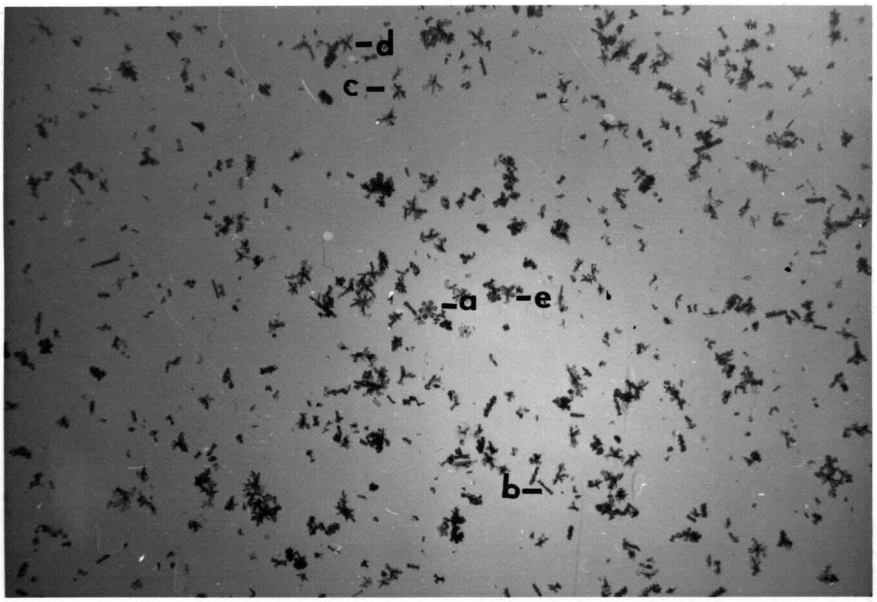

Figure 83. Crystal sample (X 2.04) for 1230 PST, 10 Mar. 1967. a broad-branched dendrites; b rimed columns; c spatial plates; d columns with side planes; e bullets.

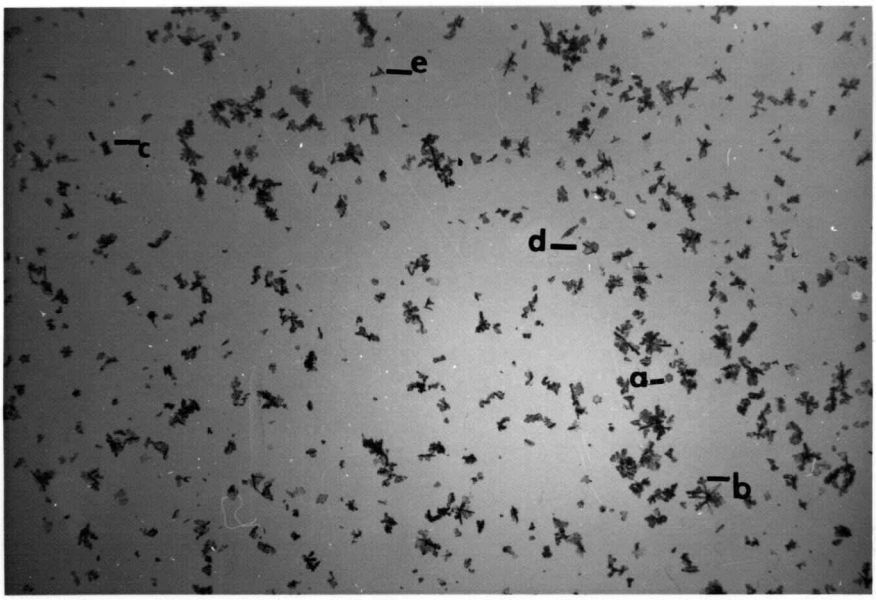

Figure 84. Crystal sample (X 2.04) for 1320 PST, 10 Mar. 1967. a plates; b spatial dendrites; c capped dolumn; d spatial plates; e capped bullets.